A Series of Novel Silicon Phthalocyanines/ Naphthalocyanine as Near Infrared Sensitizers in Organic Ternary and Quaternary Solar Cells

Eine Reihe von neuartigen Silizium-Phthalocyaninen/ Naphthalocyaninen als Nahinfrarot-Sensibilisatoren in ternären und quaternären organischen Solarzellen

Der Technischen Fakultät

der Friedrich-Alexander-Universität

Erlangen-Nürnberg

zur

Erlangung des Doktorgrades Dr.-Ing.

vorgelegt von

Lili Ke

aus Jiangxi, China

Als Dissertation genehmigt

von der Technischen Fakultät

der Friedrich-Alexander-Universität Erlangen-Nürnberg

Tag der mündlichen Prüfung: 27.01.2017

Vorsitzende des Promotionsorgans: Prof. Dr.-Ing. Reinhard Lerch

1. Gutachter: Prof. Dr. Christoph J. Brabec

2. Gutachter: Prof. Dr. Norbert Jux

Acknowledgements

First of all, my most sincere regard and deep devotion goes to my supervisor Professor Christoph J. Brabec for offering me the unique opportunity to doing research in this creative group (*i-MEET*) with a perfect combination of freedom and guidance. I appreciate all his contributions of patience, time, and ideas to conduct these interesting topics listed in this thesis. Without his support and encouragement, it is not possible for me to finish this thesis.

I am also thankful to my second supervisor Professor Rik Tykwinski for his indispensable assistance and useful suggestions throughout the systemization of all dye molecules. The first two years during my PhD period in his group really help me a lot not only in academic study but also in my daily life. His enthusiasm on science and the highest standards of research will definitely have an intense impact in my future career.

I would like to thank my group leader Dr. Tayebeh Ameri for her countless support in my academic research. She could always find the time to listen to my little problems and help me to solve them. It is really a pleasant memory to work in her ternary group under her patient instructions. Her selfless and responsible working attitude deeply inspired me a lot.

This thesis would not have been possible without the support and encouragement from my colleagues in Prof. Brabec and Prof. Tykwinski's groups. I would like to particularly thank those who directly helped with work presented in this thesis: Dr. Jie Min, Nicola Gasparini, Matthias Adam, Anna-Chiara Sale, Karen Forberich, Hong Zhang, Jose Darío Perea, Yi Hou, Chaohong Zhang, Xiaofeng Tang, Haiwei Chen, Dr. Ning Li, Stefan Langner, *etc*. I would like to thank Stefanie Rechberger and Prof. Erdmann Spiecker from the Center for Nanoanalysis and Electron Microscopy for the great help with TEM characterizations. I really appreciate the friendship of Shuai Gao, Ening Gu, Zhanyu Zhai, Carina Bronnbauer and others for their accompany in my daily life.

I would like to thank Corina Winkler, Winfried Habel and Leonid Kuper for keeping the lab always clean to maintain a nice working environment. Thanks to our secretaries Ulrike Knerr and Claudia Koch for their warm help with daily lives.

I would like to thanks the China scholarship council (CSC) for the financial support of my study in Germany. Without this financial support, it is not possible for me to have this chance to come here and finish my Ph.D study.

Last but not least, I am sincerely grateful to my beloved parents, my fiancé, my sister and brothers. Their endless love, support and encouragement made me to go through all the challenges in my life. I greatly appreciate my coming baby Xiaoqi Hu, her birth will give my life a new start.

Abstract

Bulk heterojunction (BHJ) solar cells based on polymer/fullerene blends have attracted much attention over the last decade, leading to a breakthrough in power conversion efficiency (PCE) over 10%. Several strategies are currently being pursued to achieve higher PCE, while most conjugated polymers have an intense, but rather narrow absorption band. An attractive method to broaden the absorption bandwidth is to blend near infrared (near IR) sensitizers into the host donor:acceptor binary blend system. Among them, dye molecules are the most widely used. This dissertation targets on the synthesis of novel dye molecules and fabricating of high efficiency ternary solar cells with absorption ranges extending into the near IR region.

The first part of this thesis focuses on design and synthesis of silicon phthalocyanines (**SiPCs**) and naphthalocyanine (**SiNC**) to open the possibility to modify the chemical, electronic and optical properties. Hence, a novel series of **SiPCs** (**SiPC-0**, **SiPC-1**, **SiPC-2**, and **SiPC-3**) with varying the length of alkyl chain between the pyrene ring and PC ring, and **SiNC-1** by extending the π-system structure were synthesized according to a simple method and characterized. The electronic and optical properties of all new compounds were investigated separately by using cyclic voltammetry and UV-*vis* absorption spectroscopy methods. Near IR absorption feature and suitable band gap (E_{gap}) give these molecules great potential to implement them in ternary or quaternary organic solar cells as dye sensitizers.

The second part of this thesis focuses on study of the relationship between materials' structure with their physical properties and with device application. Introducing **SiPC** compounds into P3HT/PCBM matrix, all sensitizers showed a strong photosensitivity in the near IR region and notable improvement for all performance parameters of the ternary solar cells as compared to the reference binary device. The incorporation of **SiPC-3** resulted in an increase of up to 21.9% of short-circuit current density (J_{SC}), 16.1% of open-circuit voltage (V_{OC}) and 7.2% of fill factor (FF), leading to an improvement of up to 51.6% of PCE in ternary solar cells. Charge generation, transport properties and morphology of the ternary systems were studied by using different advanced technologies to exhibit the relationship between the molecule structures with photophysical properties.

The third part of this thesis focuses on the study of ternary and quaternary concept and on the revealing the charge transfer/transport mechanism. Herein, we studied the application of **SiNC-1** as an efficient photosensitizer in ternary solar cells as well as in quaternary ones, incorporating **SiPCs** as the complementary near IR sensitizers to the **SiNC-1**. Our in-depth study based on the optoelectronic internal quantum efficiency (IQE), photoluminescence (PL) and photoinduced absorption (PIA) measurements revealed complex charge transfer and transport kinetic in ternary systems. Multi-colored dye sensitized device covering the UV-*vis* as well as near IR regions from 350 up to 900 nm outlined apparent signal characteristics of each single dye. It corroborated the effective contribution of both **SiPC** and **SiNC** dyes in enhancing the J_{SC} and device performance.

And finally, the last part of this thesis focuses on high efficiency ternary solar cells based on middle band gap polymer host systems and on V_{OC} change implementing different content of **SiPC** sensitizer. Herein, the best silicon phthalocyanine **SiPC-3** was introduced into OPV-46:PCBM and PCDTBT:PCBM host systems as the near IR sensitizer. Different to the crystalline polymer systems, amorphous ones allow more dye loading with stronger near IR photosensitivity, yielding an improvement of J_{SC}. Interestingly, different V_{OC} trend were observed for these two amorphous polymer systems.

Zusammenfassung

Organische Solarzellen, welche auf einer Polymer/Fulleren Mischung basieren, haben im letzten Jahrzehnt viel Aufmerksamkeit auf sich gezogen. Der Bulk-Heteroübergang (engl.: Bulk heterojunction (BHJ)) als Mischstruktur führte zu einem Wirkungsgrad von mehr als 10%. Konjugierte Polymere haben zwar einen intensiven, aber auch ziemlich begrenzten Absorptionsbereich, was dazu führt, dass momentan verschiedene Herangehensweisen verfolgt werden, um den Wirkungsgrad weiter zu erhöhen. Das Hinzumischen von Nahinfrarot-Sensibilisatoren in das binäre Donator:Akzeptor System ist dabei eine vielversprechende Methode den Absorptionsbereich in Richtung höherer Wellenlängen zu erweitern. Hierbei sind Farbstoffe eine der am häufigsten verwendeten Nahinfrarot-Sensibilisatoren. Das Ziel dieser Dissertation ist die Synthese von neuartigen Farbstoffen und ihre Einbindung in hocheffizienten organischen Solarzellen, um die Absorption im nahinfraroten Bereich zu verbessern.

Der erste Teil der Forschungsarbeit fokussiert sich auf das Design und die Synthese von Silizium-Phthalocyaninen (SiPC) und Silizium-Naphthalocyaninen (SiNC), wodurch die chemischen, elektrischen und optischen Eigenschaften besser modifiziert werden können. Daher wurde eine Gruppe neuartiger SiPCs (**SiPC-0**, **SiPC-1**, **SiPC-2** und **SiPC-3**) mit unterschiedlicher Alkylkettenlänge zwischen dem Pyren- und PC-Ring, sowie ein neues SiNC (**SiNC-1**) durch das Erweitern der π-Systemstruktur nach einer einfachen Methode synthetisiert und charakterisiert. Die elektrischen und optischen Eigenschaften von allen neuen Verbindungen wurden separat durch Cyclovoltammetrie und UV-*Vis* Absorptionsspektroskopie untersucht. Die Nahinfrarotfähigkeit und eine geeignete Bandlücke geben diesen Materialien ein großes Potential für die Anwendbarkeit als Farbstoffsensibilisatoren in ternären und quaternären organischen Solarzellen.

Im zweiten Abschnitt werden die Zusammenhänge zwischen Materialstruktur, physikalischen Eigenschaften und der Einfluss auf die Solarzellenleistung untersucht. Die Einlagerung von SiPC Verbindungen in die P3HT/PCBM Matrix zeigte eine deutliche Steigerung der Lichtempfindlichkeit im nahinfraroten Bereich, was folglich in einer Verbesserung aller Leistungskenngrößen der Solarzelle resultierte. Das Hinzufügen von **SiPC-3** führte zu einer

relativen Erhöhung der Kurzschlussstromdichte (J_{SC}) um 21,9%, der Leerlaufspannung (V_{OC}) um 16,1%, des Füllfaktors (FF) um 7,2% und folglich zu einer relativen Verbesserung des Wirkungsgrades um 51,6%. Um die Beziehung zwischen Molekülstruktur und photophysikalischen Eigenschaften besser zu verstehen, wurden die Ladungsträgererzeugung, Transporteigenschaften und Morphologie der ternären Materialsysteme mittels verschiedener moderner Messmethoden analysiert.

Der dritte Teil der Arbeit befasst sich mit der Erforschung des ternären und quaternären Mischkonzepts und des Ladungstransfer/Ladungstransport Mechanismus. Hier untersuchten wir die Anwendbarkeit des effizienten Photosensibilisators **SiNC-1** in ternären, sowie als Erweiterung zu den **SiPCs** in quaternären Solarzellen. Unsere gründliche Studie basierend auf optoelektronischen Messungen, wie interne Quanteneffizienz (IQE), Photolumineszenz (PL) und photoinduzierte Absoption (PIA), deckte eine komplexe Kinetik hinter dem Ladungstransfer und Ladungstransport in ternären Systemen auf. Solarzellen basierend auf mehrfarbigen Farbstoffen, mit einer wahrnehmbaren Signal-Charakteristik für jeden Farbstoff, decken mit einer hohen Absorption in den Wellenlängen 350 nm bis 900 nm sowohl den sichtbaren, als auch den nahinfraroten Bereich ab. Dies untermauert die effektive Beteiligung von **SiPC** und **SiNC** an der Steigerung des J_{SC} und des Wirkungsgrades.

Der vierte und letzte Abschnitt der Dissertation legt seinen Schwerpunkt auf hocheffiziente ternäre Solarzellen basierend auf Polymeren niedriger Bandlücke und den Ursprung der V_{OC}-Änderung, hervorgerufen durch verschiedene Massenanteile von **SiPC**. Hier wurde **SiPC-3** den binären Systemen OPV-46:PCBM und PCDTBT:PCBM als Nahinfrarot-Sensibilisator beigemischt. Im Gegensatz zu kristallinen Polymersystemen erlauben amorphe Systeme eine höhere Farbstoffbeladung mit stärkerer Nahinfrarotempfindlichkeit, resultierend in einer Steigerung der Kurzschlussstromdichte. Interessanterweise wurden für diese amorphe Polymersysteme verschiedene Änderungen der Leerlaufspannung beobachtet.

Abbreviations

AFM	Atomic Force Microscopy
Ag	Silver
AgCl	Silver chloride
Al	Aluminum
AM	Air Mass
BHJ	Bulk Heterojucntion
Ca	Calcium
CB	Chlorobenzene
CT	Charge-transfer
C60	Fullerene
$C_{61}(CO_2Et)_2$	Di(ethoxycarbonyl)methanofullerene carboxylate
CuMePc	Tetramethylsubstituted copper(II) phthalocyanine
CuPc	Copper(II) phthalocyanine
CV	Cyclic voltammetry
$CDCl_3$	Deuterated chloroform
CH_2Cl_2	Dichloromethane
D-A	Donor - Acceptor
DCB	Dichlorobenzene
E_g	Bandgap
E_{HOMO}	Energy level of Highest Occupied Molecular Orbital
E_{LUMO}	Energy level of Lowest Unoccupied Molecular Orbital
EQE	External quantum efficiency
ETL	Electron transporting layer
FRET	Förster resonant energy transfer
FTPS	Fourier Transform Photocurrent Spectroscopy
GaOHPc	Hydroxygallium phthalocyanine
HOMO	Highest occupied molecular orbital

$(3HS)_2SiPc$	Silicon phthalocyanine bis(trihexylsilyloxide
3HS-BsubPc	Tri-n-hexylsilyl oxide boron subphthalocyanine
(3HS)2-GePc	Bis(tri-n-hexylsilyl oxide) germanium phthalocyanine
H_2	Hydrogen
HCl	Hydrochloric acid
HTL	Hole transporting layer
ICBA	Indene-C60 bisadduct
IML	Intermediate layer
IPCE	Incident photon to current efficiency
IQE	Internal quantum efficiency
IR	Infrared
ITO	Indium tin oxide
j-V	Current density-voltage
KOH	Potassium hydroxide
LBG	Low band gap
LUMO	Lowest unoccupied molecular orbital
MEH-PPV	Poly[2-methoxy-5-(2'-ethylhexyloxy)-*p*-phenylene vinylene]
MeOH	Methanol
MoO_X	Molybdenum trioxide
N_2	Nitrogen
NaOH	Sodium hydroxide
NCs	Naphthalocyanines
NH_3	Ammonia gas
NIR	Near infrared
OFET	Field-effect transistors
OLED	Organic light-emitting diodes
ODCB	1,2-Dichlorobenzene
OBuOPc	1,4,8,11,15,18,22,25-octabutoxy-29*H*,31*H*phthalocyanine

OPV	Organic photovoltaic
OSC	Organic solar cell
OSCs	Organic solar cells
OXCBA	O-xylenyl C60 bisadduct
OXCMA	O-xylenyl C60 mono-adduct
OXCTA	O-xylenyl C60 trisadduct
P3HT	Poly (3-hexylthiophene-2,5-diyl)
PBHJ	Parallel-linkage BHJ ternary solar cells
PCs	Phthalocyanines
PCBM	[6,6]-Phenyl-C61-Butyric-acid-Methyl ester
$PC_{70}BM$	Phenyl-C71-Butyric-acid-Methyl ester
PCDTBT	Polymer[N-9'-heptadecanyl-2,7-carbazole-alt-5,5-(4,7)-di-2-thienyl-2',1',3'-benzothiadiazole]
PCPDTBT	Poly[2,6-(4,4-bis-(2-ethylhexyl)-4H-cyclopenta[2,1-b;3,4-b'] dithiophene)-alt-4,7(2,1,3-benzothiadiazole)]
PCE	Power conversion efficiency
PcH_2	Hydrogen phthalocyanine
(PDP)2-SiPc	Bis(3-pentadecylphenoxy)-silicon phthalocyanine
PEDOT:PSS	Poly(ethylenedioxythiophene):poly(styrene sulfonic acid)
PHJ	Planar heterojunction
photo-CELIV	Photogenerated charge carrier extraction by linearly increasing voltage
PIA	Steady-state photoinduced absorption
PL	Photoluminescence
Py	Pyrene
PtO_2	Platinum oxide
PV	Perylene tetracarboxylic derivative
PVK	Polyvinylcarbazole
RMS	Root-mean-square

SiPC	Silicon phthalocyanine
SiPcBz	Silicon phthalocyanine bis(tri-benzylsilyl oxide)
SiNC	Silicon naphthalocyanine
SubNc	Boron subnaphthalocyanine chloride
SubPc	Boron subphthalocyanine chloride
SCLC	Space-charge-limited current
TAS	Transient absorption spectroscopy
tBuSiNc	Tert-butyl-functionalized silicon 2,3-naphthalocyanine bis(trihexylsilyloxide)
TEM	Transmission electron microscopy
VB	Valence band
WF	Work function
ZnO	Zinc oxide
ZnPc	Zinc 2,3,9,10,16,17,23,24-octakis(octyloxy)-29*H*,31*H*-phthalocyanine

Symbols

A	Device active area
D	Diffusion coefficient
E_{CT}	Charge-transfer state energy
Eff.	Efficiency
E_{gap}	Energy difference between the HOMO of the electron donor and the LUMO of the electron acceptor
E_{ox}	Oxidation potential
E_{red}	Reduction potential
F_C	Ferrocene
FF	Fill factor
f_D	Normalized P3HT emission
G_{max}	Maximum generation rate of free charge carriers
I	Light intensity
J	Dipole moment
J_l	Current density under illumination at 100 mW cm^{-2}
J_d	Current density under illumination at 100 mW cm^{-2} and in the dark
J_{MPP}	Current density at the point of maximum power output
J_o	Reverse saturation current
J_{ph}	Photocurrent density
J_{SC}	Short-circuit current
k	Boltzmann constant
k^2	Dipole orientation factor
L	Active layer thickness
M_n	Number average molecular weight
M_w	Weight average molecular weight
n	Refractive index of the medium
N_A	Avogadro’s number

P_{in}	Power of the solar radiation incident on the cell
PCE	Power conversion efficiency
q	Electronic charge
Q_0	Photoluminescence quantum efficiency
ω_C	Wetting coefficient
R	Resistance
T	Transmission
U	Applied voltage
V_{eff}	Effective voltage
V_{MPP}	Voltage at the point of maximum power output
V_{OC}	Open-circuit voltage
V_0	Compensation voltage
λmax	Absorption maxima
ε	Dielectric constant
ε_A	Molar extinction coefficient
μ	Charge carrier mobility
λ	Reorganization energy
θ	Contact angle
Δ	Activation energy

Contents

Chapter 1

General Introduction

Abstract

This chapter will discuss what is currently known about bulk heterojunction (BHJ) polymer: fullerene organic solar cells. The architectures and working principles of organic solar cells will be introduced in detail. Furthermore, the concept of organic ternary solar cells will also be introduced and give insight to the fundamental principles in detail.

1.1 Introduction

In the 21st century, due to limited coal, oil and other fossil energy reserves as well as continued high prices, coupled with the human understanding of the dangers of greenhouse gas emissions and their increasing demanding, it needs more attention on new energy to replace traditional energy step by step.[1] Compared with conventional coal, oil and natural gas, wind, solar, biomass and other new energies have the advantages of clean and renewable benefits. Solar energy gets more and more attention among these new energy technologies because of its benefits, such as inexhaustible, safe and risk-free, suitable for wide application and so on. Although solar energy is one of the cleanest energy resources, it is still viewed as one of the most expensive types of renewable energy.[2] Nowadays, most commercialized solar cells are based on silicon and other inorganic semiconductor materials. However, their widespread utilization has been limited because of the high cost, high energy consumption and pollution problem during the complex production processes in these inorganic solar cells.

As the next generation solar cells, organic solar cells (OSCs) have been recently attracting more and more attention because of their advantages of low cost, lightweight, roll-to-roll large area and mechanical flexibility.[3-5] OSCs have been greatly improved and expanded in the last decade (See **Figure 1-1**). Early OSCs were made of a single organic layer sandwiched between two electrodes with different work functions. However, the built-in potential of these kind solar cells is often insufficient for exciton dissociation. Hence, they always have low efficiency of <0.1% due to the poor photocurrent generation.[6,7] A breakthrough in the field of OSCs was reported by Tang in 1986.[8] Through using a bilayer heterojunction, the device achieved ≈1% efficiency. In this structure, the donor and acceptor materials are being stacked together. However, in this bilayer structure a rather low device photocurrent can obtain because exciton dissociation can only take place at the donor-acceptor (D-A) interface. Another milestone of OSCs was reached with the introduction of the bulk heterojunction (BHJ) approach by Heeger et al.[9] In BHJ devices, a larger interfacial area compared to the bilayer heterojunction structures is created because the donor and acceptor materials are blended together. Thus exciton dissociation in BHJ is much

better than in bilayers because more excitons can be generated within the exciton diffusion length from an interface. This thesis focuses on such BHJ blends with polymers as donor and fullerenes as acceptor. On the basis of these studies, lots of researchers have developed a variety of high efficiency donor and acceptor materials, resulting in high efficiency. At the same time, there are major developments in device physics and structures, such as inverted solar cells, tandem solar cells, and ternary solar cells and so on. Hence, the prospect of OSCs is very considerable.

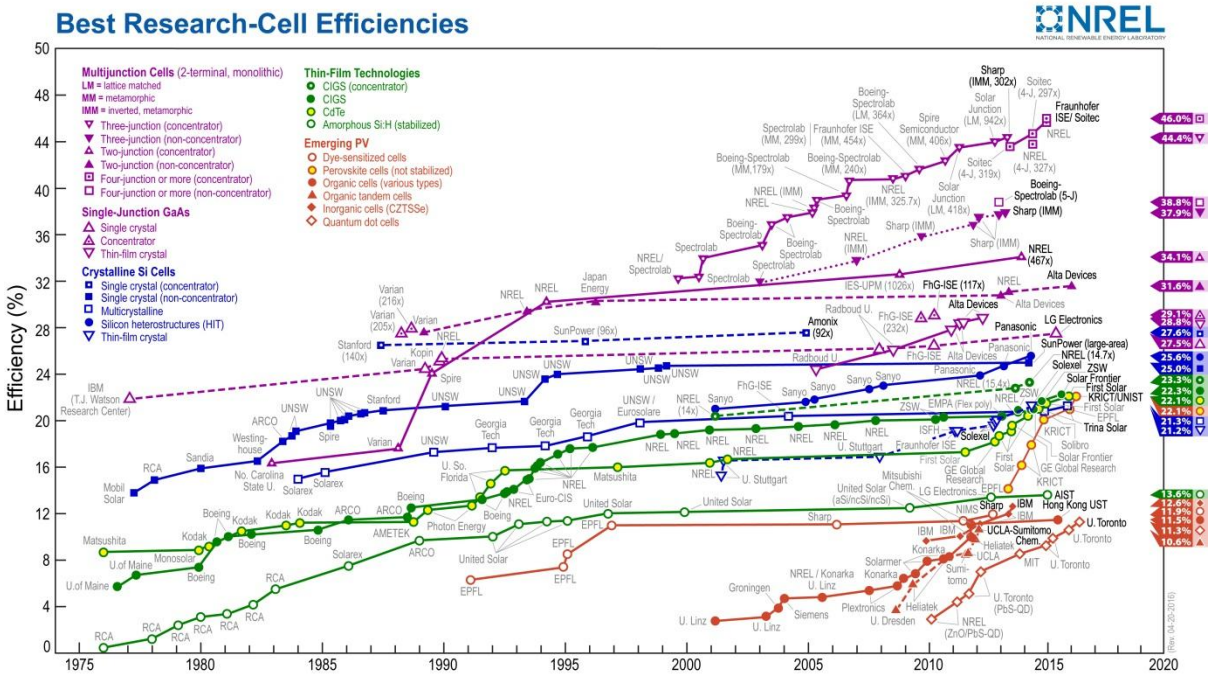

Figure 1-1 Best research-cell Efficiencies summarized by National Renewable Energy Laboratory (NREL).

1.2 Polymer:fullerene OSCs

In 1977, Shirakawa, MacDiarmid and Heeger discovered conjugated polymer with semiconducting properties, which can lead to the development of organic electronics in the fields of organic light-emitting diodes (OLEDs), field-effect transistors (OFETs) and photovoltaics (OPVs).[10] Hence, they were jointly awarded the Nobel Prize in chemistry in 2000 based on their contribution. In an organic semiconductor, the highest occupied molecule

orbital (HOMO) and the lowest unoccupied molecule orbital (LUMO) states in the delocalized π-conjugated system create the valence and the conduction band.[11] Organic solar cells (OSCs) are based on organic semiconductors, such as polymers and small molecules. Among them, bulk-heterojunction OSCs are the most widely applied, which primarily utilize two classes of materials: semiconducting polymers and fullerene derivatives to carry out the photovoltaic process, as shown in **Figure 1-2a**. These thin film OSCs are cast from blended solutions of conjugated polymers and fullerene derivatives. On the other hand, it results in lower manufacturing costs compared to the traditional inorganic counterparts due to it better solubility in common organic solvent. In the end, polymer:fullerene BHJ organic solar cells have received more and more attention as low cost, light weight, and flexible solar cells.[12-14]

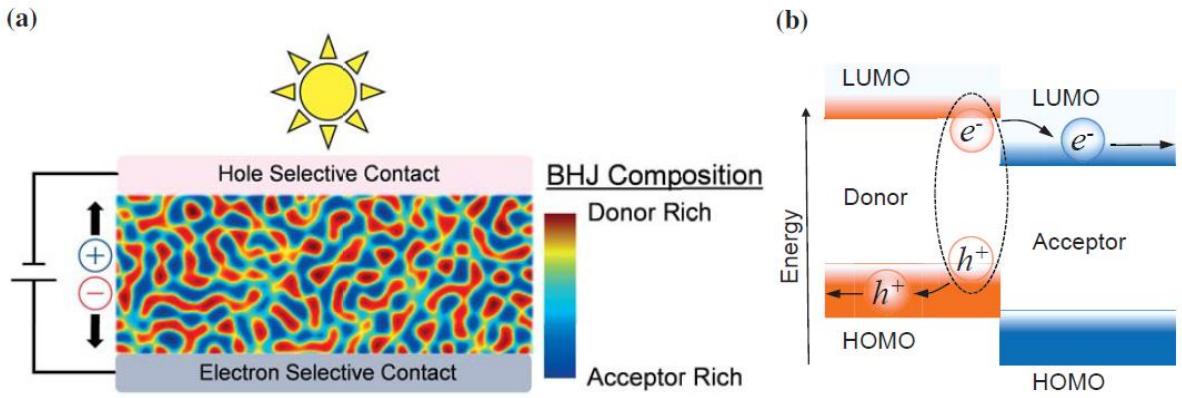

Figure 1-2 (a) An illustration of the simplest possible BHJ solar cells. The active layer is usually around 100nm thick.[15] (b) Schematic process of free carrier photogeneration in the BHJ devices.[16]

Because of their π-conjugated carbon backbone, semiconducting polymers are distinguished from normal polymers. They typically consist of alternating single and double bonds of carbon atoms, which gives rise to unique electrical properties because π-orbital electrons in the double bonds delocalized along the polymer chain.[17] Another characteristic of conjugated polymers is the strong interchain Van der Waals forces through the π-orbitals. Hence, conjugated polymers tend to aggregate in a chain-on-top of chain orientation, named as π-π stacking. Due to interchain π-orbital overlap, these kinds of π-π stacking force will in further lowers the electronic band gap and increases carrier.[16] Fullerene derivatives are the most

promising electron acceptors for polymer-based OSCs due to their high solubility and ability to form appropriate blend morphology for good charge transport.[18-20] Although the pure C_{60} material has a low conductivity with 10^{-7} Scm^{-1}, it can be dramatically enhanced by n-doping. Recently, many of the devices involved donor-acceptor polymers blended with fullerenes create the breaking record efficiencies.

Inorganic solar cells, such as silicon-base solar cells, are manufactured from an inorganic semiconductor. It is doped to form a *p*-*n* junction, which an excess of positive charges (holes) on the *p*-side, and an excess of negative charges (electrons) on the *n*-side. Due to the homojunction between *n* and *p* doped regions, *p*-*n* junction can separate photo generated free charge, and then an electric filed is formed.[21] Compared to these traditional inorganic cells, the mechanisms by converting light energy into electrical energy in OSCs are different. As know, when sunlight is absorbed by an inorganic material such as silicon, free electrons and holes are generated immediately. In organic semiconductors such as polymers, the photogenerated electron-hole pair is electrostatically bound.[22] In order to dissociate excitons into free charges, the most convenient method is to create an interface between materials. To create these interfaces, a semiconducting polymer as "*p*-type" donor material and functionalized fullerene as "*n*-type" electron acceptor material can be used as a good choose. The couple materials are normally blended in solution and then casted into a thin film.[23] After this blending process, these two materials mix intimately to result in more interface area, which creates a typical heterojunction (as shown in **Figure 1-2b**) for splitting excitons.

Polymer:fullerene bulk heterojunction blends, as schematically illustrated above, have yielded OSCs efficiencies exceeded 10% in certain cases.[24-28] In order to use as a potential alternative to inorganic solar cells, further improvements up to 15% or higher are necessary .[29]

1.3 Architectures of polymer:fullerene OSCs

To classify polymer solar cells based on the characteristics of the active layer,[30] they can divided into single cell, planar p-n heterojunction (PHJ) or bilayer cell, bulk heterojunction

(BHJ) cell, and tandem cell.[31] Among of them, the active layer of single cell consists of one single polymer. Because the cell efficiency is too low, it is not necessary to give further discussion in this thesis.

In 1986, C. W. Tang reported a novel photovoltaic cell based on organic thin films consisting of a two-layer structure.[8] The efficiency is up to 1% and lead to uproar. The bilayer solar cell structure is shown in **Figure 1-3**. In this device structure, copper phthalocyanine (CuPC) was used as *p*-type semiconductor and a perylene tetracarboxylic derivative (PV) used as *n*-type semiconductor. They were deposited by conventional vacuum evaporation. At the end, a structure of ITO/CuPC/PV/Ag was fabricated, reaching an efficiency of 1% and FF up to 0.65. *P*-type and *n*-type semiconductors were used as electron donor and acceptor material at the same time. Because of the different energy level of these two materials, exciton generated upon absorption of sunlight separated in the donor and acceptor interface, which is called the donor-accepter bilayer heterojunction cell. In 1992, N. S. Sariciftci et al. reported another successful example on bilayer solar cell.[32] In this work, there was a photoinduced electron transfer process from a conducting polymer MEH-PPV to buckminsterfullerene C_{60}. Under illumination, photo-excitation of donor was formed, and then an electron transferred to the acceptor material. At the same time, photoinduced hole at acceptor transferred to the donor. As a result, the power conversion efficiency (PCE) of the reported MEH-PPV/C_{60} bilayer cell increased more than one order of magnitude compared to the PCE of single layer MEH-PPV cell.

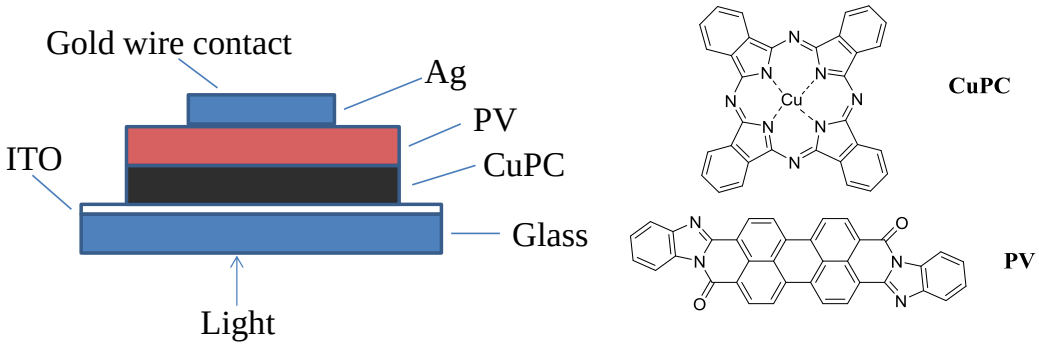

Figure 1-3 Bilayer solar cell structure reported by C.W.Tang.[8]

In bilayer device, one of the advantages is to avoid the problem of controlling the blend morphology because each component of the bilayer can be separately optimized. However, the bilayer devices are limited by the small fraction of excitons that are able to reach the donor/acceptor interface and generate free charge carriers. Although the PCEs of bilayer cell have been greatly improved compared to that of the single layer polymer cell, the separation efficiency of the excitons is still low due to the short exciton diffusion length and exciton lifetime.[33] During the charge transport process, amount of charges outside the donor-acceptor interface recombined, which limits the further improvement of PCEs. In 1995, Gang Yu et al[9] reported MEH-PPV:C_{60} blend structure, in which donor polymer MEH-PPV and acceptor fullerene C_{60} was mixed at a certain ratio. In this blend the distance from any point to donor/acceptor interface is in the nanometer level, which is called bulk heterojunction (BHJ). The formation of this BHJ structure significantly improved the donor/acceptor interface area, and further provided a more adequate place for charge separation. On the other side, the exciton diffusion distance to the donor/acceptor interface was shortened. In short, a larger interfacial area is created during the blending process of donor/acceptor materials, along with bicontinuous D-A nanoscale networks for free charges to be transported to their respective electrodes after separation. At the end, the carrier collection efficiency up to 30% and quantum efficiency reaching to 50~80% were obtained in MEH-PPV:C_{60} BHJ solar cell, yielding a PCE of 3%.

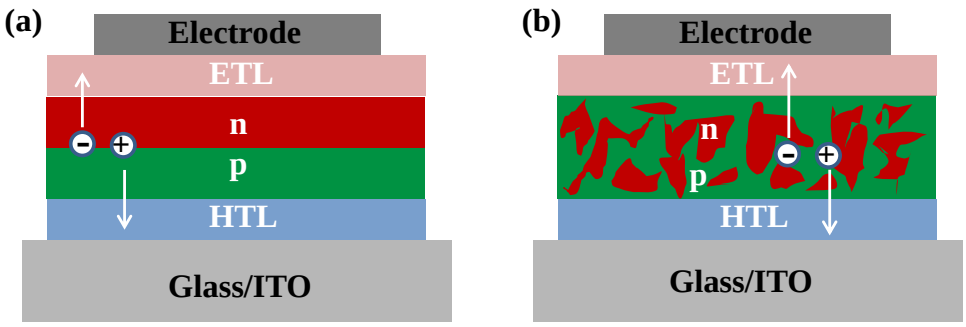

Figure 1-4 Schematic diagram of an OSC with (a) a typical PHJ (bilayer structure) or (b) a BHJ (inter-penetrating network of blended donor and acceptor materials).

In conclusion, donor and acceptor materials can be deposited as two distinct layers: planar p-n bilayer heterojunction known as PHJ and an interpenetration mixture network known as BHJ. As shown in **Figure 1-4**, these two types of layers are sandwiched between two planar electrodes. BHJ has become the standard device structure in organic solar cells because more exciton generated within the exciton diffusion length due to the larger interfacial area in the photoactive layer.

The absorption range of one single polymer based BHJ solar cell is always limited because single donor material cannot effectively absorb photons over the entire range of the solar spectrum. One useful method to improve the absorption range of the polymer is optimizing the chemical structure. Alternatively, the concept of organic tandem solar cell is another efficient way to harvest more photos in solar light effectively. It consists of two or more single cells with complementary absorption bands, and therefore can harvest a greater part of the solar spectrum compared with single junction OSCs. This concept was firstly proposed by Heeger research group.[34] They used an inverted structure with the low band-gap polymer-fullerene composite PCPDTBT/PCBM as the charge-separating layer in the front cell and the high band-gap polymer composite P3HT/PCBM as that in the back cell, as shown in **Figure 1-5a**. Although the tandem device will lose some short circuit current (J_{SC}), open circuit voltage (V_{OC}) has been greatly improved, as shown in **Figure 1-5b**. An the end, the PCPDTBT:PCBM single cell shows J_{SC} =9.2 mA/cm^2, V_{OC} =0.66 V, fill factor (FF) =0.50, and PCE =3.0%; the P3HT:PCBM single cell shows J_{SC} =10.8 mA/cm^2, V_{OC} =0.63 V, FF =0.69, and PCE =4.7%; and the tandem cell shows J_{SC} =7.8 mA/cm^2, V_{OC} =1.24 V, FF =0.67, and PCE =6.5%. Recently, there are lots of papers reported on the tandem device.[35-40] Furthermore, a PCE of 15% was predicted by Brabec et al. that can be achieved for organic tandem solar cells, which is about 1.4 times the maximum efficiency (≈11%) forecasted for single junction organic solar cells.[29]

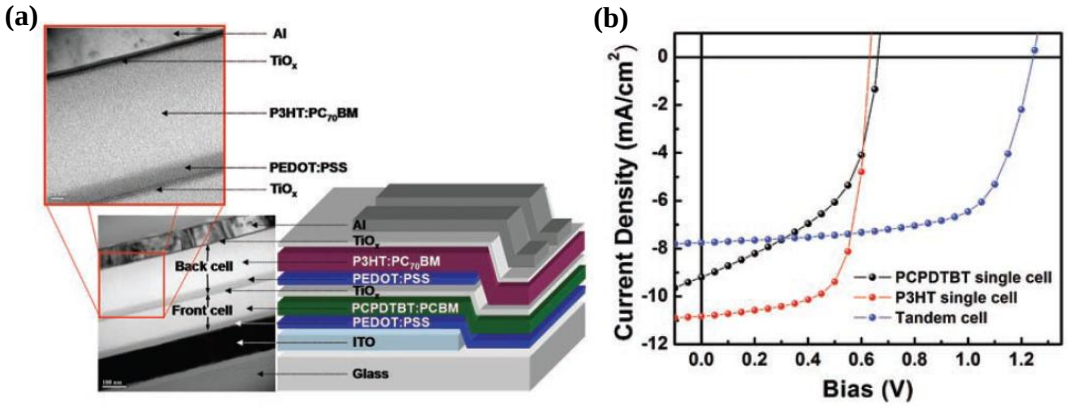

Figure 1-5 (a) The device structure (right) and TEM cross-sectional image (left) of the polymer tandem solar cells. Scale bars, 100 nm (lower image) and 20 nm (upper image). (b) *J-V* characteristics of single cells and tandem cell with PCPDTBT:PCBM and P3HT:PCBM composites under AM1.5G illumination.[34]

In addition to classify polymer solar cells from the characteristics of the active layer, they can also divide into normal device and inverted device. The structures of normal device and inverted device are similar, only the electrode is exactly opposite. For normal device, it always uses ITO as anode, PEDOT:PSS as hole transfer layer (HTL), and low work function (WF) metal as cathode such as Ca or Al. While for the inverted device structure, it always employs high WF metal as anode such as Au or Ag, MoOx as HTL, ITO as cathode, and ZnO as electrode transfer layer (ETL). The schematic diagrams of these two architectures are shown in **Figure 1-6**. As shown, compared to the normal device, the interface layers are switched each other for the inverted device. The life time and stability of the inverted architecture devices are greatly improved because they do not use PEDOT:PSS and low WF metal, which in further reduce the device preparation conditions. For example, we don't need encapsulate the inverted devices and directly characterize them in air because they avoid use of air-sensitive electrodes. Hence, inverted architecture solar cell is an important development direction in the field of polymer:fullerene solar cell industry in future.

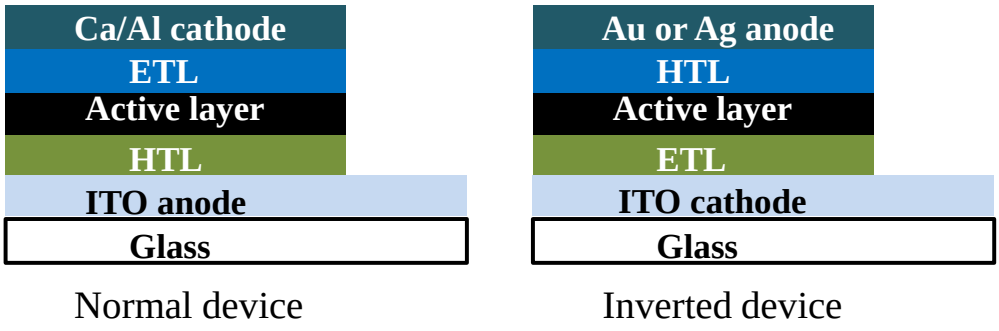

Figure 1-6 The schematic diagram of an OSC with normal and inverted solar cell devices.

1.4 Working principles of polymer:fullerene OSCs

The working processes in a polymer:fullerene BHJ OSCs are illustrated in **Figure 1-7**. After photon absorption, an electron is promoted to an excited state, usually happening in the donor, which in further forms an exciton tightly bounded by Coulombic interaction. When this exciton diffuses to a D-A interface, electron transfer can take place from donor to acceptor. Because of the low dielectric constant of organic materials, this electron transfer process can result in the formation of a bound polaron pair, rather than free charges as in inorganic semiconductors. Hence, it still needs to overcome the Coulombic interaction in order to fully dissociate this bound polaron pair into free charge carriers or polarons. At the end, these polarons need to be transported to the electrodes for photocurrent generation. In the following, details on the working principles of polymer:fullerene OSCs will be addressed.

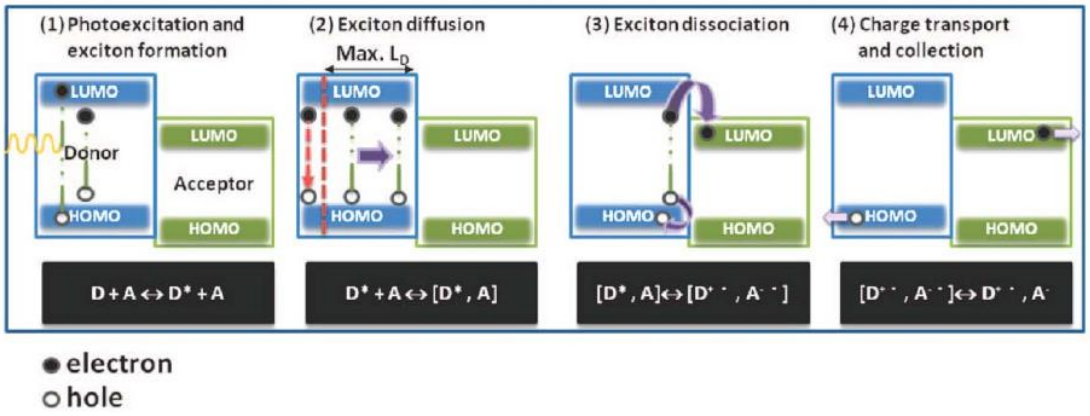

Figure 1-7 Working principles of polymer: fullerene solar cell[41]: (1) Photo excitation and exciton formation; (2) Exciton diffusion; (3) Exciton dissociation; (4) Charge transport and collection.

1.4.1 Photo excitation and formation

After the sun light irradiating onto a solar cell device, only a portion of the light is absorbed, a few partially reflected. As known, only photons with higher energy than the band gap energy of absorbing material can be absorbed, illustration that the lower bandgap materials absorb more photons.[42] When the photons are absorbed by the polymer molecular, they will not immediately separate into free charges as inorganic semiconductor do, due to the low dielectric constant of polymer (typically ε~2-4) compared to silicon (ε~12) in conventional inorganic solar cells.[43-45] As a result, photo excitation in OSCSs often generates excitons with high binding energy rather than free charges, which is named as bound electron-hole pairs. This process consists of light absorption, determining the maximum sunlight energy obtained by the solar device. Both the absorption spectrum and coefficient of the polymer are the important physical parameters to determine how much sunlight can be absorbed. Therefore, to improve the absorption spectra of the polymer, enhancing the absorption coefficient is the first step to improve the efficiency of polymer solar cells.

1.4.2 Exciton diffusion

In many bulk heterojunction devices, it still may not produce good photocurrent generation because the photo generated exciton quenching can be quite efficient.[43,46] This is frequently attributed to geminate recombination of the bound polaron pair after exciton quenching, which is a significant loss mechanism limiting the charge generation yield.[47-50] In order to allow efficient exciton dissociation, the exciton must transport to the D/A interface, which is usually described as diffusion process. Normally, the lifetime of exciton is around a scale of nanoseconds, following by photoluminescence (PL) decay path.[51] The exciton diffusion length is defined as the distance which an exciton can travel before recombination, and it is an important parameter affecting charge generation in OSCs.[33,52-54] Normally the values are

very short.[55] For example, exciton diffusion lengths are in the range of 5-10 nm for polymer materials. The exciton is likely to recombine if it cannot reach in the D/A interface within this diffusion length. Amount of excitons generated will recombine, resulting in low exciton dissociation efficiency.

Therefore, it is necessary to increase the capability of the exciton transferring to the D/A interface in order to improve the efficiency of polymer solar cells. In this process, improving phase separation of donor and acceptor is the main method to create large interfacial area, so that the exciton can diffuse quickly to the D/A interface for the next exciton dissociation process.

1.4.3 Exciton dissociation

After the exciton diffuses to the D/A interface, dissociation of the tightly bound electron-hole pairs needs to take place. Excess energy is required to overcome the Coulomb binding energy in order to separate this polaron pair into free charge carriers. The difference in electron affinities between the donor and acceptor at the interface creates a downhill driving energy for exciton dissociation.[32,56,57] If an exciton can reach an interface within its exciton lifetime, electron transfer can occur from the LUMO levels of donor to acceptor. Alternatively, hole transfer can also occur from the HOMO levels of acceptor to donor when a photon is absorbed by the acceptor instead.[58-60] It requires a driving force for both the electron and hole transfer processes to overcome the exciton binding energy. Previous studies suggest that the main driving force is the LUMO energy difference between donor with acceptor. In general this energy difference is at least 0.3-0.5 eV. Recently, it has been widely reported the mechanism for charge separation is not only a one step process via electron or hole transfer. It indicates that after exciton dissociation at D/A interface an intermediate charge transfer (CT) state may cause charge generation.[61] This CT state can be considered to be an intermediated species between a tightly bounded exciton and fully dissociated free charges. The study of CT indicates that the driving force needed in charge separation process may be less than 0.3-0.5 eV.

1.4.4 Charge transport and collection

In the next step, the separated holes and electrons have to transport along the corresponding materials to the respective electrodes. Electrons transport through the acceptor continuous phase network, while holes transport through the donor continuous phase network. In this process, the charges would be trapped due to the presence of a phase discontinuity or defect. As a result, they are unable to reach the electrode. On the other hand, charge carrier recombination can also occur during the transport process of the electrons and holes in the active layer. This can be caused by the surface traps, unsuitable contact between the active layer and collecting electrodes, and extraction of a charge carrier at the wrong electrode.[51] All these processes are called non-geminate recombination.

The charge transport efficiency is normally quantified by the material mobility μ. Meanwhile, in order to achieve efficient charge carrier transport in the active layer, balanced electron and hole mobilities are normally desired. If the difference between the electron and hole mobility is large than 2-3 orders of magnitude, the space-charge effects will become significant, which is not good.[62] After the charge carriers transport to the active layer/electrode interface, they can finally be extracted from the device in order to yield a photocurrent.

In summary, understanding these four physical processes of working principles in polymer:fullerene organic solar cells, we can study the exact methods to improve efficiency of polymer solar cells. For instance, enhancing the sunlight absorption of the active layer, improving the morphology of the active layer to increase the efficiency of exciton diffusion, optimizing the energy difference between polymer donor and acceptor, improving and balancing the carrier mobilities of polymer donor and acceptor and so on, ultimately improves the efficiency of polymer solar cells.

1.5 Characterization of polymer:fullerene OSCs

There are a variety of methods used to characterize organic solar cells. The performance of a photovoltaic device is based on its ability to convert incident light into electric current, and is

typically assessed with a current-voltage (*J-V*) curve. The *J-V* curve is used to investigate the properties of a solar cell, and provides the necessary information needed to calculate the power conversion efficiency of the device.

J-V curve is usually collected under Air Mass 1.5 (AM 1.5) illumination. Air Mass is a standardized spectrum of light to tell us how much atmosphere sunlight must travel through before it reaches the surface of the earth. Due to the photon absorption by molecules in the air, it is very important to specify this value because the spectrum of sunlight changes as it passes through the atmosphere. AM 1.5 standardized testing procedures are necessary for accurate comparison and authentication of results by different research group. This value only describes the spectrum of light, so solar cells are commonly measured at a fixed intensity of 100 mW/cm^2.[22]

The *J-V* curves of a solar cell in the dark and under illumination are shown in **Figure 1-8**. There are various parameters used to determine the power conversion efficiency (PCE) of a photovoltaic device, such as open circuit voltage (V_{OC}), short circuit current (J_{SC}) and fill factor (FF).

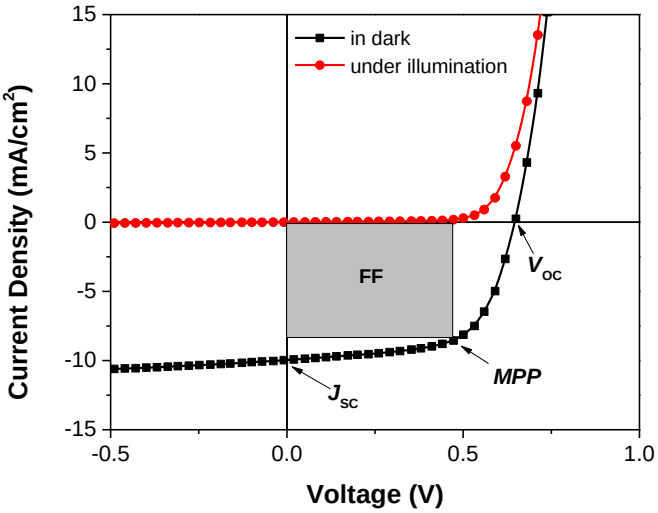

Figure 1-8 *J-V* characteristics of an organic solar cell under dark and illumination.

Open circuit voltage (V_{OC})

The open circuit voltage (V_{OC}) is the maximum voltage across the illuminate device when the short circuit current density output is 0. In BHJ polymer:fullerene OSCs, the maximum possible V_{OC} is set by the energy level difference between the HOMO level of the donor polymer and LUMO level of the acceptor fullerene.[63] At the same time, it is also rather insensitive to variation in the work function of the negative electrode.[64] However, theoretical V_{OC} is never achieved because some V_{OC} losses always occur. For example, bimolecular recombination of charge carrier will cause the V_{OC} loss in organic solar cells.[65]

Short circuit current density (J_{SC})

The short circuit current is the current produced by the illuminated device when there is no voltage. Since there is no external load on the circuit, it represents the number of charge carriers that are generated and eventually collected at the electrodes. It is a function of the amount of light absorbed by the photovoltaic materials and the efficiency of the photos converting into charges.[63] Short circuit current is typically reported short circuit density (J_{SC}), taking into account the area of the device. The primary J_{SC} limiting factor in organic solar cells is the mismatch between the absorption profile of material and the solar spectrum if morphology of the film is favorable to facility charge transport to the electrodes. A useful method to increase light absorption is increasing the thickness of the active layer, but it only works at the beginning. Further increasing the active layer thickness will cause bad effect because of the limited charge mobilities of the polymer and fullerene.

Fill factor (FF)

The fill factor (FF) is the ratio of the maximum power output of a solar cells to its theoretical maximum output.[63] The formula of FF is defined as following,

$$FF = \frac{J_{MPP}V_{MPP}}{J_{SC}V_{OC}} \qquad (1\text{-}1)$$

Where J_{MPP} and V_{MPP} are the current density and voltage at the point of maximum power output, respectively. As shown in **Figure 1-8**, FF is equivalent to the area of the shaded

rectangle divided by the area of the larger rectangle (whose edges intersect the V_{OC} and J_{SC}). High series resistance and/or low shunt resistance within the device can lead to a low FF.

Power conversion efficiency (PCE)

The power conversion efficiency (PCE) is the ratio of the photogenerated power output to incident light input.[63] It represents the efficiency of the solar cell and can be calculated from a *J-V* curve by,

$$PCE = \frac{J_{MPP}V_{MPP}}{P_{in}} = \frac{J_{SC}V_{OC}FF}{P_{in}} \quad (1\text{-}2)$$

Where P_{in} is power of the solar radiation incident on the cell.

1.6 Requirements for an ideal polymer:fullerene OSCs

To design a high efficiency polymer:fullerene OSC with an optimized J_{SC}, V_{OC} and FF, the following requirements should be fulfilled:

(1) The broaden absorption spectrum range and a high absorption coefficient of the materials to enhance photo harvesting.
(2) Suitable HOMO and LUMO levels, which not only realize the effective charge separation but also ensure adequate V_{OC}.
(3) Polymer donor material should have a high hole mobility, contributing to the transport of the photo-generated carriers.
(4) Ideally, the polymer donor material should have a certain molecular self-assembly capability. If so, an ideal morphology of active layer and superior continuous charge transport networks will be formed through the solution treatment, thermal treatment or additive adding methods.
(5) The high solubility of materials used in organic solar cells is necessary for solution processing. The excellent chemical stability and light stability are also important for commercial applications of OSCs.

1.7 Ternary polymer:fullerene OSCs

In the past few years, although the PCE of organic solar cells has obtained a breakthrough (>10%), it is still lower than that of inorganic solar cells. As known, the narrow absorption profile of organic semiconductor material is the main factor limiting the performance for organic solar cell. In order to overcome this limitation, researchers have followed different strategies from various aspects. For example, one useful method to broaden absorption window is designing and synthesizing various low bandgap polymers, which can further harvest more photons in the near IR region and increase J_{SC}.[66-74] However, it is very difficult to design a single conjugated polymer which can harvest photons effectively from visible to near IR range. Hence, the concept of organic tandem solar cells is proposed using as another alternative way to harvest more photons in solar cells effectively. The tandem solar cell involves stacking two or more cells with complementary absorption spectra in series or parallel connection, which harvests photons at the highest possible potential.[29,35-38,75] Although Brabec et al. predicted that the PCE of organic tandem solar cells could research a value of 15%,[38] there are still lots of disadvantages in organic tandem solar cell. Firstly, it is necessary to make sure the photocurrents generated both top and bottom cells balanced because the overall photocurrent is limited to that in the lower current cell in a series connection. Secondly, although in terms of production cost all solution processed organic tandem solar cells are the most desired, it is not easy to implement it technically. Thirdly, it is necessary to design and optimize a suitable combination of HTL+ETL, so called interlayer/intermediate layer, between the top and bottom cells in order to guarantee the perfect recombination of the holes+electron extracted from their corresponding active layer within this interlayer/intermediate layer.

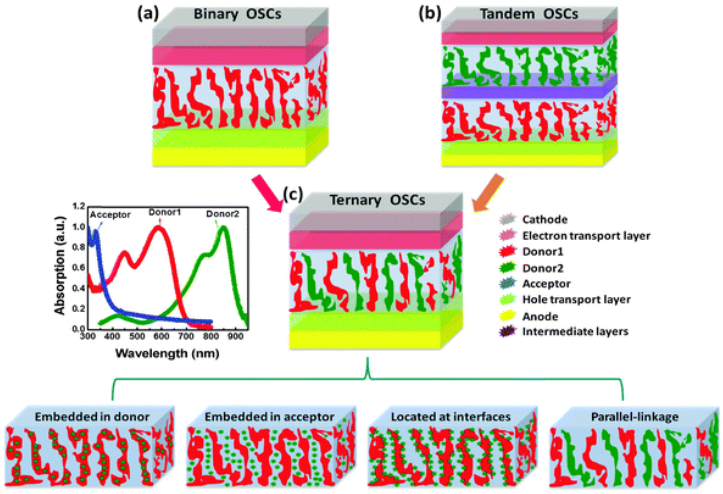

Figure 1-9 The schematic diagram of the (a) binary OSCs, (b) tandem OSCs, and (c) ternary OSCs with four possible active layer morphologies as the location of the third component is different.[76]

In summary, it is very important to develop a useful method to harvest much more photons effectively in a simple structured and simple processed-device. Alternatively, the concept of ternary sensitization cells has been introduced, which uses a third component with different optical properties to act as a second donor or acceptor in BHJ solar cells.[77-88] As shown in **Figure 1-9**, organic ternary solar cells benefit the advantages of both tandem solar cells and single bulk heterojunction solar cells: enhancing light absorption by incorporating multiple organic materials and simplicity of processing conditions.

In general, there are three components in the active layer for a ternary solar cell: the host donor/acceptor (D/A) system and the third component. The third component can be polymer, small molecules, dye and nanoparticle.[89-94] The ternaries are categorized in three main groups based on the function of the third compound: two donors/one acceptor ($D_1/D_2/A$),[95-97] one donor/two acceptor ($D/A_2/A_1$),[98-100] donor/nonvolatile additive/acceptor.[101-103] Compared to a binary solar cell, the mechanisms controlling the photovoltaic behavior in a ternary solar cell are much more complicated because it is affected by many parameters such as the nature and the amount of the sensitizer. Moreover, as shown is **Figure 1-10**, there are four possible fundamental configurations of the active layer classified based on the position of the

sensitizer and its correlation to the other components for a ternary solar cell. These four morphologies include as following: the third component embedded in one donor or acceptor phase, located in the interfaces, forming a parallel-like structure with the primary donor or acceptor, and an alloy with either the donor or acceptor material.

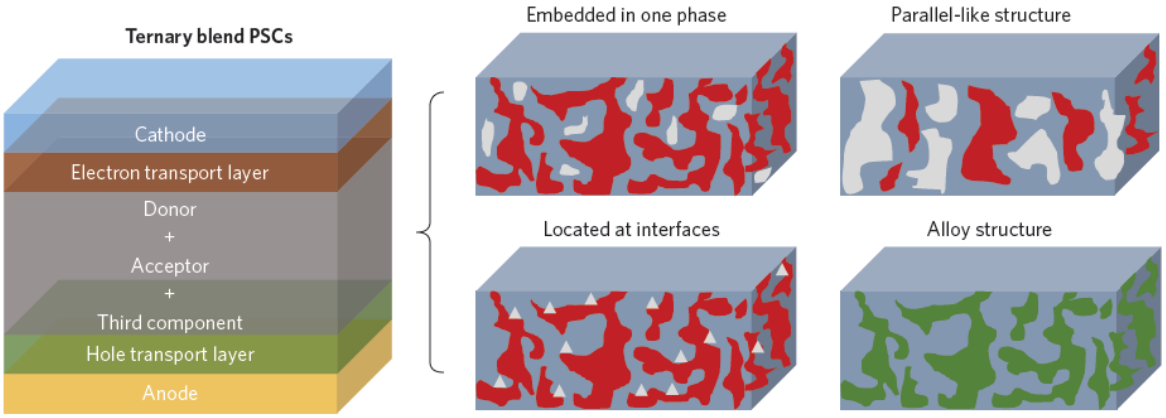

Figure 1-10 Structures of ternary blend BHJ polymer:fullerene solar cells with four possible active layer morphologies.[89]

In ternary solar cells, mainly based on the location of the third component in the ternary active layer, there are three fundamental principles: charge transfer, energy transfer, and parallel-linkage or the alloy model.

1.7.1 Charge transfer

The charge transfer and transport in ternary systems are not a simple superposition of charge transfer and transport properties at all stages. It is determined by the combination of various mechanisms, such as the position of the photosensitive material in the binary host film, electronic energy levels and the bandgap of the three materials, the content of photosensitive material, and the final microstructure of the ternary film. For example, the position of the energy level of the photosensitive material relative to the donor and acceptor levels of the host system determines the exciton dissociation and the possibility of charge transfer at each interface. Locating the HOMO and LUMO level of the third component between the HOMOs and LUMOs of host components (cascade energy level), which can provide several effective

ways for charge transfer and transport. As shown in **Figure 1-11**, in a typical ternary blend, this cascade charge transfer is illustrated. The electron can be transferred from the photo excited host donor to either acceptor or the sensitizer. Subsequently the sensitizer has to transfer an electron to acceptor. And the photo excited sensitizer is alternatively capable of transferring holes to the host donor while transferring electrons to the acceptor. For the charge transfer mechanism, a cascade energy level alignment is useful to reduce the charge transfer barrier, ensuring efficient exciton dissociation and charge transport to the corresponding electrodes.

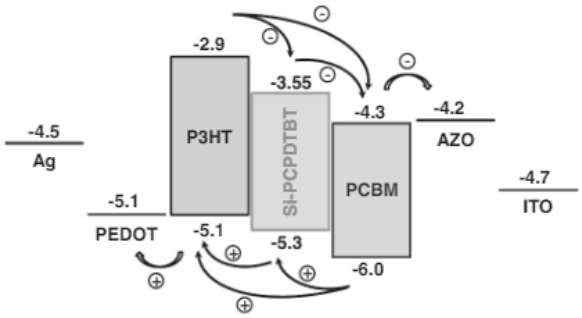

Figure 1-11 Schematic representation of the cascade charge transfer in a ternary solar cell, where the P3HT:PCBM is employed as the host system and Si-PCPDTBT as the near IR sensitizer.[82]

Several methods are used to probe charge transfer happening between different materials. Among them, the widely used method is photoluminescence (PL) measurement. For example, if there is charge transfer occurring between two donors, the PL intensity of one donor would be quenched without increasing the PL intensity of another donor. One the other hand, with the PL intensity of one donor quenching, if the increased PL intensity is observed for the other donor, it indicates that energy transfer exists between these two donors. The charge transfer between P3HT and SMPV1 was investigated by Deng et al. through measuring PL of P3HT:SMPV1 blend films by increasing the SMPV1 content.[104] As shown in **Figure 1-12a**, the PL emission intensities of both the pristine P3HT and SMPV1 films are reduced when mixing them together. By increasing SMPV1 doping ratios in donors, the PL intensities of those two donors quench more. This trend indicated that charge transfer happening between P3HT and SMPV1. At the same time, they also proposed another useful method to verify the

charge transfer by investigating the *J-V* curves of solar cells. Without the acceptor, three solar cell devices base on different active layers: pristine P3HT based device, pristine SMPV1 based device, and P3HT:SMPV1 (1:1) blend device were fabricated. As shown in **Figure 1-12b**, the current density of the solar cells with P3HT:SMPV1 (1:1) blend device is much larger than that of P3HT based and SMPV1 based devices, which should be due to the effective charge transfer between P3HT and SMPV1.

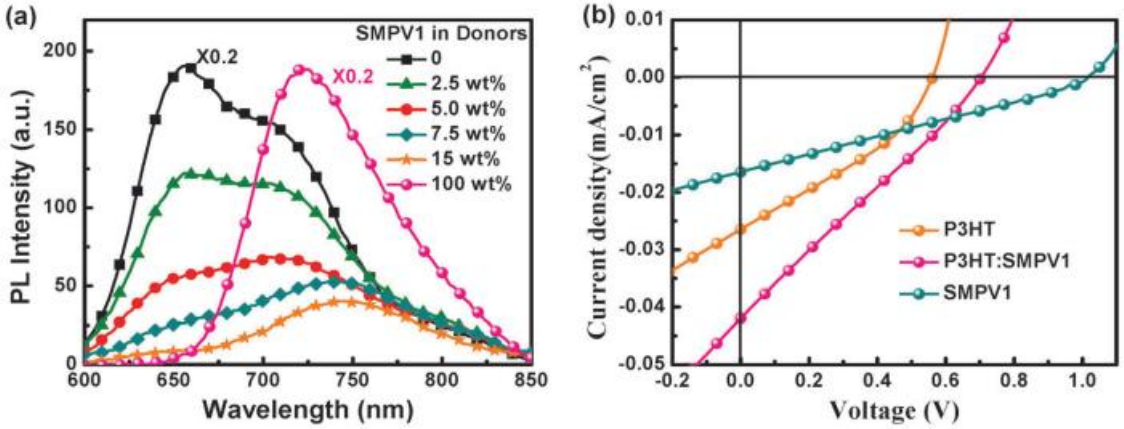

Figure 1-12 (a) PL spectra of P3HT:SMPV1 films with different contents of SMPV1 by exciting all films at 490 nm wavelength; (b) *J-V* curves of OSCs with P3HT, SMPV1, and P3HT:SMPV1 as active layers under AM 1.5 illumination at 100 mW cm^{-2}.[104]

Through steady-state photoinduced absorption (PIA) measurement, Koppe et al. investigated the charge carrier dynamics in ternary solar cells by employing the P3HT:PCBM blend as the host matrix and the low band gap polymer PCPDTBT as the near IR sensitizer.[79] As shown in **Figure 1-13**, the PCPDTBT radical cations are formed when exciting the PCPDTBT/PCBM films under the pump energy of 1.59 eV, while P3HT/PCBM films cannot be excited by 1.59 eV. Exciting the film at 2.33 eV resulted in the typical polaron peak of P3HT at 1.25 eV. Interesting, exciting P3HT/PCPDTBT/PCBM (0.8/0.2/1) film under the pump energy of 1.59 eV yielded a pronounced absorption peak at around 1.25 eV, which suggested that P3HT polaron is generated by photo excitation of PCPDTBT. These observations indicated that there is a hole transfer from PCPDTBT to P3HT in ternary solar cells.

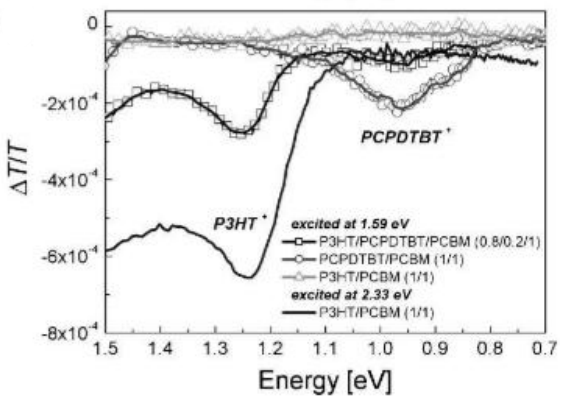

Figure 1-13 PIA spectra of annealed thin film of P3HT/PCPDTBT/PCBM (0.8/0.2/1), PCPDTBT/PCBM (1/1) and P3HT/PCBM (1/1), which were all excited at 1.59 eV. P3HT/PCBM (1/1), excited at 2.33 eV, serves as a reference for the spectroscopic position of the P3HT polaron.[79]

1.7.2 Energy transfer

Compared with the charge transfer, the energy transfer in ternary blend films should be a completing process among the materials. It is known that there are several energy transfer mechanisms including Förster (Fluorescence) resonance energy transfer, resonance energy transfer and electric energy transfer.[83] Substantial overlapping of the one material emission spectrum and the other material absorption spectrum is the necessary condition for an efficient energy transfer, as shown in **Figure 1-14**. But the overlap of these two spectra is not sufficient for the energy transfer to happen. Lu et al. verified that although the absorption of the primary donor polymer showed enough overlap with the emission of the third component, while at the end the dominating mechanism for ternary solar cells is charge transfer but not energy transfer.[105]

In the ternary solar cells, the third component could be the “energy donor” or the “energy acceptor”. Due to the limited radius of energy transfer, it required that the location of the “energy donor” is required to be close to the “energy acceptor”.

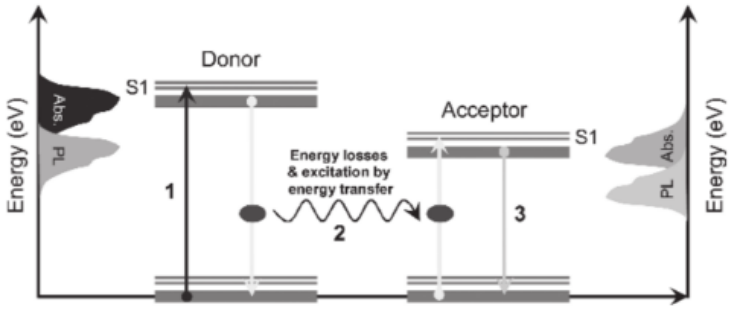

Figure 1-14 Schematic representation of the resonant energy transfer mechanism, as donor absorbs light (arrow 1) and transfer the energy to acceptor (arrow 2), which fluoresces (arrow 3). The abbreviation of Abs. and PL represent the absorption and photoluminescence spectra of the donor and acceptor, respectively.[83]

Figure 1-15 illustrates the schematic of the energy transfer in ternary solar cells with the third component (D_2 or A_2) as an "energy acceptor".[76] Lots of examples are used to study energy transfer pathway based on the $D_1/D_2/A$ ternary solar cell system, exciton energy in D_1 can be transferred to D_2 via Förster resonance energy transfer, as shown in **Figure 1-15a**. The energy transfer can also happen in $D/A_2/A_1$ ternary system. Cnops et al. fabricated a series of planar BHJ solar cells with α-sexithiophene (α-6T) as a donor and both boron subnaphthalocyanine chloride (SubNc) and boron subphthalocyanine chloride (SubPc) as acceptors.[106] The SubNc layer can serves as an energy acceptor for excitons generated in the SubPc layer, as shown in **Figure 1-15b**.

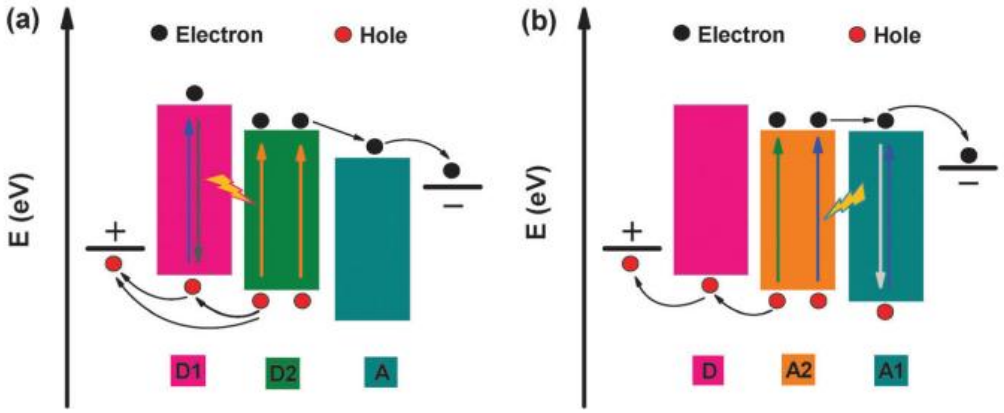

Figure 1-15 Schematic of the energy transfer in ternary OSCs based on (a) $D_1/D_2/A$ and (b) $D/A_2/A_1$ system, the lightning bolts indicate the potential energy transfer pathway, and the arrows indicate the possible charge transfer and transport pathway.[76]

It can distinguish the energy transfer and charge transfer between two materials by measuring the PL spectra of their blends or individual pristine. As shown in **Figure 1-16**, the PL spectra of P3HT:SQ blends by increasing the amount of SQ doping ratios are measured to verify the energy transfer between P3HT and SQ molecules.[107] Under exciting all blends at 490 nm, the PL intensity of P3HT significantly decreased while SQ emission intensity continuously increased when increasing the amount of SQ doping ratios. In fact, the PL intensity of pristine SQ is very weak. The relatively strong emission intensity of SQ region in blend cases should be attributed to the efficient energy transfer from P3HT to SQ molecules.

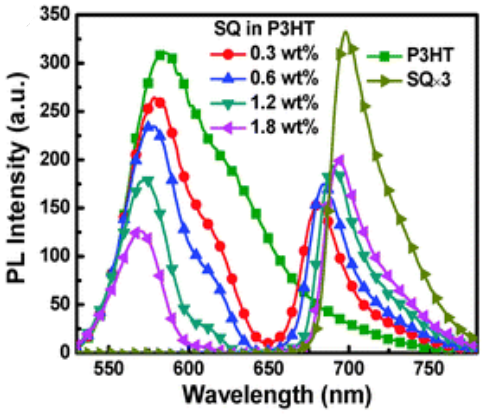

Figure 1-16 PL spectra of pristine P3HT, pristine SQ, and P3HT:SQ blends with different SQ doping ratios under 490 nm light excitation.[107]

1.7.3 Parallel-linkage or the alloy model

Alternative to the charge transfer and energy transfer mechanisms, parallel-linkage mechanism do not require some conditions, such as accurate engineering of locations, band gaps and energy levels of all involved materials. For the same system of D_1:D_2:A, the excitons form in each individual donor domain. Then they diffuse to the interface of the domain:A and dissociate to free charges. **Figure 1-17** presents a typical D_1:D_2:A ternary solar

cells with the parallel-linkage mechanism, where polymer 1 and polymer 2 are employed as the complementary absorbers.[83] The excitons generated in each individual polymer domain will migrate to the respective polymer/acceptor interface and then dissociated into free electrons and holes. Subsequently, these generated holes are transported to the anode through their corresponding donor channels. At the same time, the collected electrons are transported to cathode through the acceptor channels, which is the same as normal binary solar cells.

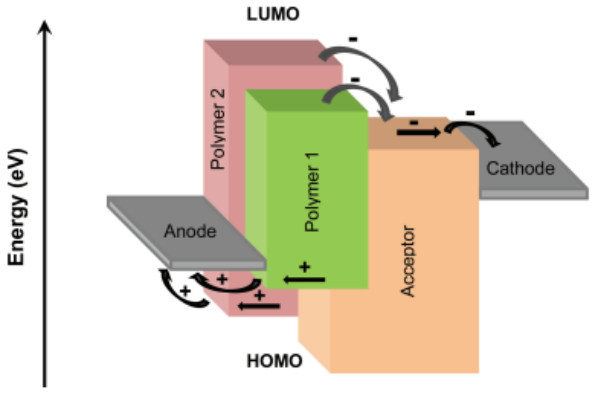

Figure 1-17 Schematic representation of the parallel-linkage mechanism in a ternary solar, with two polymer donors and an acceptor.[83]

The most efficient parallel-linkage BHJ ternary solar cells (PBHJ) to date was reported by Yang et al.[108] Two polymer donors DTffBT and DTPyT with different band gaps and HOMO levels were employed into ternary system at a weight ratio of 0.5:0.5. The solar cells were fabricated according to **Figure 1-18a**. In this PBHJ, free charge carriers travel through their corresponding donor-polymer-linked channels and fullerene-enriched domain to the electrodes, equivalent to a parallel-like connection. As shown in **Figure 1-18b**, the J_{SC} of the PBHJ solar cell (13.5 mA/cm^2) is nearly identical to the sum of those of the individual "subcells" (7.86 and 6.99 mA/cm^2 for DTffBT:PCBM and DTPyT:PCBM, respectively), V_{OC} is between those of the "subcells".

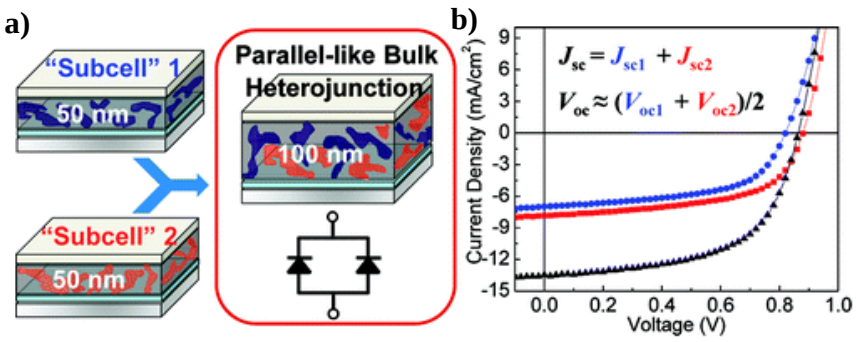

Figure 1-18 (a) Schematic representation of the parallel-like BHJ ternary cell of DTffBT:DTPyT:PCBM and the corresponding binary subcells of DTffBT:PCBM and DTPyT:PCBM. (b) *J*-*V* characteristics of the respective cells.[108]

In some ternary system, either two donors or two acceptors, Thompson et al. proposed another model to explain charge transport with increasing J_{SC} and tuning V_{OC}, named alloy model.[109-112] Different with the parallel-linkage mechanism, which illustrate each component forming its own independent charge carrier transport network, two components used in an alloy model are electronically similar. When they are applied in ternary active layers, it forms an electronic alloy with the same HOMO and LUMO based on the average value of these two components. **Figure 1-19** represents a new charge transfer state, as shown as the rectangle included sparse diagonal. This phenomenon can be attributed to the nature of delocalized intermolecular electrons and holes. In an alloy model ternary system, electronically similar molecules form the same HOMO and LUMO levels instead of each component forming separate channels as a charge pathway. The new HOMO and LUMO energy level values are in between the two corresponding energy levels of two donors or two acceptors, which are very depended on the ratio of these two components. For both the parallel-linkage and alloy model, an increased J_{SC} may be realized in the ternary solar cells.[108,113] The doping ratios of the third component are always very high for efficiently harvesting photons. The similar chemical and physical natures of two donors or two acceptors are necessary for good compatibility when blending them together.

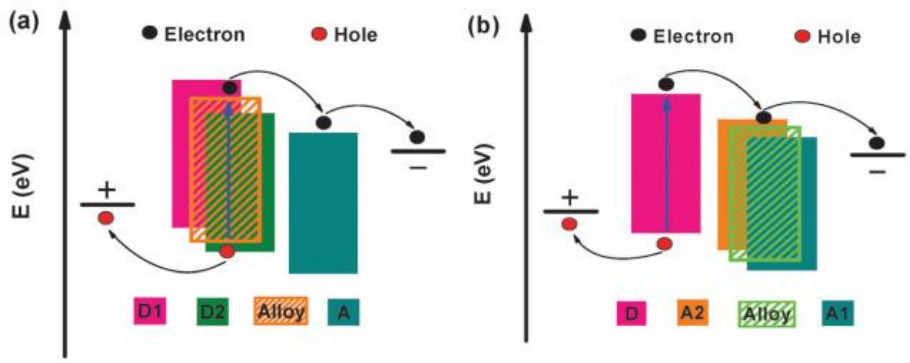

Figure 1-19 Schematic representation of the alloy model in (a) $D_1/D_2/A$ and (b) $D/A_2/A_1$ based ternary solar cells.[76]

As discussed above, the fundamental principles of ternary solar cells, charge transfer, energy transfer, and the parallel-linkage or alloy model, have their own advantages and limitations. They are distinctly different from each other. In one ternary solar cell, there may be not only one mechanism governing the photovoltaic process.

1.8 Outline of this thesis

Chapter 1 gives a background introduction on the organic semiconductors, the evolution, development, working principles and characterization of the polymer:fullerene organic solar cells. Particularly, it gives an introduction on the ternary polymer:fullerene OSCs and describes the aim of this thesis.

Chapter 2 is devoted to give a detail introduction on the fundamental principles of ternary solar cells, and on the key function of the third component in ternary blend systems. Furthermore, it summarizes a brief review on the ternary polymer:phthalocyanine:fullerene OSCs.

Chapter 3 introduces all the materials used in this project. The deposition techniques and processing recipe used in this thesis for device fabrication are discussed in detail. At last, experimental methods used to characterize the devices' performance, their morphology and charge transfer/transport mechanism are introduced.

Chapter 4 prevents the detail synthesis procedures of silicon phthalocyanines and naphthalocyanine by incorporating of four bulky *tert*-butyl substituents to the periphery position and two pyrene groups in the ligand position. The electronic properties are studied by cyclic voltammetry, and the optical properties are studied by UV-*vis* solution absorption.

Chapter 5 describes the implementation of four silicon phthalocyanines (**SiPC-0**, **SiPC-1**, **SiPC-2**, and **SiPC-3**), by varying the alkyl chain length between the PC ring and pyrene ring, into P3HT:PCBM matrix as near IR photosensitizers in ternary blends. The corresponding ternary devices are fabricated. Ternary films and devices both are characterized by employing advance optoelectronic techniques. The relationship between the molecule structures and device performance will also be investigated.

Chapter 6 describes the implementation of the novel silicon naphthalocyanine **SiNC-1** into P3HT:PCBM matrix as near IR photosensitizers in ternary blends. Similarly, the ternary films and devices both are characterized by advance optoelectronic techniques. The charge transfer/transport mechanism is investigated to explain the detailed origin of **SiNC-1** photosensitivity. Furthermore, the quaternary devices are designed and fabricated by introduce **SiPC** and **SiNC** as complementary near IR absorbers to achieve multi-colored dye sensitization.

Chapter 7 describes the implementation of the best silicon phthalocyanine **SiPC-3** into two high efficiency systems of OPV-46:$PC_{70}BM$ and PCDTBT:$PC_{70}BM$. Compared to the P3HT-based systems, the difference between the crystalline polymer ternary systems and amorphous polymer ternary systems by incorporating are investigated and explained.

Chapter 8 summarizes the main achievements of this thesis. Limitations and future challenges of OSCs are supplied as an outlook.

Chapter 2

State of the art

Abstract

This chapter will focus on the introduction of ternary solar cells. The key function of the third component will be presented. Furthermore, this chapter will also discuss some of the recent advances in ternary dye sensitized polymer:phthalocyanine:fullerene organic solar cell research. At the end, the current challenges and aims of this thesis will be illustrated.

Recently, as one of the promising candidates, ternary solar cells exhibit great potential to obtain high performance. As discussed in **Chapter 1**, ternary solar cells enjoy both the enhanced photon harvesting in tandem solar cells and simple fabrication conditions that is used in single BHJ solar cells. At the same time, all the methods used to optimize the performance of single BHJ solar cells can be also applied in ternary solar cells. In order to design a nice ternary solar cell, it not only needs that the third component has a complementary absorption profile with the host system, but also the cascade energy level configurations and balance carrier mobility between electron acceptor and electron donor is required. In a ternary system, the HOMO and LUMO values of each component are important parameters to decide the properties of OSCs. The key parameters, V_{OC}, J_{SC} and FF, can be individually or simultaneously optimized to their maximum values through some experiment methods, such as adjusting the donor or acceptor doping ratios, adjusting phase separation or adopting interfacial layer and so on.

2.1 Key function of the third component

Ternary organic solar cells have certain advantages compared with the traditional binary organic solar cells. By means of reasonable design, a suitable third material is introduced into the host system, and both the energy level and the absorption spectrum of the active layer can be adjusted. The adjustment of the energy level helps to increase the voltage of the organic solar cell, and thus improves the power conversion efficiency of the device. Similarly, the extension of the absorption spectrum of the active layer can increase the capture of the solar photon and further enhance the short circuit current. In addition, the cascade energy level structure can promote the carrier transport. At the same time, the improvement of morphology is beneficial to the exciton dissociation and carrier collection, energy transfer can help exciton dissociation and improve exciton dissociation efficiency. Comprehensive use of these advantages can improve the understanding of mechanism in ternary organic solar cell, which further helps to promote the development of organic solar cells.

2.1.1 Broaden spectrum or enhancing J_{SC}

As the second electron donor, the near IR narrow band gap material can be simply doped into the wide bandgap host system. Hence, the absorption spectrum of the active layer can be extended to the near IR region. This can increase the capture of the solar photon by the more active layer, which further increases the short circuit current J_{SC}.[82,94,114] According to the study of Minnaert et al., the PCE of polymer solar cells can be increased by 35% if the width of the absorption window of the active layer expands from the actual 200 nm to the ideal 400 nm.[115] Gesquiere et al. studied the near IR sensitization phenomenon based on P3HT:PCPDTBT:PCBM ternary organic solar cell systems with increasing doping concentration of PCPDTBT in the host system. **Figure 2-1** showed absorption spectra of active layer films and EQE spectra of the corresponding devices.[94] As observed, the intensity of the absorption spectra at 650-900 nm is gradually increased, and similar phenomena can be seen from the EQE spectra. At the end, the short-circuit current of the solar cell was increased from 10.55 mA/cm^2 to 12.67 mA/ cm^2, and the maximum energy conversion efficiency was up to 3.33%. Koppe et al. also reported the similar work by incorporating PCPDTBT into the dominating P3HT:PCBM system to extend the spectroscopic response into the near IR regions.[79]

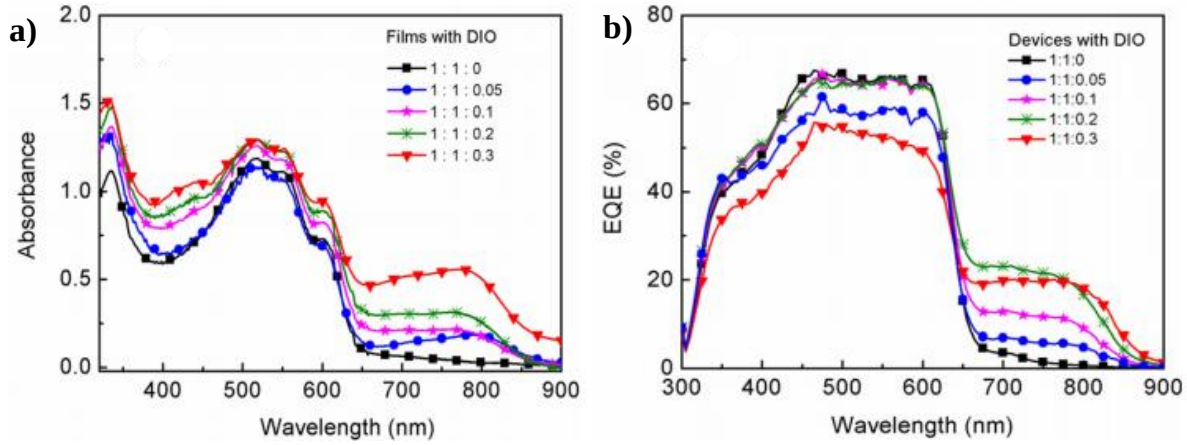

Figure 2-1 (a) Absorption spectra of active layer films and (b) EQE spectra of corresponding devices with various PCPDTBT adding concentration.[94]

Ameri et al. also did a series of studies based on ternary organic solar cells.[82-84,116] As shown in **Figure 2-2**, the addition of Si-PCPDTBT into P3HT:ICBA host system can effectively extend the absorption spectrum of the active layer to the near IR region.[84] As a result, the J_{SC}

of the organic solar cell increased from 7.9 mA/cm^2 to 10 mA/cm^2, and the PCE increased from 3.9% to 5.1% when incorporating Si-PCPDTBT into the P3HT:ICBA system. The response region of the absorption spectra was extended to 850 nm by adding Si-PCPDTBT.

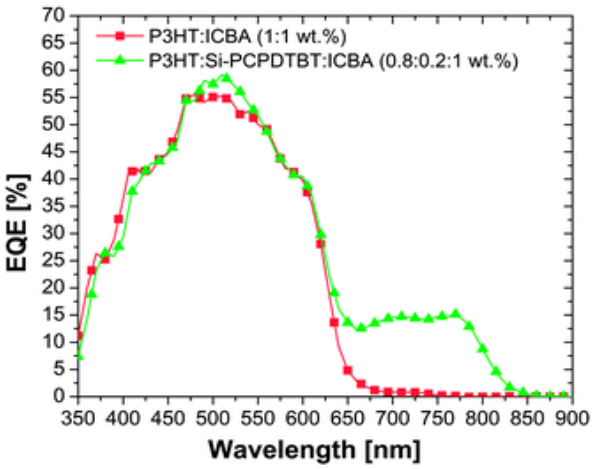

Figure 2-2 EQE spectra of 1:1 wt% P3HT:ICBA (squares) and 0.8:0.2:1 wt% P3HT: Si-PCPDTBT:ICBA (triangles).[84]

2.1.2 Adjusting the energy level or V_{OC}

In a ternary solar cell, it usually includes two donor materials or two acceptor materials. The energy level of active layer changes by adjusting the dual donor or dual acceptor mass ratio, and then adjusts V_{OC} of OSCs.[109,112,117,118] Compared with binary system, the change of V_{OC} in ternary system is very complex, so it is not easy to do projection by simple formula. All parameters deciding the transporting mechanisms in ternary cell, such as the amount of the third component, the locating of sensitizer, band gap of the composing elements, morphology of the active layer and so on, will lead to tune V_{OC} for performance optimization.[104,119]

Park et al. reported that two anthracene-based star-shaped conjugated small molecules, HBantHBT and BantHBT, are used as electron-cascade donor materials by incorporating them into PBTADN:$PC_{70}BM$ based host systems.[120] Through appropriate energy level alignment and optimal domain sizes for charge carrier transfer, it yielded complementary absorption spectra. At the end, the addition of HBantHBT into PBTADN:$PC_{70}BM$ host system caused the V_{OC} increasing from 0.83 V to 0.89 V for the corresponding devices,

leading to a PCE improvement from 3.0% to 4.1%. Meanwhile, the addition of BantHBT yielded a V_{OC} of 0.91 V and PCE of 5.6%, an increasing of 87% compared to the standard device.

Wang et al. also reported a ternary solar cell with dual acceptors, using P3HT as the donor and mixed PCBM and ICBA acceptor.[118] In this ternary system, the proportion of the ICBA and PCBM in acceptor was varied, while the overall proportion of donor (P3HT) to acceptor (ICBA and PCBM) was maintained at 1:1. The relationship between the ratio of PCBM:ICBA and V_{OC} was investigated. As listed in **Table 2-1**, the V_{OC} of organic solar cell improved gradually with increasing the amount of ICBA. Actually, Thompson et al. also demonstrated that the V_{OC} of P3HT/ICBA/PCBM based ternary solar cells can be changed by varying the amount of ICBA in acceptors as well as maintaining high FF and J_{SC}.[109]

Table 2-1 Parameters for the investigated devices.[118]

PCBM:ICBA	V_{oc} (V)	J_{sc} (mA/cm^2)	FF (%)	PCE (%)
1:0	0.667	7.09	70.0	3.31
0.9:0.1	0.679	6.89	68.3	3.20
0.7:0.3	0.700	6.59	67.9	3.13
0.5:0.5	0.721	6.45	67.6	3.14
0.3:0.7	0.743	6.51	65.8	3.18
0.1:0.9	0.834	7.16	68.2	4.07
0:1	0.887	7.52	70.4	4.70

Khlyabich et al. have described an intriguing example to show that the actual situation is much more complex.[109] They fabricated a series of ternary blend solar cells using P3HT as donor and two different fullerene derivatives (PCBM and ICBA) as acceptors. The results showed that if the total amount of acceptors kept constant, the V_{OC} could be varied gradually over the full range in a near-linear fashion by changing the weight ratio of PCBM and ICBA. Kang and coworker, however, observed a different effect.[121] In this study, o-xylenyl C60 mono-adduct (OXCMA) and P3HT are used as host system, using either the o-xylenyl C60 bisadduct (OXCBA) or the o-xylenyl C60 trisadduct (OXCTA) as the second acceptor. As reported, the V_{OC} of the P3HT:OXCMA:OXCTA was increased only by small amount of the second acceptor (W_{OXCTA}<0.3). However, the V_{OC} drastically decreased in higher values of

OXCTA>0.7. The behavior of V_{OC} in this system can be divided into two regimes. In the first regime where the V_{OC} of the system is increasing, the second acceptor has a bridging effect between P3HT and OXCMA. However, by increasing the amount of OXCTA in the system, OXCMA plays as a trap and thus preventing the efficient charge transport and promote the recombination.

There are various factors which have an effect on the V_{OC} in different degrees, such as microstructure, energetic disorder, charge-transfer (CT) state and so on. Actually, in many literatures the effect of CT states on V_{OC} has been reported.[122,123] In polymer:fullerene BHJ solar cell, V_{OC} is determined by the interfacial CT states between polymer and fullerene. Fourier-transform photocurrent spectroscopy (FTPS) and electroluminescence (EL) spectra are used to extract the relevant interfacial molecular parameters. Vandewal et al. reported an analytical expression linking these properties to V_{OC}.[124] According to this study, an analytical expression for V_{OC} as a function of EQE_{EL} and the parameters E_{CT}, λ and f evaluated at short circuit is shown in the formulation of Eq. (2-1).

$$V_{OC} = \frac{E_{CT}}{q} + \frac{kT}{q} ln\left(\frac{J_{SC}h^3c^2}{fq2\pi(E_{CT}-\lambda)}\right) + \frac{kT}{q} ln(EQE_{EL}) \quad (2\text{-}1)$$

Where k is Boltzmann's constant and T is the absolute temperature. E_{CT} is the free-energy difference between the CT complex ground state and the CT excite state and λ is a reorganization energy associated with the CT absorption process. f is related to CT absorption strength. EQE_{EL} is EL external quantum efficiency.

2.1.3 Improving morphology

The morphology of the active layer can be adjusted even when a small amount of the donor material or the acceptor material is incorporated in the host system. For example, the incorporation of the acceptor material has a similar effect as a solvent additive. It results that the distribution of the acceptor material in the host system is more uniform, so the contact area of the donor/acceptor material is increased, and further improving the exciton

dissociation efficiency. The improvement of morphology also helps to enhance the collection of carriers on the electrodes.[125-127]

Lin et al. studied the effect of polyvinylcarbazole (PVK) on the P3HT:ICBA system.[128] ICBA has a trend to diffuse and aggregate into large clusters because it is a highly symmetric molecule. At the end, it results in a huge horizontal phase separation, further leading to a significant drop in PCE. By the addition of PVK into P3HT:ICBA system, it could effectively prevent the clustering of ICBA crystalline molecules, thereby improving the phase separation. As shown in **Figure 2-3**, ICBA molecules are clustered together without doped PVK into the active layer. The interphase network of the bulk heterojunction becomes disordered after PVK is incorporated into the active layer. This avoids the ICBA aggregation into an isolated island and further facilitates the dissociation of excitons.

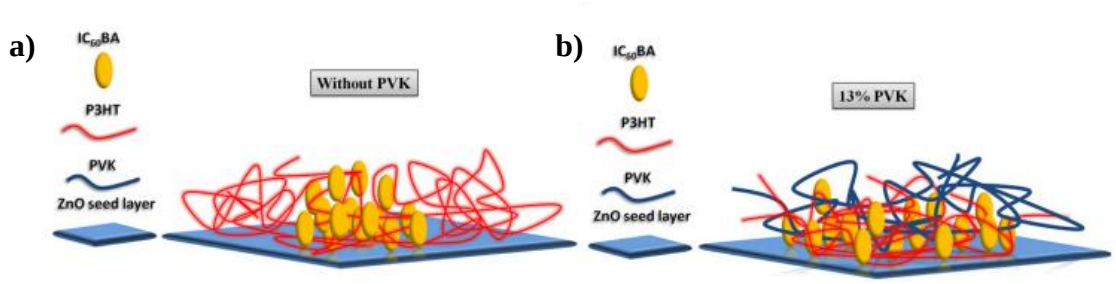

Figure 2-3 Schematic structure of molecular chain distribution in the active layer is blended a) without PVK and b) 13% PVK. Which dispersed ICBA aggregation cluster by the PVK molecular chain.[128]

The effect of a small perylene dye on the performance of organic solar cells based on P3HT:PCBM blends was investigated by Okada et al. **Figure 2-4** illustrated AFM images of P3HT:PCBM blending films with various perylene doping concentration. The surface root-mean-square (RMS) roughness of the film without perylene standard system was 1.58 nm. When increasing the dye doping concentration, the surface roughness of the film decreased gradually. It indicated that doping the proper concentration perylene could make the active layer surface smooth, further increasing the PCE.

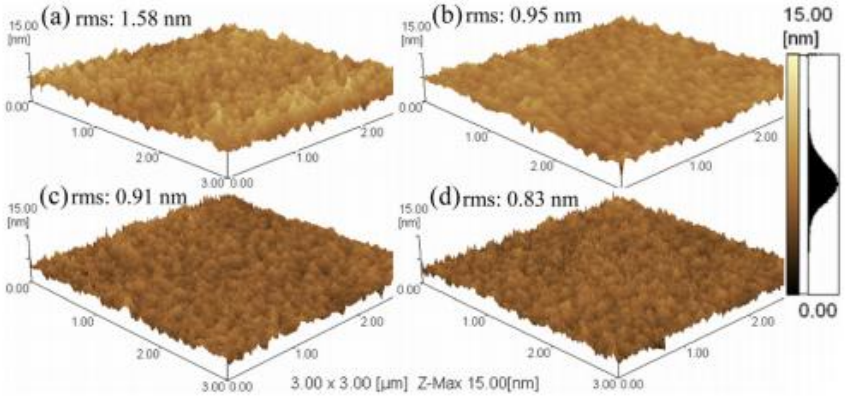

Figure 2-4 AFM images of P3HT:PCBM blending films with various perylene doping concentration.[129]

2.2 A brief review of ternary polymer:phthalocyanine:fullerene OSCs

Over the past few years, there are amount of papers published to investigate the use of phthalocyanines in thin-film polymer:fullerene organic solar cells. The addition of phthalocyanines primarily improved light harvesting to enhance the efficiency of these devices. This section will address the key findings of each study. Device data for each paper has been listed in **Table 2-2** below.

Table 2-2 Device data for ternary polymer:phthalocyanine:fullerene solar cells. Some information is absent as it was not provided in the publications.

Year	D:A	Sensitizer	Thickness (nm)	J_{SC} (mA/cm^2)	V_{OC} (V)	FF	PCE (%)
2006	MEH-PPV: C_{60}	PCH_2	150	0.00027	1.40	0.69	-
2007	P3HT: $C_{61}(CO_2Et)_2$	GaOHPc	200	-	-	-	-
2009	P3HT:PCBM	OBuOPc	-	-	-	-	-
2009	P3HT:PCBM	ZnPc	100	6.2	0.48	0.37	1.1
		$(3HS)_2$-SiPc	100	7.9	0.58	0.59	2.7
2010	P3HT:PCBM	SiPc+SiNc	-	10.9	0.57	0.69	4.3

2010	MEH-PPV:PCBM	CuPc	-	5.04	0.75	0.37	1.41
2011	P3HT:PCBM	CuMePc	-	16.3	0.58	0.56	5.3
2014	P3HT:PCBM	tBuSiNc	220	11.4	0.62	63	4.46
2014	P3HT:PCBM	$(3HS)_2$-SiPc	-	9.84	0.57	0.59	3.29
		$(3HS)_2$-GePc	-	0.62	0.16	0.24	0.03
		$(3HS)_2$-BsubPc	-	9.20	0.55	0.58	2.92
		$(PDP)_2$-SiPc	-	9.49	0.59	0.54	3.02
2015	P3HT:PCBM	$(3HS)_2$-SiPc	220	12.1	0.58	0.62	4.4
		SiPcBz6	220	13.4	0.58	0.60	4.8
		SiPcBz	220	12.0	0.54	0.58	3.8

In 1986, the first heterojunction bilayer device was reported by Tang, using copper phthalocyanine (CuPc) as donor and a perylene derivative as acceptor, reaching a power conversion efficiency of 1%.[8] Thin film devices based on a metal phthalocyanine and fullerene have applied in many fields, such as co-deposited single layer,[130] bilayer,[131] multilayer[132] and gradient deposition[133] devices. All these devices require the complicated processing conditions. For example, all materials used need to be vacuum deposited in high temperature. So it is necessary to develop solution deposited thin film organic solar cells through using conducting polymers and soluble fullerenes. Herein, soluble phthalocyanines are required to incorporate into that architecture, which is the main focus of this literature survey.

Ltaief et al. were the first to introduce a phthalocyanine into a MEH-PPV/C_{60} heterojunction device, and the absorption window of the active layer became broaden because of the photosensitization of phthalocyanine.[134] As shown in **Figure 2-5**, it found that the addition of hydrogen phthalocyanine (PCH_2) to the device could increase the V_{OC}, J_{SC} and FF. Although the relevance of this is questionable considering the very low device efficiency, the width of absorption spectrum increases drastically. They also incorporated the dye coumarin 343 into some devices to achieve a similar outcome. Through photoluminescence (PL) measurements,

they hypothesized that the addition of PcH_2 improved the device properties by extending the spectra response and improving the concentration of photogenerated pairs.

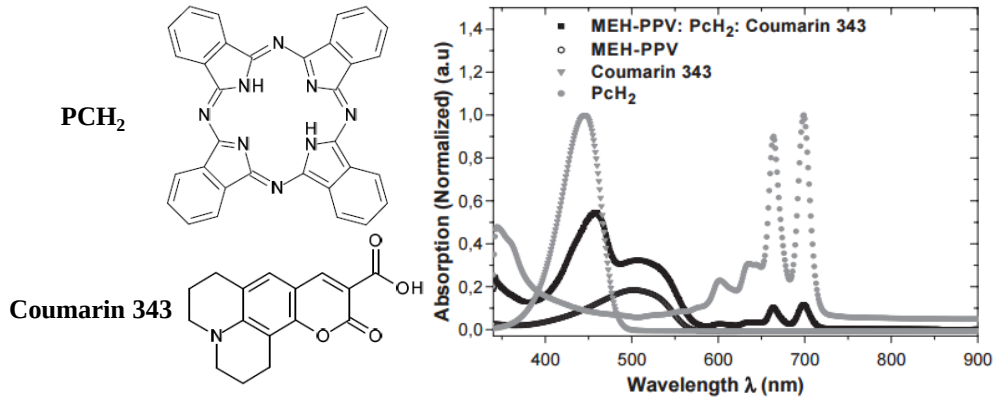

Figure 2-5 The molecular structures of PCH_2 and coumarin 343, and the absorption of the pristine materials and MEH-PPV:PCH_2:Coumarin 343 ternary blend thin film.[134]

Kaulachs et al. attempted to incorporate the electron donating porphyrinoid hydroxygallium phthalocyanine (GaOHPc), as shown in **Figure 2-6**, into P3HT:fullerene based solar cell. It can extend the spectral response of the reference cell into the near IR region.[135] When incorporating this phthalocyanine into P3HT:fullerene matrix, the light absorption window is broaden with a region in the 350–1000 nm because its complementary absorption profile with the host system. However, compared with the GaOHPc CT band at 830 nm, charge carrier photogeneration efficiency was 3 times higher for illumination in P3HT absorption. The highest reported EQE of any ternary device was less than 3%, so there appears to be little benefit in doing so when the performance of the resulting is so poor.

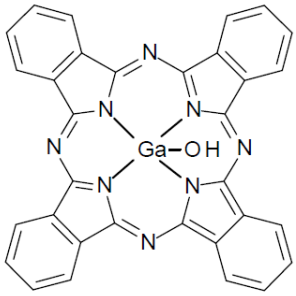

Figure 2-6 Chemical structure of hydroxygallium phthalocyanine (GaOHPc).

Johansson et al. also studied the extending spectral response of a P3HT:PCBM solar cell by utilizing the dye 1,4,8,11,15,18,22,25-octabutoxy-29*H*,31*H*- phthalocyanine (OBuOPc). Compared to a device without such dye sensitization, a photo conversion spectrum extending more than 150 nm toward longer wavelengths was observed.[136] The efficiency of the device was found to be dependent on the concentration of OBuOPc. It displayed an increase in device EQE with only the lowest concentration of 5% OBuOPc, while the device EQE decreased with higher concentrations of up to 33%. The authors reasoned that OBuOPc is unable to transfer charge directly to the electrodes by itself. Transient absorption spectroscopy (TAS) measurements show that after excitation of the OBuOPc there is an electron transfer from the dye to PCBM and a subsequent hole transfer from the dye to P3HT, which results in a long-lived ($P3HT^{+}$/dye/$PCBM^{-}$) charge-separated state, as shown in **Figure 2-7**. It also indicated that the efficiency of hole transfer to P3HT is reduced in blends of higher dye concentration. Thus higher concentration of dye will not improve device performance but rather hinder the charge transport.

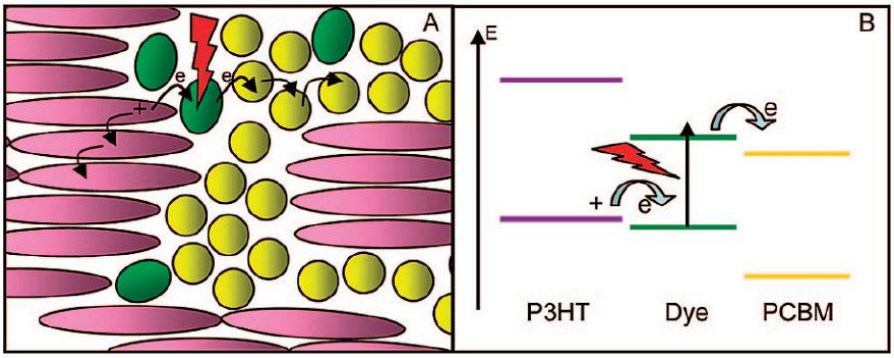

Figure 2-7 Proposed model of charge transfer with the P3HT:dye:PCBM device.[136]

The relationship between device performance and the formation of dye aggregates was studied by Honda et al. through introducing two near IR absorption phthalocyanine dye molecules, zinc 2,3,9,10,16,17,23,24-octakis(octyloxy)-29*H*,31*H*-phthalocyanine (ZnPc) and silicon phthalocyanine bis(trihexylsilyloxide) ($(3HS)_2$-SiPc), into P3HT/PCBM matrix.[137] The molecular structures of these two dyes are shown in **Figure 2-8**. They identified that one major efficiency limiting factor is the propensity of the dye to form aggregates in the film. By testing UV-vis spectra for both the solution and thin film, it observed that the ZnPc

absorption peak was greatly reduced in thin film even the peak was clearly visible in solution. This trend indicated that significant aggregation of ZnPc was occurring. In contrast, the bulky axial ligands on the $(3HS)_2$-SiPc suppress the formation of aggregates within the ternary blend film. As a result, it yielded an improvement in PCE from 2.2% for P3HT:PCBM control solar cell to 2.7% for $(3HS)_2$-SiPc base ternary devices, while the equivalent blend using ZnPc suffered a decrease in performance to 1.1%. Interesting, EQE spectra of the $(3HS)_2$-SiPc ternary blend showed not only a strong peak in $(3HS)_2$-SiPc absorption band, but also an increase from 50% to 60% of the peak associated to P3HT absorption. These findings suggest that there are two origins for the increase in the photocurrent by the introduction of $(3HS)_2$-SiPc. $(3HS)_2$-SiPc serve not only as a light harvesting photosensitizer but also as an energy funnel for P3HT excitons at the P3HT/PCBM interface.

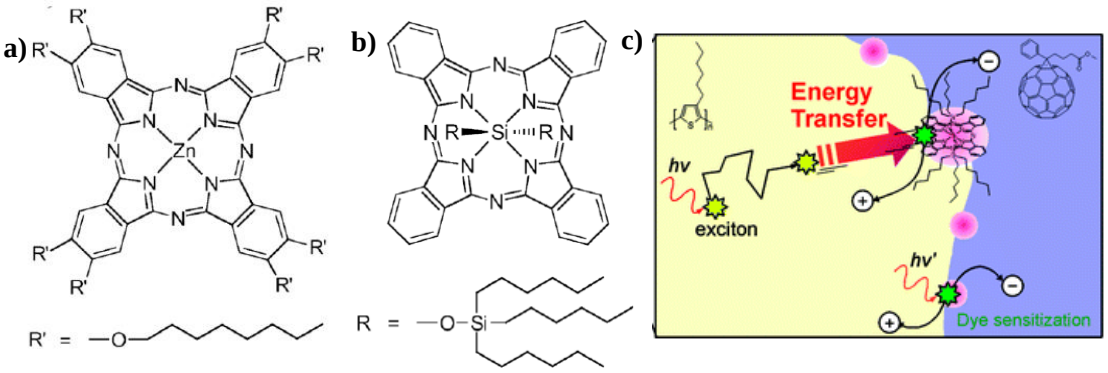

Figure 2-8 The molecular structures of (a) ZnPc and (b) $(3HS)_2$-SiPc, and (c) schematic illustrations of P3HT: $(3HS)_2$-SiPc:PCBM device.[137]

Afterwards, Honda et al. did some more investigations based on silicon phthalocyanine (SiPc) sensitized ternary solar cells using P3HT:PCBM as host system.[138,139] They proposed that SiPc molecules localized in disordered P3HT phases at the interface between P3HT and PCBM rather than in the crystal domains through absorption and surface energy measurements.[138] As identified, surface energy and crystallization of the host matrix are the two driving forces for SiPc locating at the interface: the former is the primary driving force and the latter acts as assistance to the main driving force. They also studied transient

absorption spectroscopy (TAS) to investigate the light harvesting mechanism in P3HT:SiPc:PCBM ternary blends.[139]

In order to harvest more photons in the near IR region, multi-colored dye sensitization using two dyes as co-sensitizers has been demonstrated. These two dyes, SiPc and silicon naphthalocyanine bis(trihexylsilyl oxide) (SiNc), were incorporated into the P3HT/PCBM binary blends because they had complementary absorption bands in the near IR region,.[140] The highest PCE of 4.3 with a J_{SC}=10.9 mA/cm2, V_{OC}=0.57 V and FF=69% was obtained for a P3HT:SiPc:SiNc:PCBM quaternary solar cell. The photocurrent increased by about 10% in the individual ternary blend solar cells and interesting increased by about 20% in the quaternary blend solar cells. **Figure 2-9** showed the quaternary solar cells exhibited two sharp EQE peaks at 670 and 780 nm, corresponding to the absorption of SiPc and SiNc.

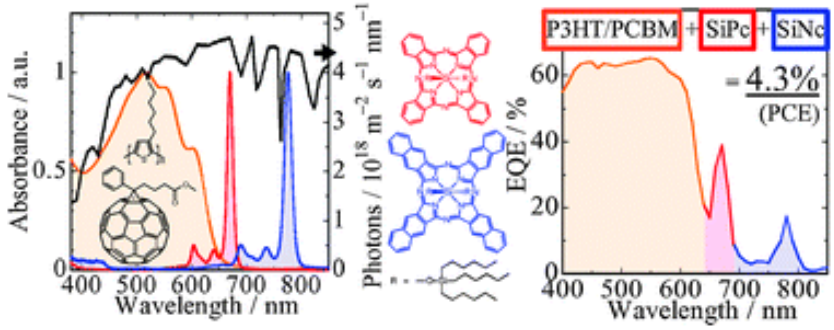

Figure 2-9 The absorption spectra and molecular structures of P3HT:PCBM, SiPc and SiNC, and the EQE spectra of quaternary cell of P3HT:SiPc:SiNc:PCBM.[140]

Chen et al. incorporated 15% (by weight) of dye copper(II) phthalocyanine (CuPc), shown in **Figure 2-10**, into MEH-PPV:PCBM host system as the near IR absorption dye. As a result, it can broad light absorption window because MEH-PPV:PCBM binary control cell does not absorb light at wavelengths longer than 550 nm.[141] The introduction of CuPc yielded an increase of 12% for the efficiency of the device, which they attributed primarily to an increase in J_{SC} through enhanced light absorption. However, it resulted in a decrease in device performance because of the reduced V_{OC} and J_{SC} when the concentration of CuPc beyond 15%. SEM images identified large (>600nm) aggregates of CuPc in ternary blended

films contained 30% CuPc. They also proved that these large CuPc aggregates formed interfacial potential barriers between the polymers, which further hindered charge transport and mobility.

Xu et al. demonstrated the incorporation of tetramethylsubstituted copper(II) phthalocyanine (CuMePc) nanocrystals into the P3HT:PCBM matrix.[142] The molecular structure of this dye is shown in **Figure 2-10**. Two broad absorption peaks at 617 and 708 nm were investigated for the spin-coated film of the CuMePc nanocrystals. Mobility measurements showed that the P3HT:CuMePc composite including identical volumes of P3HT and CuMePc exhibited the high mobility of 2.5×10^{-2} cm^2/Vs, exceeding the mobility of pure P3HT (7.3×10^{-3} cm^2/Vs). Herein, it illustrated best photovoltaic performance with a J_{SC}=16.3 mA/cm2, V_{OC}=0.58 V and FF=56% and a PCE=5.3% for P3HT:CuMePc:PCBM (1:1:2) based ternary solar cell. Compared to the control P3HT:PCBM reference, it resulted in about 40% enhancement. This is due to the higher mobility and the wider absorption of the ternary case.

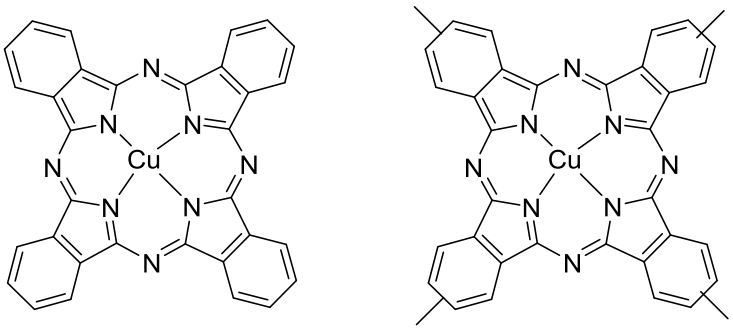

Figure 2-10 The chemical structures of CuPc and CuMePc.

Similarly, a tert-butyl-functionalized silicon 2,3-naphthalocyanine bis(trihexylsilyloxide) (tBuSiNc) dye molecule was incorporated by Lim et al. into P3HT:PCBM host blend BHJ solar cell as a near IR photosensitizer, resulting in increased near IR absorption.[143] Prominently, as shown in **Figure 2-11**, the addition of tBuSiNc yielded more than 150 nm red shift compared to the control binary cell, further resulting an increase of up to 40% in J_{SC} and up to 19% in PCE in photovoltaic devices. It showed that the tert-butyl functionalization enable an increase in the volume fraction of the dye molecule by testing two-dimensional

grazing incidence wide-angle X-ray scattering (2-D GIWAXS). That means large amount of tBuSiNc can be incorporated into host system without destroying the device morphology compared to the unfunctionalized one. This resulted in an increase in the spectral bandwidth of the absorption.

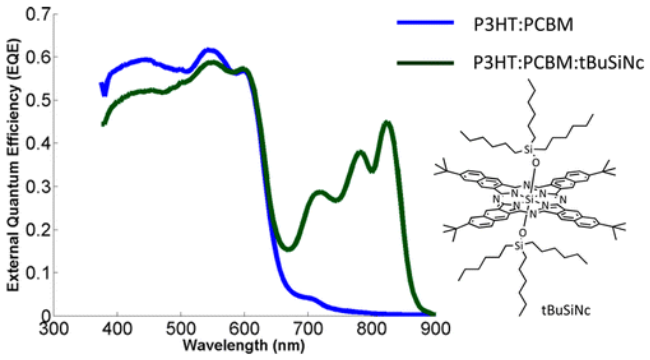

Figure 2-11 EQE spectra of P3HT:PCBM binary and P3HT:PCBM:tBuSiNc ternary solar cells, and the molecular structure of tBuSiNc.[143]

In 2014, Bender et al. explored the molecular characteristic of $(3HS)_2$-SiPc which makes it so effective in increasing the OPV device performance to verify the results of Honda et al.[144] Therefore, similar dyes using different core elements such as germanium and boron, the structures shown in **Figure 2-12**, were synthesized by them. And then the resulting dyes were applied in BHJ OPV devices. It was found that the addition of $(3HS)_2$-GePc resulted in a large decrease in PCE and EQE, and the presence of 3HS-BsubPc resulted in a nonstatistical increase in J_{SC} and PCE. One the other hand, they kept the SiPc core and substituted the tri-n-hexylsilyl soluble groups with pentadecyl phenoxy groups, named $(PDP)_2$-SiPc. The performance of $(PDP)_2$-SiPc based ternary OSCs was worse than that of $(3HS)_2$-SiPc based ternary OSCs. Therefore, $(3HS)_2$-SiPc is a unique additive. During their study, it concludes that tert-n-hexylsilyl substituents offers the necessary solubilizing properties offering case for crystallization for a SiPc when in the solid state, which results in favorable dispersion and charge transfer between the D:A matrix.

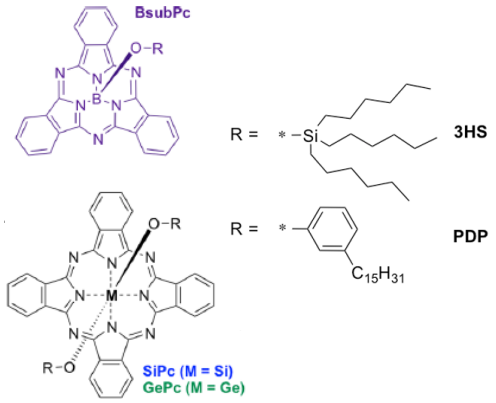

Figure 2-12 The chemical structures of bis(tri-n-hexylsilyl oxide) silicon phthalocyanine ((3HS)2-SiPc), bis(3-pentadecylphenoxy)-silicon phthalocyanine ((PDP)2-SiPc), tri-n-hexylsilyl oxide boron subphthalocyanine (3HS-BsubPc), bis(tri-n-hexylsilyl oxide) germanium phthalocyanine ((3HS)2-GePc).[144]

Xu et al. synthesized heterostructured silicon phthalocyanine derivative (SiPcBz6) as a novel near IR dye and studied interface engineering for this new dye blend ternary polymer solar cells.[145] One axial ligand is tri-n-hexylsiloxy substituent, which is compatible with P3HT with a low surface energy. The other ligand is tri-benzylsiloxy substituent, which is compatible with PCBM with a higher surface energy. For comparison, they also synthesized two other homostructured SiPc molecules, $(3HS)_2$-SiPc and SiPcBz. Because of the compatibility with both materials, SiPcBz6 preferentially located at the P3HT/PCBM interface, which can be loaded up to 15 wt% and hence can boost the photocurrent generation by 30%. However, only 5 wt% for $(3HS)_2$-SiPc and SiPcBz can locate in the interface before destroying the device performance. From EQE spectra shown in **Figure 2-13**, the near IR sensitization for SiPcBz6 is up to 60%, while only 30% for $(3HS)_2$-SiPc and SiPcBz.

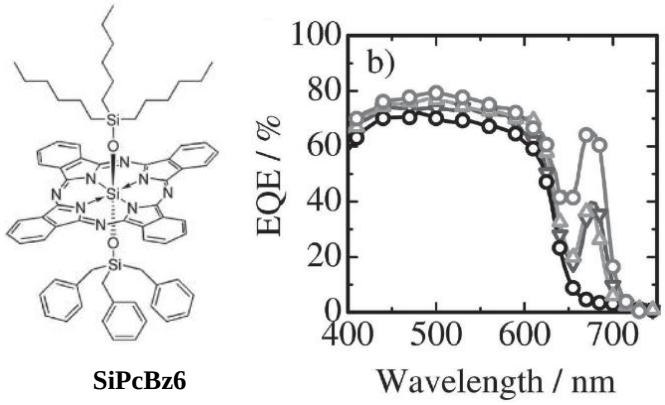

SiPcBz6

Figure 2-13 The chemical structure of SiPcBz6 and EQE spectra of P3HT/PCBM/SiPc ternary solar cells: $(3HS)_2$-SiPc (triangles), SiPcBz6 (gray circles), SiPcBz (inverted triangles), and no dye (black circles).[145]

2.3 Challenges and aims

According to the above discussion, an increasing number of research groups have adopted phthalocyanine/naphthalocyanine materials as third components in polymer:fullerene organic solar cells. However, most of them focus on reporting the improvements for device efficiency by comparing ternary blend device to the binary reference device. The performance of the reported reference devices was often very poor. Thus, even when an improvement has been reported, the effectiveness of the addition of a phthalocyanine material is in many cases questionable. Phthalocyanine compounds, used as a functional near IR sensitizer in OSCs, have been synthesized with a variety of substituents. However, a fundamental understanding of the ternary devices' performance in correlation with morphology and transport mechanism is always absent in some literature. On the other hand, the influence of phthalocyanine engineering on the ternary devices' performance is not studied too much for some publication.

Another challenge is that the addition amount of phthalocyanine/naphthalocyanine materials is always very low. As known, they have a great tendency to form insoluble aggregates because of their planar aromatic structure. This phenomenon not only inhibits the properties presented by phthalocyanine/naphthalocyanine but also produces a side effect on the performance of PCE. One useful method is the functionalization of the molecules.

Hence, this thesis aims to provide a systematic study of the phthalocyanine sensitized ternary blend OSC devices. Firstly, rational design and synthesis of novel phthalocyanine/ naphthalocyanine is done, and afterward the relationship between the molecule structures and their physical and chemical properties is investigated in detail. Secondly, the compounds properties are correlated to the ternary devices' performance and their functionality. Finally, a full-fledged characterization is carried out to get insights into the morphology and charge transfer/transport mechanism of the functional ternary devices. Various factors, such as structural property, miscibility and the suitable energy levels of the third component may influence the microstructure formation and charge transfer/transport in ternary systems.

This thesis seeks to address above mentioned, to better understand this complex field of study, and design high efficiency and reproducible ternary solar cells.

Chapter 3

Materials and Methods

Abstract

This chapter describes the materials, solar cells preparation, and device structures using in this thesis, followed by the description of the applied measurement techniques and characteristic methods.

3.1 Materials

The photophysics of BHJ organic photovoltaic devices are based on the concept of photoinduced electron transfer from donor-type conjugated polymers into acceptor molecules such as fullerene. The choice of semiconductor polymers, fullerene acceptors and interface materials all play an important role in the construction of an organic solar cell. The materials in this thesis were either commercially available, or were designed and synthesized by our collaborators. All materials were used as received.

3.1.1 Active layer materials

The donor and acceptor materials applied in this thesis are listed in **Table 3-1**. The materials were used as received without further purification. Regioregular P3HT used for the study was provided by BASF (Sepiolid P200, M_n=13.4 kg/mol, M_w=21.8 kg/mol, PDI=1.63 (GPC)). Low band gap polymer PCDTBT and OPV-46 were provided by our collaborators. $PC_{60}BM$ and $PC_{70}BM$ were purchased from Solenne B.V. The chemical structures of the donor and acceptor materials are illustrated in **Figure 3-1**.

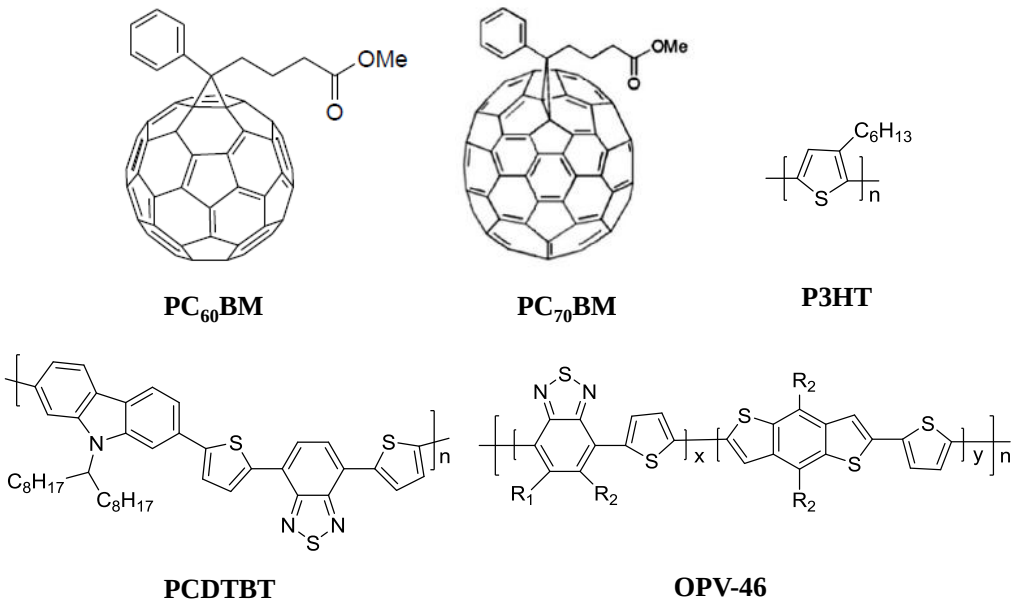

Figure 3-1 Chemical structures of active layer materials used in this thesis.

Table 3-1 Active layer materials (donors and acceptors) used in this thesis.

	Materials	Provider	M_W (kg/mol)	Purity
Donor	P3HT	BASF	21.8	–
	PCDTBT	Collaborator	–	–
	OPV-46	Collaborator	–	–
Acceptor	$PC_{60}BM$	Solenne	–	99.5
	$PC_{70}BM$	Solenne	–	99

3.1.2 Interface materials

ZnO nanoparticles with the size of 10 nm (*Nanograde-N10*) are dissolved in isopropanol to 2.5%, which used as electron transfer layer (ETL) material. Before coating, the solution should be shaken, unltrasonicated and filtered through 0.45 μm FTPE filter. Evaporated molybdenum oxide (MoOx) was purchased from Sigma-Aldrich, which used as hole transfer layer (HTL) material.

3.2 Device architectures and sample layout

Bulk heterojunction (BHJ) organic solar cells are constructed in layer, which can divide into normal device and inverted structure as shown in **Figure 1-6**. For comparison, all devices are fabricated in inverted structures in this thesis as shown in **Figure 3-2a**. Although other transparent materials such as polymer sheets may also be employed, the device is usually built onto a glass substrate. Indium tin oxide (ITO) is usually coated on the glass substrate, which is used as an optically transparent cathode. Because the solar cell is illuminated through this layer, it is very important that the transparent electrode absorbs as little visible light as possible. A thin film consisting of ZnO nanoparticles (normally 40 nm) is then applied to the ITO layer by doctor blading, which is used as electron transfer layer (ETL). The next layer is the active layer, which is a blend of the electron-donating semiconducting polymer and electron-accepting fullerene. For ternary solar cell, it is also necessary to blend the third component into active layer. The active layer absorbs light and generated

photocurrent. Finally, a 10 nm MoOx used as HTL interface layer and 100 nm metal anode (typically Ag) are vacuum deposited to complete the cell.

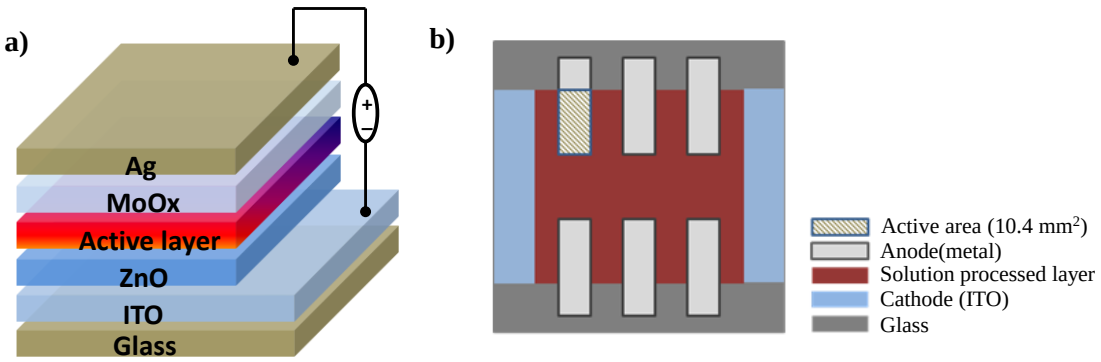

Figure 3-2 a) General structure of an inverted BHJ organic solar cell used in this thesis; b) Sample layout of organic device.

The sample layout is shown in **Figure 3-2b**. The solar cells were processed on glass substrates (2.5×2.5 cm^2) with pre-patterned bottom ITO electrode. Afterwards, all solution-processed layers were deposited over the whole substrate area using doctor-blading or spin-coating technologies, and then structured before the top metal electrode (Ag) deposition through a shadow mask via thermal evaporation. The overlap of top and bottom electrodes defined the active area (10.4 mm^2). Each substrate had 6 devices.

3.3 Deposition methods

a) Doctor Blading

Most solution processed layers in this thesis have been deposited by doctor-blading in air. Because its simplicity and efficient material usage, doctor blading technology is widely used. Meanwhile, doctor-blading can be employed in both sheet-to-sheet and roll-to-roll processing. As shown in **Figure 3-3a**, the solution is applied in the slit between the substrate and the blade. Then the blade moves with a defined speed over the substrate to apply the wet film. After drying, the ~nm or μm thickness film of the applied material finds itself on the substrate. There are several parameters which can control the thicknesses of layers, including the speed of blade, the temperature of bottom, the slit height between substrate and blade.

Normally, the thickness of the film is mainly dependent on the speed of the blade and the solution concentration.

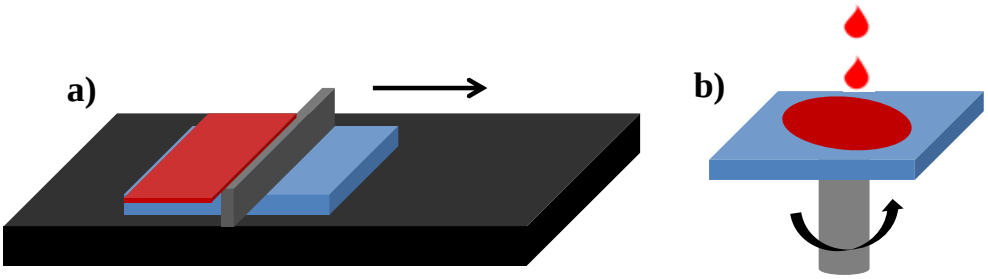

Figure 3-3 Depiction of solution deposition procedures including a) doctor-blading and b) spin-coating.

b) Spin-coating

Spin-coating is another simple procedure used to deposit uniform thin films to flat substrates, where it can be used to create uniform thin films with nanoscale thicknesses, as depicted in **Figure 3-3b**. A typical process involves depositing a small puddle of a fluid material onto the center of a substrate and then spinning the substrate at high speed. After solvent evaporation, a solid film is generated. For the spin-coating procedure, the film thickness is mainly controlled by the concentration of the solution and the rotation speed. In addition, for a constant spinning speed, the same dependency is obtained for the spinning time. The longer the spinning time is, the smaller gets the film thickness.

3.4 Methods of characterization

3.4.1 Film characterization

Absorption spectrum measurements: Absorption profiles were recorded with a Perkin Elmer Lambda-35 absorption spectrometer from 300 to 1000 nm using the thin film cast from CB solution. The absorption spectroscopy is a helpful characterization method for ternary solar cells. In order to have better photon absorption, complementary polymers are used in ternary active layer. According to Beer-Lambert Law,[146] the absorbance (A) can be defined as following equation (3-1):

$$A = \log\left(\frac{I_0}{I}\right) = \varepsilon_A CL \qquad (3\text{-}1)$$

Where A is absorbance or optical density, I_0 is intensity of light incident upon sample cell, I is intensity of light leaving sample cell. C is the molar concentration of solution, L is the length of absorption medium, ε_A is Molar absorption coefficient.

Film thickness measurement: The thickness of thin films was measured using a profilometer (Tencor). A profilometer scans a surface with a small needle and registers height differences. The lateral resolution is the in the μm range due to the diameter of the tip of the needle, but the height resolution is in the nm range. The thickness of a film can be measured by removing a part of the film via scratching and measuring the difference from surface of the film to the bottom of the gap.

Atomic Force Microscopy (AFM): In this thesis, AFM was used to study the surface morphology and roughness of thin films. And topographical measurements were performed with AFM (Veeco Model D3100) in tapping mode.

Transmission electron microscopy (TEM): The active layers for the TEM investigations were prepared as plan view specimens. Therefore films of PEDOT:PSS and active layers with a thickness of 50 nm were deposited on glass using doctor-blading under ambient conditions. To float off the active layer, the sample was put into a vessel with distilled water, where PEDOT:PSS dissolved, and the active layer was transferred to a Cu TEM supporting grid. The TEM investigations were performed using an FEI Titan Themis 300 TEM with a high brightness field emission gun (X-FEG) operated at 200 kV equipped with a high resolution Gatan Imaging Filter (GIF Quantum) used for electron energy-loss spectroscopy (EELS) and energy filtered TEM (EFTEM). Elemental maps were calculated using the three window technique.

Photoluminescence (PL): The schematic of PL setup are shown in **Figure 3-4**.[147] PL describes spontaneously emission of light from a material under optical excitation. When the incident photon has enough energy, it is absorbed and then an electronic excitation will

happen. The excited electrons may have a radiative relaxation as a light which can be collected and analyzed. In this thesis, all PL measurements were performed on thin layers. After preparing the corresponding solutions, different active layer films were doctor bladed on glass under ambient conditions. The films were excited at 375 nm and 445nm, employing a chopped argon laser beam. The PL emission of the films was dispersed by a 600 lines per mm grating monochromator (HRS-2) and detected by a Germanium detector (ADC 403L) through the lock in technique.

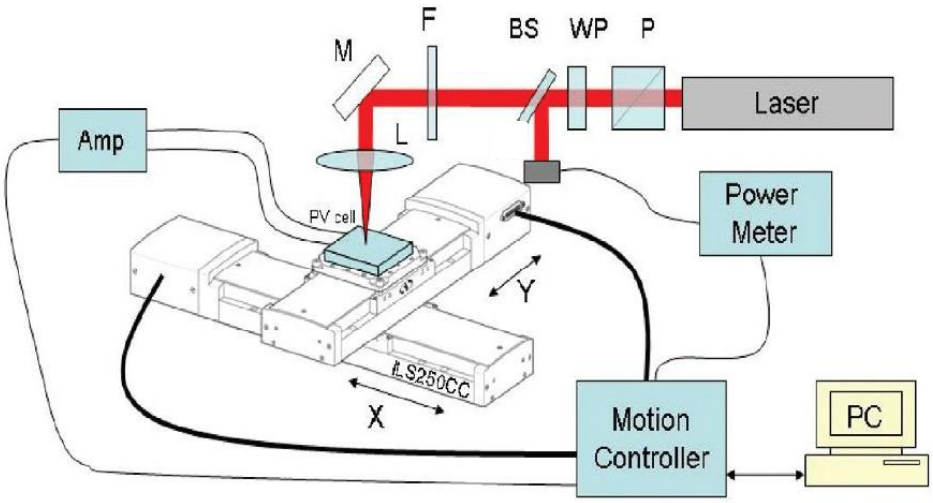

Figure 3-4 The schematic of photoluminescence setup.[147]

Surface Energy: The contact angle between three solvents' drops (ultrapure water and ethylene glycol) and the surface energy of the pristine films were measured using a contact angle instrument from Dataphysics (model OCA20). Surface energies were calculated by the values of the initial contact angles using the SCA20-U software and the Owens-Wendt and Kaelble method. The measured surface energies for pristine materials are averaged values based on 10 measurements per film. Subsequently, the wetting coefficient (ω) can be calculated by using the values of surface energies of different materials. For example, the wetting coefficient of material C (ω_C) in blends of materials A and B can be calculated by Young's equation as following,[148,149]

$$\omega_C = (\gamma_{C-B} - \gamma_{C-A})/\gamma_{A-B} \quad (3\text{-}2)$$

Where γ_{X-Y} is the interfacial surface energy between X and Y, calculated by Neumann's

equation as following

$$\gamma_{X-Y} = \gamma_X + \gamma_Y - 2(\gamma_X\gamma_Y)^{0.5}\exp[-\beta(\gamma_X-\gamma_Y)^2] \quad (3\text{-}3)$$

Where β= 0.000115 $m^{-4}\,mJ^{-2}$.

3.4.2 Device characterization

Current density-voltage (*J-V*): *J-V* characteristics of solar cells were measured using a source measurement unit from BoTest. Illumination was provided by a solar simulator (Oriel Sol 1A, from Newport) with AM1.5G spectra at 100 mW cm^{-2} which was calibrated by a certified silicon solar cell. The light intensity was modulated with a series of neutral color density filters, allowing changing the intensity from 100 to 0.4 mW cm^{-2}. All devices were tested in air.

External quantum efficiency (EQE): EQE spectra were recorded with an Enli Technology (Taiwan) EQE measurement system (QE-R), and the light intensity at each wavelength was calibrated with a standard single-crystal Si photovoltaic cell. EQE characterization shows the response of a photovoltaic device and is defined in equation (3-4):

$$EQE = \frac{number\ of\ collected\ charges}{number\ of\ incident\ photons} \quad (3\text{-}4)$$

By recording the response of the sample to a monochromatic light illumination at different wavelengths, the EQE spectrum is obtained. Significantly, J_{SC} can be calculated by integrating the spectrum over the scanned area, as shown in the following equation (3-5):

$$J_{SC}(E_g) = e\int_{E_g}^{\infty} I_{ph}(E) * EQE(E) * dE \quad (3\text{-}5)$$

Where E_g is the energy band gap of the absorber and I_{ph} is the spectrum of the sunlight at AM 1.5G.

Photogenerated charge carrier extraction by linearly increasing voltage (Photo-CELIV): In photo-CELIV measurements, the devices were illuminated with a 405 nm laser-diode. Current transients were recorded across an internal 50 Ω resistor of an oscilloscope (Agilent

Technologies DSO-X 2024A). We used a fast electrical switch to isolate the cell and prevent charge extraction or sweep out during the laser pulse and the delay time. After a variable delay time, a linear extraction ramp was applied via a function generator. The ramp, which was 60 μs long and 2 V in amplitude, was set to start with an offset matching the V_{OC} of the cell for each delay time.

Photo-induced absorption (PIA): PIA studies were performed by exciting the sample with a 786 nm laser while simultaneously probing the sample with a white lamp. The PIA spectra of the sample were dispersed by a 1200 lines mm-1 grating monochromator (iHR320) and detected by a silicon detector and a InGaAs detector separately through lock-in technique. Photo induced absorption spectroscopy involves measuring the linear absorption spectrum of the excited state of the system. The working principle of PIA spectroscopy is shown in **Figure 3-5**. And the detail explanation of this measurement is discussed as following to give an insight understand.

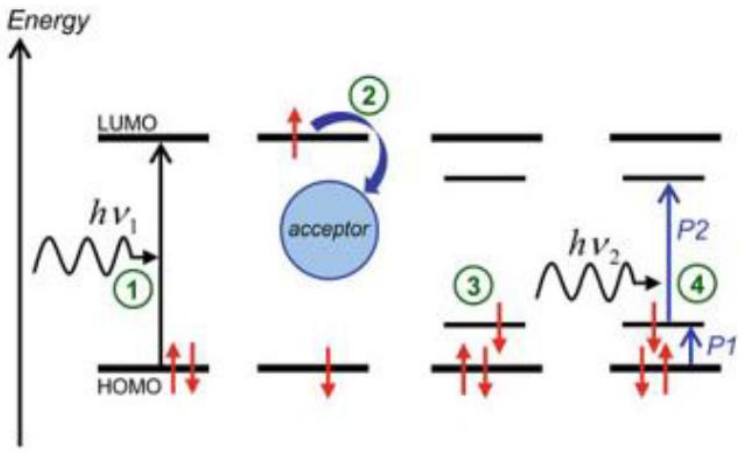

Figure 3-5 Working principle of PIA spectroscopy.[150]

A laser beam is used to excite the polymer, and then electron-hole pairs are created. If there is an electron acceptor, the excited electron gets transferred to electron acceptor, leaving behind the hole in the polymer. If the polymer has either donated an electron or accepted a hole, the resulting positive charge on the polymer causes a restructuring of the conjugation along the polymer backbone that is observed spectrally as an opening of states below the bandgap of

the polymer. This hole will form a polaron with energy levels with HOMO-LUMO gap of the neutral molecule. Now the sample is irradiated by a white light (lamp), absorption occurs at photon energies corresponding to transitions involving the polaron levels. Therefore the transmission of the excited sample will differ from the transmission of the ground state. The difference of these two transmissions gives the photo induced absorption (PIA) signal.[150]

Chapter 4

Synthesis of near IR sensitizers: silicon phthalocyanines (SiPCs) and silicon naphthalocyanine (SiNC-1)

Abstract

To overcome absorption limitations in organic photovoltaic (OPV), several strategies are currently pursuing to achieve enhanced PCE. Hence, the concepts of ternary and quaternary cells have been introduced, which incorporate one component or two components into the host system. Among them, dye sensitized solar cells have already attracted significant attention because their complementary absorption characteristics. In this chapter, several dye molecules are synthesized and characterized.

The synthetic routes and molecular characterizations of related near IR sensitizers can be found in the following published article:

(1) **L. Ke**, J. Min, M. Adam, N. Gasparini, Y. Hou, J. D. Perea, W. Chen, H. Zhang, S. Fladischer, A. C. Sale, E. Spiecker, R. R. Tykwinski, C. J. Brabec and T. Ameri, A series of novel pyrene-substituted silicon phthalocyanines as near-IR sensitizers in organic ternary solar cells: Synthesis and device fabrication, *Adv. Energy Mater.* **2016**, *6*, 1502355.

(2) **L. Ke**, N. Gasparini, J. Min, H. Zhang, M. Adam, S. Rechberger, K. Forberich, C. Zhang, E. Spiecker, R. R. Tykwinski, C. J. Brabec and T. Ameri, Panchromatic quaternary polymer/fullerene BHJ solar cells, based on the novel silicon naphthalocyanine and silicon phthalocyanine dye sensitizers, *J. Mater. Chem. A*, **2016**, DOI: 10.1039/C6TA08729A.

4.1 Introduction

As mentioned in **Chapter 2**, dye sensitized organic solar cells have already been widely studied because they are easy to adapt in host matrix in respective to microstructure compatibility and spectral sensitivity. Among the dye molecules, phthalocyanines (**PCs**) and naphthalocyanines (**NCs**) have been developed as an interesting class of semiconducting materials and used in dye sensitized OSCs.[137,140,142] They are planar π-electron macroheterocycles that consist of four isoindole subunits linked together through nitrogen atoms (The structures are shown in **Figure 4-1**).[151-154] Normally, these kinds of molecules have intense absorption spectra generated by their extensively conjugated systems, presenting two major bands: the Q and the Soret B band. The Q band, usually observed in the near IR region, is the strongest with the molar absorptivity values exceeding 10^5 L $mol^{-1}cm^{-1}$. While for the Soret band, lying near 350 nm, is generally much broader and less intense.

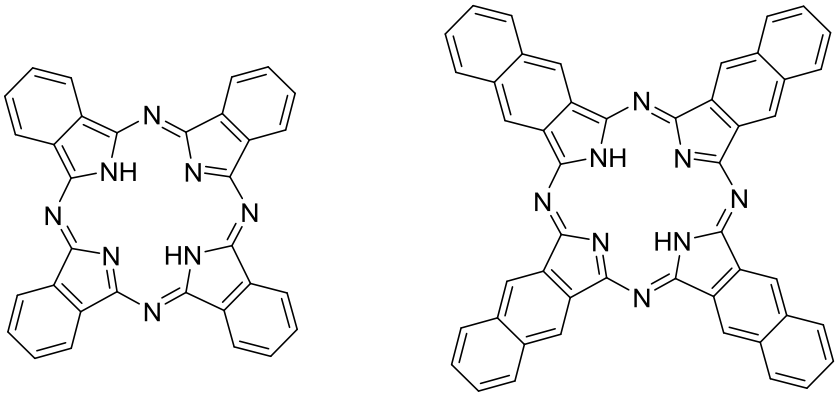

Figure 4-1 The basic skeleton of phthalocyanine and naphthalocyanine as a metal free-base.

Phthalocyanines and naphthalocyanines are known to have high chemical, thermal and optical resistances, making them ideal candidates as efficient dyes.[155-158] However, **PCs** and **NCs**, due to their planar aromatic structure, have a great tendency to form insoluble aggregates.[159,160] This intrinsic characteristic not only inhibits the properties presented by **PCs** and **NCs** at the molecular level but also produces a side effect on the performance of PCE, which in further limit their technological applications. One useful method is employed to prevent the formation of aggregating trend is the functionalization of the molecules if possible.[161-163] Two strategies, the addition of a metal into the ring[164] and the substitution of a variety of ligands at axial and/or peripheral position[165], are used to tailoring of the physical and optical properties of **PCs** and **NCs**. Because the high quantum yields and long fluorescence lifetime of axially substituted silicon **PCs** and **NCs**, they are widely studied.[151,166-169] Compared to zinc- and aluminum- **PCs** and **NCs**, these kinds of compounds have the advantages of the hexacoordinate nature of hypervalent silicon. This feature leads the possibility to functionalize the axial valences, yielding silicon phthalocyanines and naphthalocyanines derivatives whose tendency to aggregation is minimal.[170-172]

On the other hand, Pyrene and its derivatives gain researcher's interests because of their unique photophysical characteristics.[173] The molecular structure of pyrene is shown in **Figure 4-2.** As alternant flat polycyclic aromatic hydrocarbon systems, they include a relatively long lifetime and a high quantum yield.[174,175] They are also the most useful moiety among the fluorescent chromophores. Pyrene and its derivatives have often been used as anchor groups

to facilitate electron transfer into the acceptor domains.[176] In addition, pyrene containing compounds have been shown to adsorb specifically onto the surface of carbon nanotubes by means of no covalent π-π stacking interaction.[177] Here, we employ these advantages to substitute the silicon phthalocyanines with pyrene moiety.

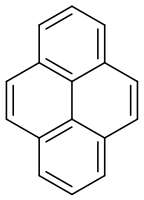

Figure 4-2 The structure of pyrene ring.

Although phthalocyanines and pyrene moieties appear to be promising candidates and both molecules have been widely studied, there are only few work reports on the combination of these two moieties.[178-180] In this chapter, a novel series of silicon phthalocyanine dyes (**SiPC-0**, **SiPC-1**, **SiPC-2**, and **SiPC-3**) and novel silicon naphthalocyanine (**SiNC-1**) are synthesized and characterized. Incorporation of four bulky *tert*-butyl substituents to the periphery position can improve solubility in common organic solvents and reduce the possibility of large scale aggregation, while two pyrene groups in the ligand position can cause a red shift of absorption by *π*-stacking between the pyrene and PC moiety and in parallel can control the intermolecular interactions.

4.2 Experimental section

4.2.1 Material and reagents

All chemicals were purchased from commercial suppliers and used as received. All solvents were distilled prior to use. Methanol (MeOH) was normally rotovaped (with NaOH pellets added beforehand) sitting over molecular sieves in case it had to be water-free. Distill pyridine was sitting over solid KOH and then stored it over 4Å molecular sieves. NH_3 and H_2 were also reagent-grade. 1-Pyrenecarboxylic acid, 1-pyreneacetic acid and 1-pyrenebutyric acid were purchased from Sigma-Aldrich.

4.2.2 Characterization equipment and instrument

Analytical TLC was performed on Al plates coated with 0.20 mm silica gel and containing a fluorescent indicator (Macherey-Nagel, ALUGRAM.SILG/UV254), visualizing via UV-light (264/364 nm) or standard coloring reagents. Column chromatography was carried out on silica gel (Macherey-Nagel, M-N Silica Gel 60A, 230−400 mesh). The solution UV–vis characterization was performed on a Cary 5000 UV–vis–NIR (Varian) spectrometer. ^{1}H NMR spectra were recorded at ambient conditions on a Bruker Avance 300 spectrometer and referenced to the residual solvent signal (^{1}H: $CDCl_3$, δ=7.24 ppm) and recorded at ambient conditions. Mass spectra were obtained by a Shimadzu AXIMA confidence (MALDI TOF) and a maXis 4G (Bruker, APPI HRMS).

Cyclic voltammetry (CV) studies were carried out using a BASi Voltammetric Analyzer CV−50W. The measurements were performed using a 0.1 M solution of n-Bu_4NPF_6 in CH_2Cl_2, with a platinum working electrode, a platinum counter electrode, and an Ag/AgCl reference electrode. The cyclovoltammograms were recorded from −2.5 V to 1.5 V (vs. F_C/F_C^+) with a scan rate of 60 mV s^{-1}. The concentration of the analyzed compounds is stated in the caption of the corresponding cyclovoltammogram, with a value of 1.0 mM. All solutions were degased with N_2 before and were layered with N_2 during the CV measurement. The potential values (E½) were calculated using the following equation $E½=(E_{red} + E_{ox})/2$, where E_{red} and E_{ox} correspond to the cathodic and anodic peak potentials, respectively. Potentials are referenced to the ferrocene/ferrocenium (F_C/F_C^+) couple used as an internal standard. The HOMO and LUMO energies were calculated with the empirical relation:[181]

$$E_{HOMO} \approx -\left(E_{\frac{1}{2}}^{ox} + 4.8\ eV\right) \qquad (4\text{-}1)$$

$$E_{LUMO} \approx -\left(E_{\frac{1}{2}}^{red} + 4.8\ eV\right) \qquad (4\text{-}2)$$

Thereby, all redox potentials were referred to the F_C/F_C^+ couple which were set to 0 V.

4.2.3 Synthesis of the precursors

1-pyrenepropionic acid.

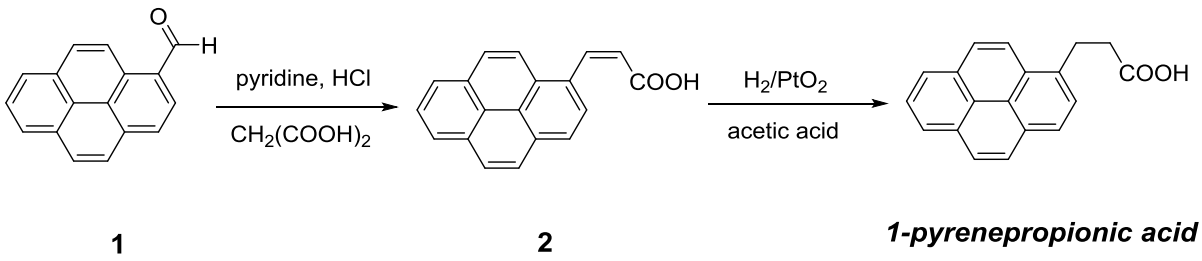

Scheme 4-1 Synthesis route of ***1-pyrenepropionic acid***.[182]

The synthesis procedure of ***1-pyrenepropionic acid*** is shown in **Scheme 4-1**. Via adaptation of a known procedure,[183] to a solution of 1-formylpyrene (461 mg, 2.00 mmol) in pyridine (1.5 mL) was added malonic acid (1.04 g, 9.99 mmol), and the solution was stirred for 9 h at 100 ºC. The solution was cooled, and HCl (1.0 M, 6 mL) was added to quench the reaction. The solid was filtered to afford 3-(1-pyrenyl) acrylic acid **2** (533 mg, 98%) as yellow granules. Hydrogenation of **2** (140 mg, 0.514 mmol) was performed by stirring a solution of **2** in acetic acid (50 mL) under a H_2 atmosphere (1 atm) in the presence of PtO_2 (14.0 mg, 0.0617 mmol) for 15 h at room temperature. The catalyst was removed by filtering and the solvent evaporated, the residue was dissolved in ether (20 mL). The ethereal solution was washed with water (200 mL) and dried over Na_2SO_4. The solvent was removed to give the crude product, which was purified by recrystallization from hexane/CH_2Cl_2 (50:1 mL) to give the result compound (90.0 mg, 65%) as a light yellow solid. ^{1}H NMR ($CDCl_3$): δ 2.90–2.96 (m, 2H), 3.68–3.73 (m, 2H), 7.92–8.30 (m, 9H). Spectral and physical data were similar to that reported in reference 35.

tert-Butyl SiPCCl$_2$.

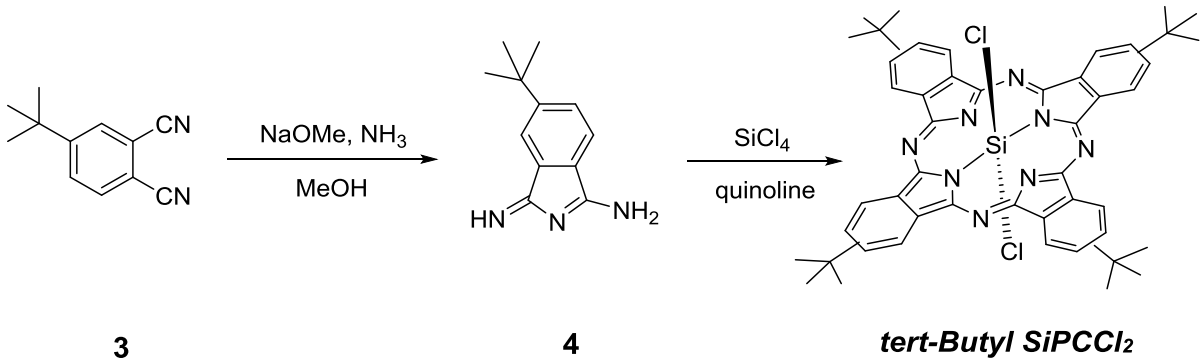

3 **4** ***tert-Butyl SiPCCl₂***

Scheme 4-2 Synthesis route of ***tert-Butyl SiPCCl₂***.[182]

The precursor ***tert-Butyl SiPCCl₂*** was synthesized according to Lo et al. and Lim et al.[184,185] The synthesis route was shown in **Scheme 4-2**. Anhydrous NH_3 was bubbled into a stirred mixture of compound **3** (300 mg, 1.63 mmol), sodium (40.7 mg, 1.77 mmol), and dry methanol (15 mL) for about 20 h while it was at reflux. After cooling, the solvent was removed, and the product was purified by column chromatography (silica gel, methanol). The solvent was removed, affording **4** (328 mg, 71%), as a yellow–white powder.

Tetrachlorosilane (0.240 mL, 2.10 mmol) was added to a suspension of compound **4** (300 mg, 1.49 mmol) in quinoline (10 mL) at room temperature under nitrogen. The mixture was heated to 210 °C and stirred for 2 h. After slowly cooling to room temperature, methanol (15 mL) was added, and the resulting mixture was stirred overnight. The green precipitate was plugged over a pad of silica gel with CH_2Cl_2 as solvent. After removing the solvent, the residue was purified by column chromatography (silica gel, ethyl acetate/hexanes 1:2) to remove all quinoline and side products, and the solution evaporated. The dark blue mixture was recrystallized from methanol (30 mL), filtered, and dried in vacuo to yield ***tert-Butyl SiPCCl₂*** (240 mg, 77%) which was used for subsequent reactions without further purification.

tert-Butyl SiNCCl₂.

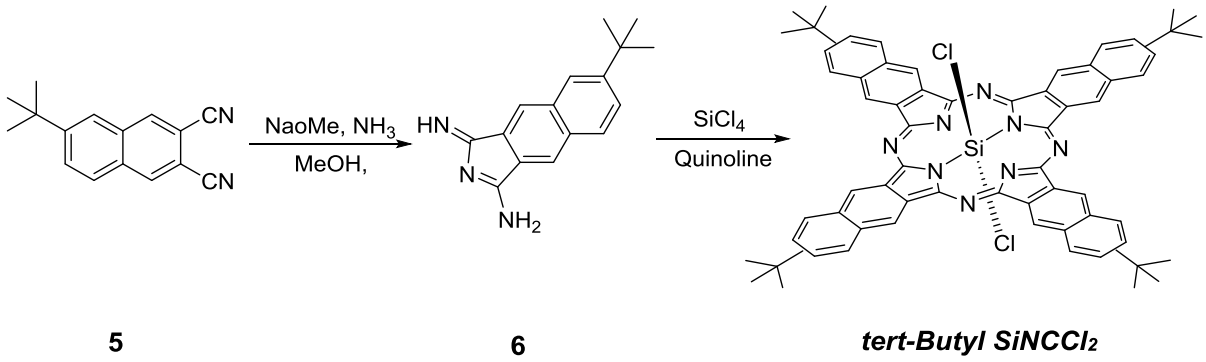

5 **6** ***tert-Butyl SiNCCl₂***

Scheme 4-3 Synthesis route of ***tert-Butyl SiNCCl₂***.[186]

The synthesis procedure ***tert-Butyl SiNCCl₂*** was shown in **Scheme 4-2**, which is similar with the synthesis of ***tert-Butyl SiNCCl₂***. Anhydrous NH_3 was bubbled into a stirred solution of compound **5** (285 mg, 1.00 mmol), sodium (23.0 mg, 1.00 mmol), and dry MeOH (15 mL) for about 20 h while the reaction was held at reflux. The reaction mixture was cooled to room temperature, and the solvent was evaporated. The resulting solid was purified by column chromatography (silica gel, MeOH) to give compound **6** (180 mg, 0.716 mmol, 71%) as light yellow powder.

In the next step, tetrachlorosilane (0.10 mL, 0.873 mmol) was added to a suspension of compound **6** (150 mg, 0.598 mmol) in quinoline (3 mL) at room temperature under nitrogen. The mixture was heated to 210 °C and stirred for 2 h. After cooling to room temperature, MeOH (15 mL) was added, and the resulting mixture was stirred overnight. The reddish-brown solid was filtered, washed with MeOH (10 mL), and then dried to yield ***tert-Butyl SiNCCl₂*** (80.0 mg, 52%), which was used for subsequent reaction without further purification.

4.2.4 Synthesis of new compounds

4.2.4.1 Synthesis of SiPCs

Silicon phthalocyanines **SiPC-0**, **SiPC-1**, **SiPC-2** and **SiPC-3** were synthesized as described

in **Scheme 4-4**. The target silicon phthalocyanines were obtained via a condensation reaction between precursor ***tert-Butyl SiPCCl₂*** and an excess of pyrene acids with varying different length of alkyl chains in dyglime at high temperature.[187,188] The target compounds were characterized by ^{1}H NMR, UV-vis spectroscopy, and HR-APPI-MS. All data collected were consistent with the predicted structures. Detailed synthesis procedures and their characterizations are shown as following.

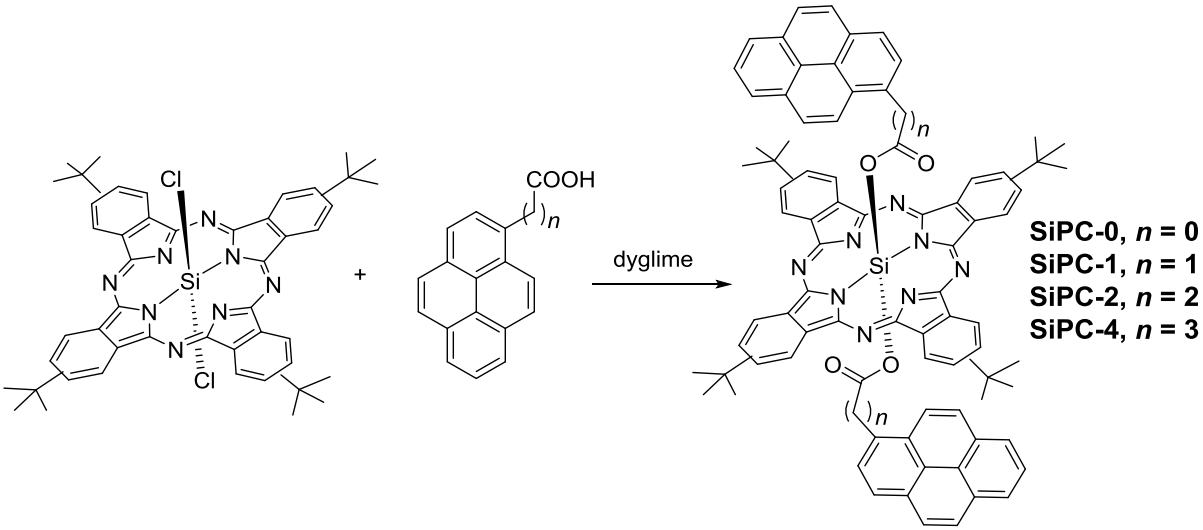

Scheme 4-4 Synthesis route of **SiPCs**.[182]

SiPC-0

A mixture of ***tert-Butyl SiPCCl₂*** (100 mg, 0.120 mmol), 1-pyrenecarboxylic acid (88.6 mg, 0.360 mmol), and dyglime (3 mL) was added to a flask under nitrogen. The mixture was stirred at 160 °C for 5 h. After cooling to room temperature, the green solid was plugged through silica gel using CH_2Cl_2. After removing the solvent, the residue was purified by column chromatography (silica gel, CH_2Cl_2/hexanes 1:1) and the solvent evaporated. The green solid was recrystallized from methanol (20 mL), filtered, and dried in vacuo to afford **SiPC-0** as a green powder (40.0 mg, 27%). UV–vis (CH_2Cl_2) λ_{max} 356, 624, 695 nm; ^{1}H NMR ($CDCl_3$): δ 1.80 (s, 36H), 5.49 (d, *J* = 6.0 Hz, 2H), 5.72–5.75 (m, 2H), 6.78 (d, *J* = 9.0 Hz, 2H), 6.97 (d, *J* = 9.0 Hz, 2H), 7.39 (d, *J* = 9.0 Hz, 2H), 7.62–7.83 (m, 8H), 8.45 (d, *J* = 9.0 Hz, 4H), 9.58–9.77 (m, 8H). The ^{1}H NMR spectrum was shown in **Figure 4-3**. APPI

HRMS calc. for $C_{82}H_{66}N_8O_4Si$ [M^+], 1254.4971, found 1254.4976.

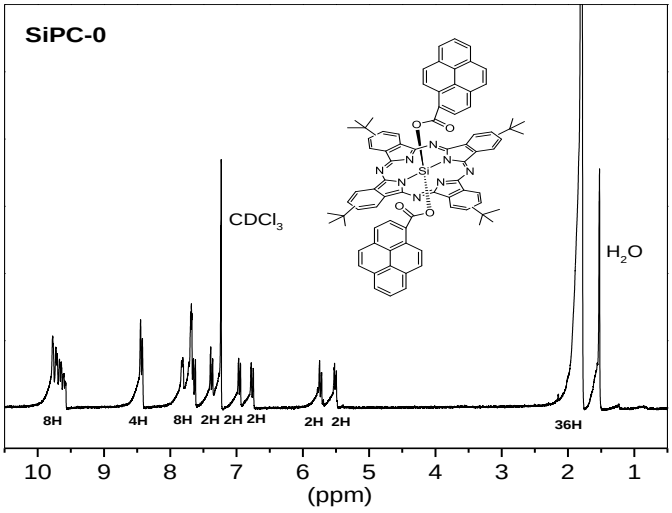

Figure 4-3 The ^{1}H NMR spectrum for **SiPC-0**.[182]

SiPC-1

A mixture of ***tert-Butyl SiPCCl$_2$*** (50.0 mg, 0.0598 mmol), 1-pyreneacetic acid (62.5 mg, 0.240 mmol), and dyglime (2 mL) was added to a flask under nitrogen. The mixture was stirred at 160 °C for 7 h. After cooling to room temperature, the green solid was plugged through silica gel using CH_2Cl_2. After removing the solvent, the residue was purified by column chromatography (silica gel, ethyl acetate/hexanes 3:1) and evaporated. The green solid was recrystallized from methanol (20 mL), filtered, and dried in vacuo to yield **SiPC-1** as a green powder (30.0 mg, 39%). UV–vis (CH_2Cl_2) λ_{max} 361, 623, 693 nm; ^{1}H NMR ($CDCl_3$): δ 1.87 (s, 36H), 5.38–5.42 (m, 2H), 5.53–5.56 (m, 2H), 6.66–6.74 (m, 4H), 7.55 (d, *J* = 9.0 Hz, 2H), 7.85 (d, *J* = 9.0 Hz, 2H), 7.99–8.28 (m, 10H), 8.45–8.55 (m, 2H), 8.65–8.81 (m, 2H), 9.15–9.20 (m, 2H), 9.41–9.42 (m, 2H), four protons coincident with adventitious solvent and not observed. The ^{1}H NMR spectrum was shown in **Figure 4-4**. APPI HRMS calc. for $C_{84}H_{70}N_8O_4Si$ [M^+] 1282.5284, found 1282.5271.

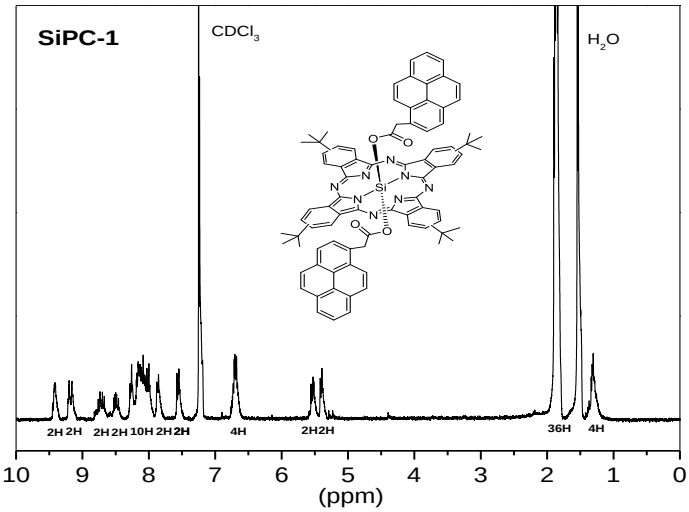

Figure 4-4 The ^{1}H NMR spectrum for **SiPC-1**.[182]

SiPC-2

A mixture of ***tert-Butyl SiPCCl$_2$*** (100 mg, 0.120 mmol), 1-pyrenepropionic acid (131 mg, 0.478 mmol), and dyglime (3 mL) was added to a flask under nitrogen. The mixture was stirred at 160 °C for 4 h. After cooling to room temperature, the green solid was plugged through silica gel using CH_2Cl_2. The solvent was evaporated the residue was purified by column chromatography (silica gel, CH_2Cl_2/hexanes 2:1) and then recrystallized from methanol (20 mL) to afford **SiPC-2** as a green powder (38.0 mg, 24%). UV–vis (CH_2Cl_2) λ_{max} 331, 345, 623, 694 nm; ^{1}H NMR ($CDCl_3$): δ –0.10 to –0.05 (m, 4H), 1.08–1.10 (m, 4H), 1.79 (s, 36H), 6.06–6.09 (m, 2H), 6.58–6.62 (m, 2H), 7.23–7.35 (m, 4H), 7.78–7.94 (m, 8H), 8.03–8.06 (m, 2H), 8.28–8.32 (m, 4H), 9.18–9.28 (m, 2H), 9.34–9.43 (m, 2H), 9.61–9.71 (m, 4H). The ^{1}H NMR spectrum was shown in **Figure 4-5**. APPI HRMS calc. for $C_{86}H_{74}N_8O_4Si$ [M^+] 1310.5597, found 1310.5589.

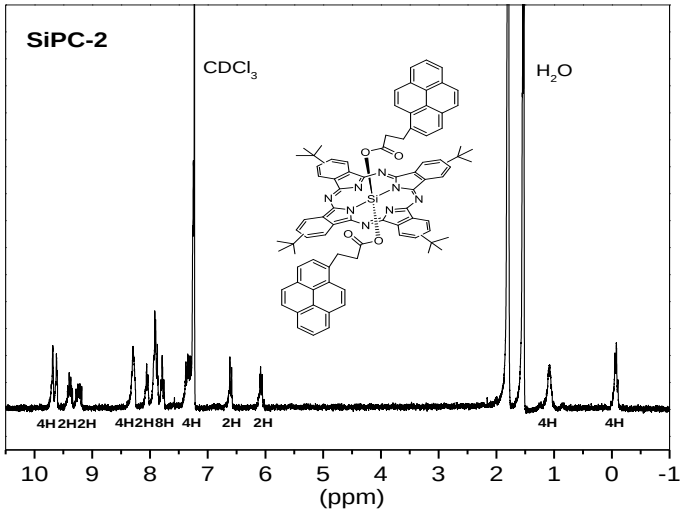

Figure 4-5 The ^{1}H NMR spectrum for **SiPC-2**.[182]

SiPC-3

A mixture of ***tert-Butyl SiPCCl$_2$*** (100 mg, 0.120 mmol), 1-pyrenebutyric acid (138 mg, 0.479 mmol), and dyglime (3 mL) was added to a flask under nitrogen. The mixture was stirred at 160 °C for 4 h. After cooling to room temperature, the green solid was plugged through silica gel using by CH_2Cl_2. The solvent was evaporated and the residue was purified by column chromatography (silica gel, CH_2Cl_2/hexanes 2:1) and then recrystallized from methanol (20 mL) to afford **SiPC-3** as a green powder (40.0 mg, 25%). UV-vis (CH_2Cl_2) λ_{max} 330, 345, 362, 623, 693 nm; ^{1}H NMR ($CDCl_3$): δ –0.44 to –0.22 (m, 4H), –0.20 to –0.09 (m, 4H), 1.35–1.41 (m, 4H), 1.75 (s, 36H), 6.50–6.57 (m, 2H), 7.17 (d, *J* = 9 Hz, 2H), 7.53–7.56 (m, 2H), 7.67 (d, *J* = 9.0 Hz, 2H), 7.78–8.08 (m, 10H), 8.32–8.39 (m, 4H), 9.48 (d, *J* = 9 Hz, 2H), 9.55 (d, *J* = 9 Hz, 2H), 9.69–9.76 (m, 4H). The ^{1}H NMR spectrum was shown in **Figure 4-6**. APPI HRMS calc. for $C_{88}H_{78}N_8O_4Si$ [M^+] 1338.5910, found 1338.5919.

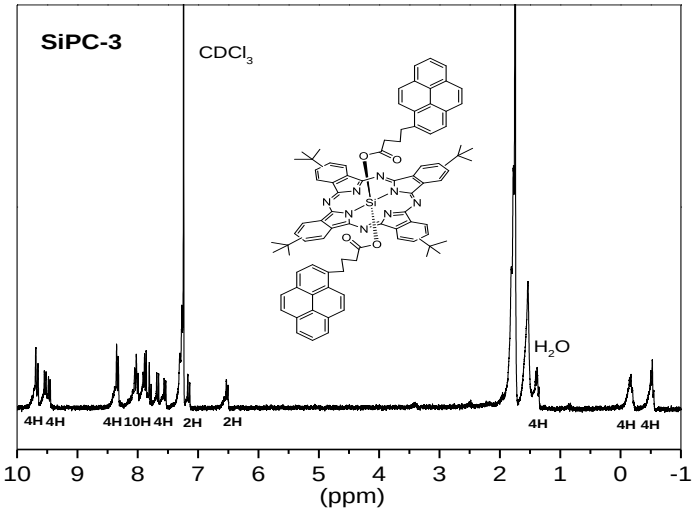

Figure 4-6 The ^{1}H NMR spectrum for **SiPC-3**.[182]

4.2.4.2 Synthesis of SiNC-1

Scheme 4-5 presents the synthetic route to silicon naphthalocyanine **SiNC-1**, which features axial substitution with two pyrene acetic acid groups. Furthermore, the periphery of the naphthalocyanine incorporates four bulky *tert*-butyl groups, which improve the solubility of the dye molecule and reduce the dye aggregation to allow high dye loading. Displacement of the two chloride ligands of ***tert-Butyl SiNCCl$_2$*** with pyreneacetic acid gave **SiNC-1**.[182,187,188] The product **SiNC-1** was characterized by ^{1}H NMR and UV-vis spectroscopy as well as APPI HRMS, and all data were consistent with the proposed structure. The detailed synthetic procedure is described as following.

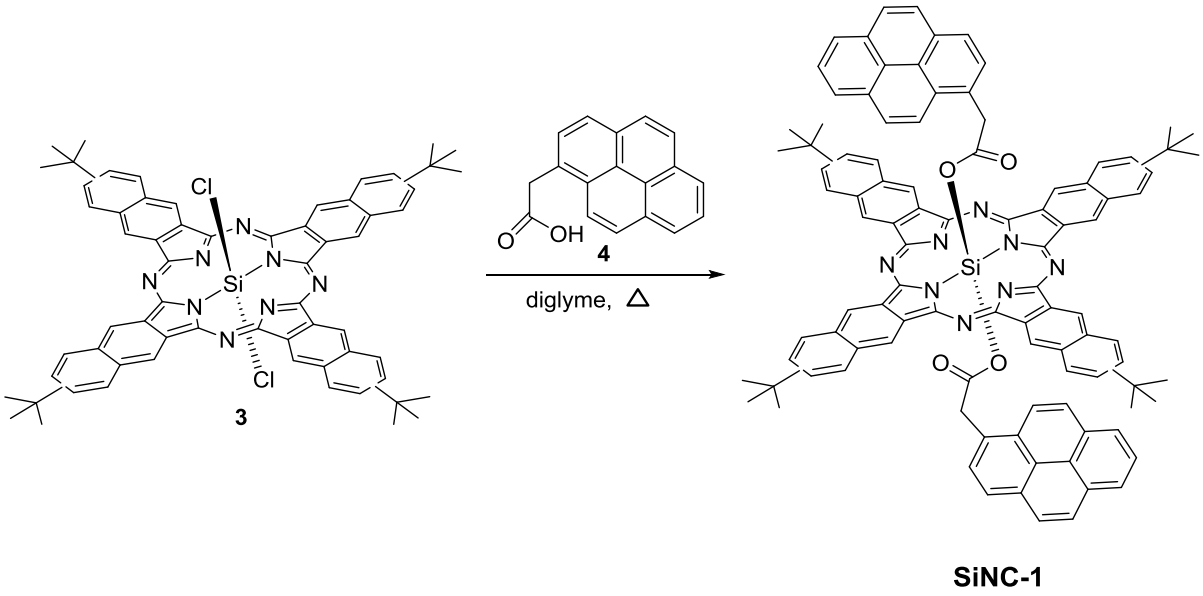

Scheme 4-5 Synthesis route of **SiNC-1**.[186]

A mixture of ***tert-Butyl SiNCCl₂*** (56.0 mg, 0.0540 mmol), 1-Pyreneacetic acid (50.0 mg, 0.192 mmol) and dyglime (2 mL) was added into a flask under nitrogen. The mixture was stirred at 160 °C for 6 h. After cooling to room temperature, the yellow solid was passed through a plug silica gel using CH_2Cl_2. After removing the solvent, the residue was purified by column chromatography (silica gel, CH_2Cl_2/ hexanes 1:1 to 1.5:1) and the solvent evaporated. The yellow solid was recrystallized from MeOH (20 mL), and then filtered. The solid was further washed using acetone (20 mL) and the filtrate was evaporated to afford ***SiNC-1*** as yellow powder (20.0 mg, 25%). UV–vis (CH_2Cl_2) λ_{max} 245, 279, 347, 721, 813 nm; ^{1}H NMR ($CDCl_3$): δ 1.75 (s, 36H), 2.14 (s, 4H), 5.65 (d, *J*=6.0 Hz, 2H), 5.75 (d, *J*=9.0 Hz, 2H), 6.66 (d, *J*=9.0 Hz, 4H), 7.22–7.24 (m, 4H), 7.54 (d, *J*=9.0 Hz, 2H), 7.69–7.72 (m, 2H), 7.83–7.88 (m, 2H), 8.00–8.07 (m, 8H), 8.42–8.51 (m, 8H), 9.24–9.41 (m, 4H). The ^{1}H NMR spectrum of ***SiNC-1*** is shown in **Figure 4-7**. APPI HRMS m/z: calc. for $C_{100}H_{78}N_8O_4Si$ (M^+), 1482.5896; found 1482.5910. MALDI TOF (matrix) *m/z* 1482 (M^+, 10%), 1223 (M-$PyCH_2CO_2$–, 50%).

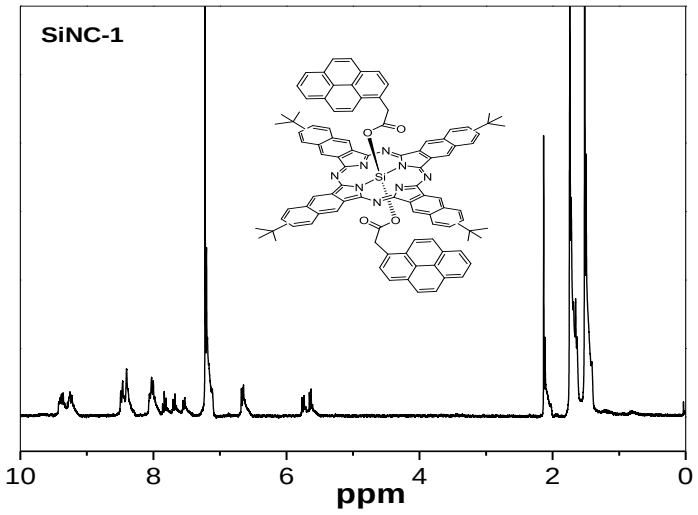

Figure 4-7 The ^{1}H NMR spectrum for **SiNC-1**.[186]

4.3 Results and discussion

4.3.1 The electronic investigation by cyclic voltammetry

As mentioned in **Chapter 2**, phthalocyanines show interesting optoelectronic properties and they have been already used in organic solar cells. Unfortunately, unsubstituted phthalocyanines show poor solubility in common organic solvents and are easy to form aggregation. As a result of the insolubility and the easy trend to aggregate of unsubstituted **PCs**, efforts have been directed to the functionalization of phthalocyanines. Hence, **SiPC-0**, **SiPC-1**, **SiPC-2**, and **SiPC-3** are synthesized. On the other hand, it allows changing the optoelectronic properties with the purpose to decrease the HOMO−LUMO gap to better apply in organic electronic devices. To extend the π-system of silicon phthalocyanines toward improving device characteristics, a novel naphthalocyanine derivative **SiNC-1** with more benzyl ring at the periphery position has been explored.[189,190] As shown in **Table 4-1**, the additional benzyl ring to π-system result in a decrease in the oxidation potential 0.07 V to for **SiNC-1** compared to 0.42 V observed for **SiPC-1**, yielding a lower HOMO−LUMO gap.

Table 4-1 The Cyclic voltammetry[a] results of **SiPCs** and **SiNC-1**.[190-192]

Compound	$E_{1/2}^{ox1}$ [b]	$E_{1/2}^{red1}$ [b]	$E_{1/2}^{red2}$ [b]	E_{HOMO}[c]	E_{LUMO}[c]	E_{gap}[d]

	[V]	[V]	[V]	[eV]	[eV]	[eV]
SiPC-0	0.51	-1.13	-1.62	5.31	3.67	1.64
SiPC-1	0.42	-1.26	-1.63	5.22	3.54	1.68
SiPC-2	0.48	-1.19	-1.53	5.28	3.61	1.67
SiPC-3	0.50	-1.20	-1.63	5.3	3.60	1.70
SiNC-1	0.07	-1.32	-1.66	4.87	3.48	1.39

[a]Cyclic voltammetry was performed according to the method showing in Section 3.2.2.

[b]The potential values (E½) were calculated using the following equation $E½=(E_{red} + E_{ox})/2$, where E_{red} and E_{ox} correspond to the cathodic and anodic peak potentials, respectively.

[c]The HOMO and LUMO values were calculated according to the empirical relations $E_{HOMO} \approx -(E_{1/2}^{ox} + 4.8\ eV)$ and $E_{LUMO} \approx -(E_{1/2}^{red} + 4.8\ eV)$.

[d]Electrochemical HOMO−LUMO gaps determined by $E_{gap} = E_{ox} - E_{red}$.

The cyclic voltammetry plots of **SiPC-0**, **SiPC-1**, **SiPC-2**, **SiPC-3**, and **SiNC-1** are shown in **Figure 4-8**. For **SiPCs** each show one reversible oxidation event in the range of 0.42 to 0.51 V, and the second quasi-reversible oxidation process is not obvious. Unfortunately, there is no clear trend observed for the oxidation potentials based on the different alkyl chain length between the pyrene ring and PC ring. At the same time, they all show one revisable reduction event in the range of -1.26 to -1.13 V, and a second reduction process in the range of -1.56 to -1.63 V. Similar to that observed for the oxidation potentials, there is no obvious trend that can be identified in the reduction potentials based on the alkyl chain length. For **SiNC-1** the first oxidation value is 0.07 V, which is much lower than those of **SiPCs**. The first reduction value is -1.32 V and the second reduction value is -1.66 V, slightly lower than the reduction range of **SiPCs**. This behavior can be explained with the extending of the π-system in **SiNC-1** that allows for better electronic communication between the intermolecular moiety, resulting in smaller HOMO−LUMO gaps, 1.39 eV for **SiNC-1** and with a range from 1.64 to 1.70 eV for **SiPCs**.

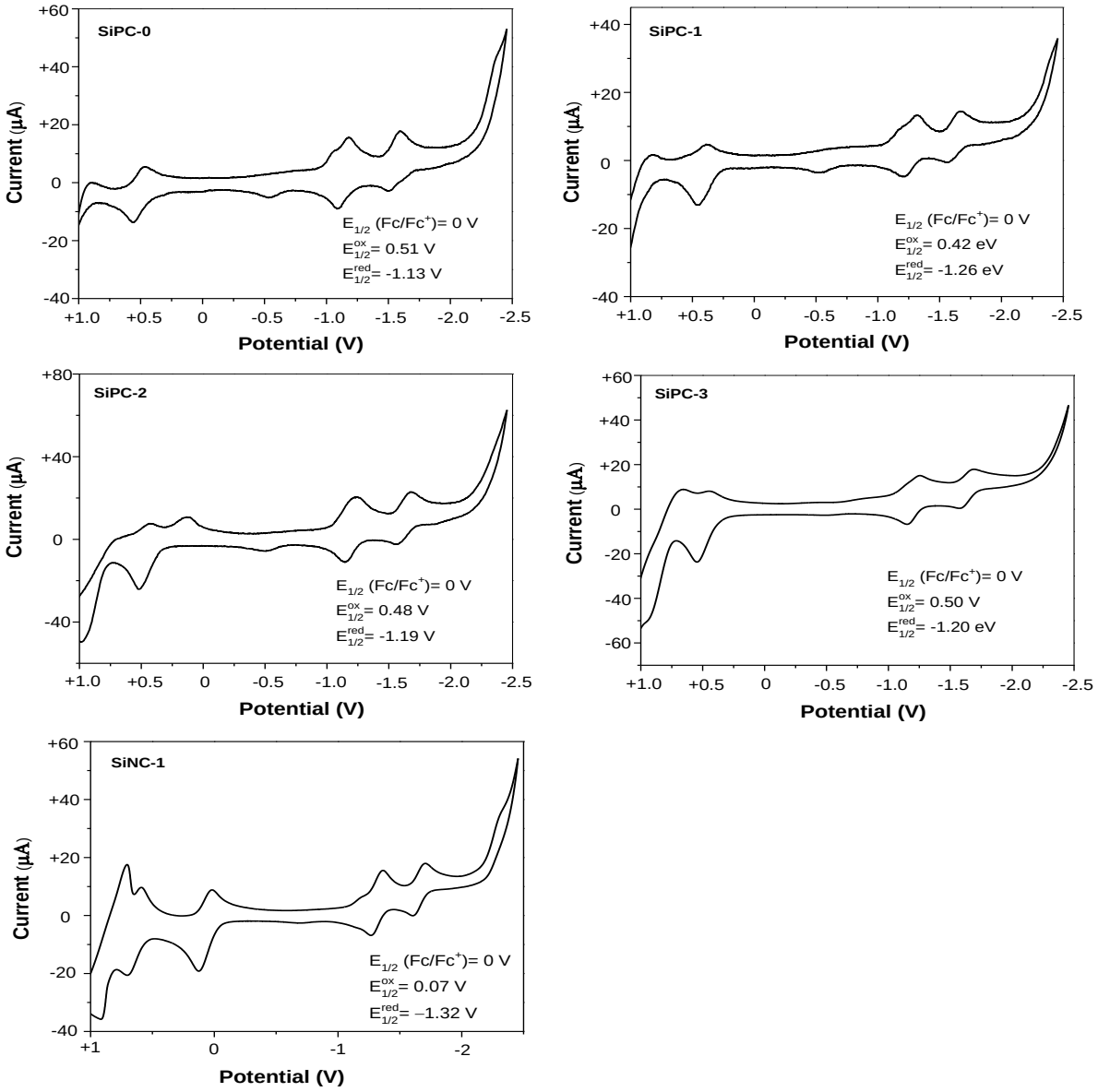

Figure 4-8 The cyclic voltammetry plots of **SiPC-0**, **SiPC-1**, **SiPC-2**, **SiPC-3**, and **SiNC-1**. The potentials are measured vs F_C/F_C^+, using Ag/AgCl as reference electrode. Ferrocene was measured separately.[182,186]

4.3.2 The optical investigation by UV-Vis absorption

a) Absorption in solution

The normalized absorption spectra of **SiPC-0**, **SiPC-1**, **SiPC-2**, **SiPC-3** and **SiNC-1** in solution state are shown in **Figure 4-9**. It demonstrates that the spectra of all **SiPCs** combine the absorption features of both silicon-phthalocyanine (B-band: 300–450 nm and Q-band:

600–730 nm) and the ligand pyrene (300–400 nm). The Q-band with a peak around 696 nm is much stronger than the B-band with a peak around 350 nm, showing a high intensity. This phenomenon is similar to the reported work.[193] Interestingly, **SiPC-0** exhibits a slightly broader B-band compared to **SiPC-1**, **SiPC-2**, and **SiPC-3**, possibly caused by a stronger face– to –face interaction between the pyrene groups and the PC ring in the case of **SiPC-0**.

Most significantly, all **SiPCs** examined have a strong red shift compared to other axial substituents in previous reports.[137,143,194] In Honda's work, employing two trihexylsilyl oxide groups in the ligand position of Si core, the characteristic absorption region of SiPC is at around 650 nm to 700 nm, while for our case it shows a range of 550 nm to 735 nm. This red shift can be explained by π–π interactions between the planar face of PCs and the pyrene group, effectively lowering the band gap. With the pyrene moiety in the axial ligand position, the tendency to form intermolecular aggregates is likely to be reduced, as extensive aggregation would lead to fluorescence quenching and a broadened, blue-shifted Q-band absorption.

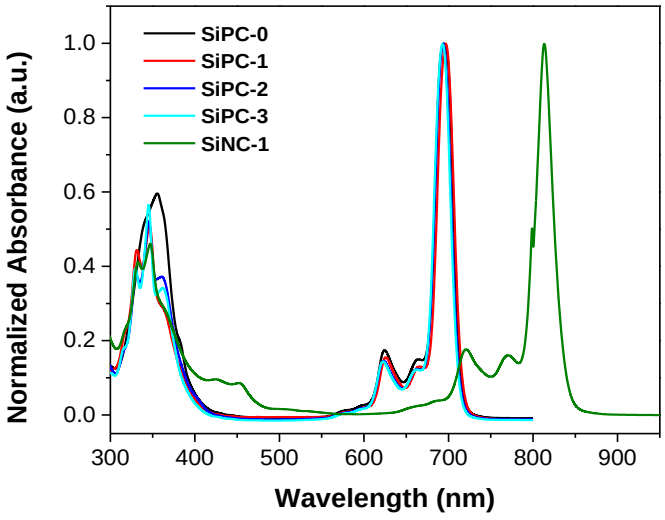

Figure 4-9 Normalized absorption spectra of pristine **SiPC-0**, **SiPC-1**, **SiPC-2**, **SiPC-3** and **SiNC-1** in solution (CH_2Cl_2).

On the other hand, **SiNC-1** shows a strong red shift compared to **SiPCs**, providing a broader absorption in the near IR region. This is well attributable to the expanded conjugated system, with in turn decreasing molecular HOMO-LUMO bandgap, being consistent with the HOMO

and LUMO energy levels estimated by cyclic voltammetry see **Table 4-1**. **SiNC-1** combines the absorption features of both silicon naphthalocyanine (B-band: 300–500 nm and Q-band: 620–880 nm) and the ligand pyrene (300–400 nm), which also shows a strong red shift compared to other axial substituents.[143]

b) Absorption in solid state

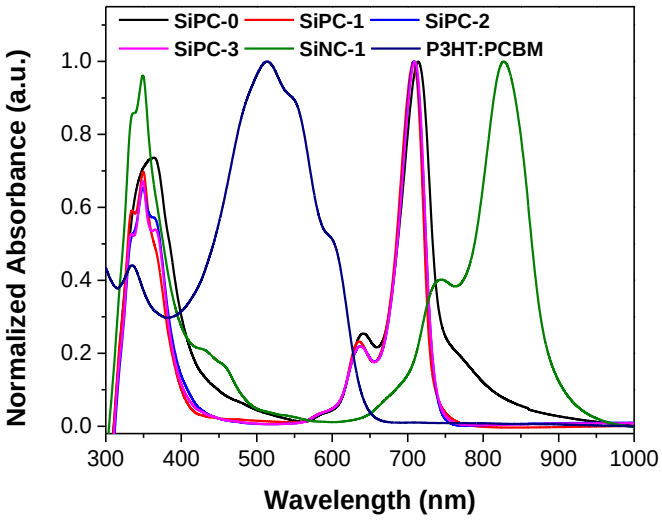

Figure 4-10 Normalized absorption spectra of pristine **SiPC-0**, **SiPC-1**, **SiPC-2**, **SiPC-3**, **SiNC-1**, and P3HT:PCBM in solid state.

The absorption spectra of pristine **SiPC-0**, **SiPC-1**, **SiPC-2**, **SiPC-3** and **SiNC-1** in thin films are shown in **Figure 4-10**. For **SiPC-1**, **SiPC-2**, and **SiPC-3**, the absorption profiles show a slight red shift compare to those in solution state, while the absorption sharp looks similar for both in solution and in film. In this case, the different length of alkyl chains does not significantly affect the absorption region of the molecule. Interestingly, it demonstrates that the spectrum of **SiPC-0** combines the B-band of 300–550 nm and Q–band of 560–950 nm, exhibiting a much broader absorption range compared to other three dyes. This phenomenon possibly caused by a stronger face– to –face interaction between the pyrene groups and the PC ring in the case of **SiPC-0**. The similar trend was observed for **SiNC-1** absorption, yielding a much broader absorption range and a stronger red shift in solid state compared to that in solution. Most significantly, **SiNC-1** also shows a strong red shift compared to **SiPCs**, providing a broader absorption in the near IR region. This is well attributable to the expanded

conjugated system, with in turn decreasing molecular HOMO-LUMO bandgap, being consistent with the HOMO and LUMO energy levels estimated by cyclic voltammetry.

In order to study whether either **SiPCs** or **SiNC-1** can be widely applied in polymer/fullerene systems, we also added the absorption spectrum of P3HT:PCBM (the most widely studied system) in **Figure 4-10**. As shown, the complementary absorption profiles of **SiPCs** and **SiNC-1**, which do not significantly overlap with that of P3HT:PCBM, promise to allow enhanced solar harvesting in ternary and quaternary systems. Herein, these dye molecules emerge not only suitable HOMO-LUMO band gaps which is matching with that of P3HT and PCBM, but also a complementary absorption windows with P3HT/PCBM system, so they should work as photosensitizers in P3HT/PCBM base ternary solar cell system.

4.4 Conclusion

In this chapter, substitution of silicon phthalocyanine and naphthalocyanine opens a possibility to modify the chemical, electronic, and optical properties. By incorporating of four bulky *tert*-butyl substituents to the periphery position and two pyrene groups in the ligand position, a novel series of silicon phthalocyanines (**SiPC-0**, **SiPC-1**, **SiPC-2**, and **SiPC-3**) with varying the length of alkyl chain between the pyrene ring with PC ring, and one silicon naphthalocyanine (**SiNC-1**) were synthesized according to a simple method and characterized.

All compounds have been investigated by cyclic voltammetry. The results obtained for **SiPCs** reveal that the alkyl chain length between PC rings with the axial substituent pyrene does not change the electronic properties. At the end, four silicon phthalocyanines gain the similar E_{ox}, E_{red} and E_{gap}. Comparing the results with **SiNC-1**, extending of the π-system in **SiNC-1** allows for better electronic communication between the intermolecular moieties, resulting in smaller HOMO−LUMO gaps.

Finally, all synthesized new compounds have been studied by UV-*vis* absorptions both in solution and in solid state. Either **SiPCs** or **SiNC-1** show distinguish absorption

characteristics for both silicon phthalocyanines/naphthalocyanine and pyrene ring. **SiNC-1** shows a strong red shift compared to **SiPCs**, providing a broader absorption in the near IR region, which is consist with the results estimated by cyclic voltammetry. At the same time, much broader absorption profiles were observed for **SiPC-0** and **SiNC-1** in solid state compared to those in solution state. The near IR absorption feature gives **SiPC-0**, **SiPC-1**, **SiPC-2**, **SiPC-3** and **SiNC-1** great potential to apply in ternary or quaternary organic solar cells as dye sensitizers.

Chapter 5

A series of pyrene-substituted silicon phthalocyanine as near–IR sensitizers in organic ternary solar cells

Abstract

An attractive method to broaden the absorption bandwidth of polymer/fullerene based bulk heterojunction (BHJ) solar cells is to blend near IR sensitizers into the host system. Among them, silicon phthalocyanines have attracted wide attention because their complementary absorption characteristics and suitable energy levels. Different axial substitutions were already designed to modify the thermodynamic properties of PCs, but the impact of extending the π-conjugation of the axial ligand on the opto-electronic properties, as a function of the length of the alkyl spacer, has not been investigated yet.

As mentioned in **Chapter 4**, a novel series of pyrene-substituted **SiPCs** (**SiPC-0**, **SiPC-1**, **SiPC-2**, and **SiPC-3**) with varying lengths of alkyl chain tethers were synthesized. In this chapter, the synthesized **SiPCs** are introduced into the P3HT/PCBM matrix, and the corresponding organic ternary devices are fabricated. Moreover, the relationship between the rational structures of dye sensitizer with device performance has been investigated in detail.

The relative results in detail can be found in the following published article:

L. Ke, J. Min, M. Adam, N. Gasparini, Y. Hou, J. D. Perea, W. Chen, H. Zhang, S. Fladischer, A. C. Sale, E. Spiecker, R. R. Tykwinski, C. J. Brabec and T. Ameri, A series of novel pyrene-substituted silicon phthalocyanines as near-IR sensitizers in organic ternary solar cells: Synthesis and device fabrication, *Adv. Energy Mater.* **2016**, *6*, 1502355.

5.1 Introduction

As mentioned in **Chapter 2**, to overcome absorption limitation in organic photovoltaic (OPV), the concept of ternary sensitization cells has been introduced. Among them, dye sensitized ternary solar cells have already attracted significant attention because they are easy to adapt in ternaries in respective to microstructure compatibility and spectral sensitivity.[142,195,196] On the other hand, the strong near IR absorption of silicon phthalocyanine, dedicates it as the third component in P3HT:PCBM ternary devices.[137,144,156,194,197] Taking advantage of the hexacoordinate nature of silicon core, it is easy to functionalize the axial positions of Si core.[188] One of the most efficient ways to enhance the light harvesting ability of PCs is the introduction of elongate π-systems in the ligand position of the Si core.

By tailoring and substituting the function groups including axial ligand and periphery position, silicon phthalocyanine molecules can be designed to realize a low band gap, strong and broad absorption, resulting in improved PCEs of devices. Most of the attention was focused on ternary solar cells with symmetrical axially substituted silicon phthalocyanine derivatives, but the impact of respective alkyl chain on the silicon phthalocyanine based ternary solar cells was not studied to sufficient detail. In fact, carefully designing and controlling the position of the alkyl chain length can not only adjust suitable solubility of materials in common used organic solvents but also balance the band structure and morphology in the solid state, and thus improve their photovoltaic properties.

Actually, there are numbers of papers reported the relationship between the alkyl terminal chains length and the device performances. Our group also successfully reported the effects

of alkyl chains on the molecular solubility and blend morphology as well as their performance in BHJ organic solar cell.[198,199] Those studies demonstrated first attempt to study the structure-property relationship based on the star-shaped TPA-based small molecular with various lengths of alkyl end groups (methyl, ethyl, hexyl, and dodecyl), and $DTS(Oct)_2$-$(2T\text{-}DCV\text{-}Me)_2$ with methyl terminal chains and $DTS(Oct)_2$-$(2T\text{-}DCV\text{-}Hex)_2$ with hexyl terminal chain to understand the special effects of alkyl chains on film morphology, charge generation/transport mechanisms in device. Therefore, the utility of length engineering on small molecules is of crucial importance to elucidate structure-property relationships. Insight into such relationships will be beneficial for the judicious choice of new molecules based on appropriate conjugation length for use in OPVs. Although many efforts have already done to investigate the effects of alkyl chains length on physical and photovoltaic performance, almost no paper reports their effect on silicon phthalocyanine derivatives based OSCs, especially using as spacer. Thus, we designed and synthesized four silicon phthalocyanines with varying the alkyl chain length between the axial ligand with the main PC ring. The detail synthesis route is in **Chapter 4**. Their structures are shown in **Scheme 5-1**.

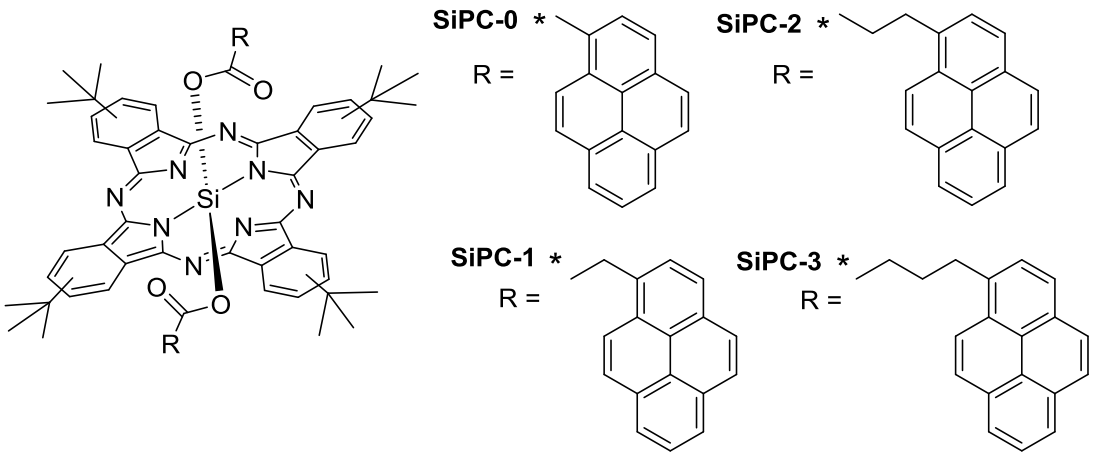

Scheme 5-1 The structures of synthesized **SiPCs**.[182]

5.2 Experiment methods

5.2.1 Solution preparation

Regioregular P3HT was purchased from BASF (Sepiolid P200), PCBM was purchased from Solenne BV and used without further purification. The solutions of P3HT, PCBM and different sensitizers (**SiPC-0**, **SiPC-1**, **SiPC-2**, and **SiPC-3**) were prepared at a concentration of 20 mg mL^{-1} in dichlorobenzene (DCB). All these solutions were left overnight to stir on a hot plate under 85 °C to ensure complete dissolution of the compounds in DCB. The different sensitizer solutions were then mixed separately with P3HT and PCBM solution in controlled amounts to vary the final mount of dyes in the ternary blend film. These mixed solutions were allowed to spin on a hot plate for at least 1.5 h at 85 ^{0}C to ensure that the solutions were fully mixed before blading.

5.2.2 Device fabrication

All devices were fabricated using doctor blading technology under ambient conditions with the structure of **Figure 5-1**. Pre–structured indium tin oxide (ITO) substrates were cleaned with acetone and isopropyl alcohol in an ultrasonic bath for 15 minutes each. After drying, the substrates were successively coated with 40 nm of zinc oxide (ZnO), following by annealing in air on a hot plate at 80 °C for 5 min. Finally a 120 nm thick active layer based on P3HT:sensitizers:PCBM (20 mg/mL) was bladed. The whole stack was annealing on a hot plate at 140 °C for 5 min in the glove box. To complete the fabrication of the devices 10 nm of MoOx and 100 nm of Ag were thermally evaporated through a mask (with a 10.4 mm^2 active area opening) under a vacuum of ~$5x10^{-6}$ mbar.

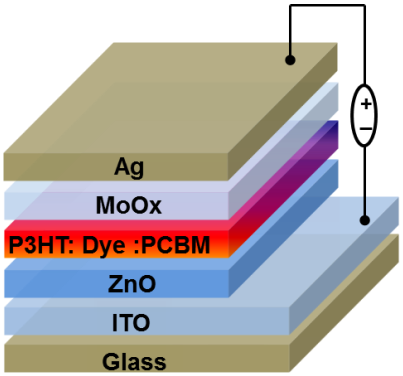

Figure 5-1 Schematic illustration of the employed ternary solar cell architecture.

5.2.3 Acknowledgments

Most of measurements shown in this chapter were done by Lili Ke. At the same time, we thank our colleagues for their contributions to some technique measurements as following. Photoinduced charge carrier extraction by linearly increasing voltage (photo-CELIV) was done by N. Gasparini. Transmission electron microscopy (TEM) was done by S. Fladischer. Atomic force microscopy (AFM) was done by Hong Zhang.

5.3 Results and discussion

5.3.1 Film characterization

a) Absorption Properties of blend ternary films

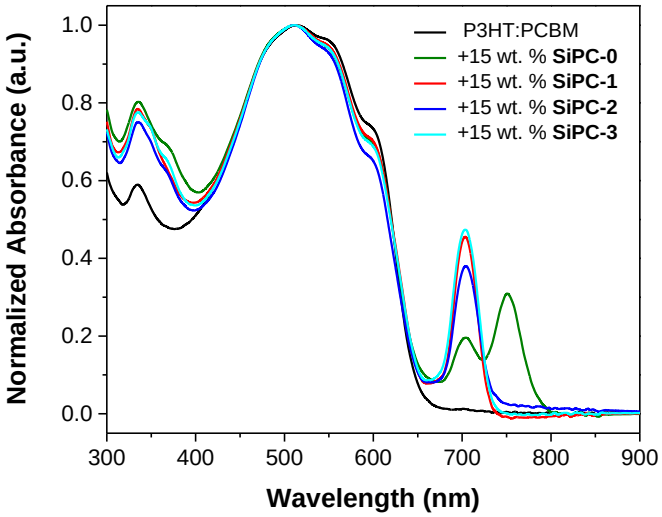

Figure 5-2 Normalized absorption spectra of blended thin films (P3HT:15 wt.% dye:PCBM), dyes: **SiPC-0**, **SiPC-1**, **SiPC-2**, and **SiPC-3**.[182]

The absorption characteristics of ternary films comprised of 15 wt.% sensitizers (**SiPC-0**, **SiPC-1**, **SiPC-2**, and **SiPC-3**) are shown in **Figure 5-2**. A constant film thickness of ca. 120 nm was targeted for all blends to precisely access the changes of absorption profiles and intensities. In the solid state, the distinguished vibration bands at around 500–600 nm were

observed for all films, which are indicative of the crystallization of P3HT. The crystallization of P3HT was not disturbed because the vibrational bands of P3HT were clearly observed even in the presence of **SiPC** molecules. In the range of 300–400 nm, it integrates the absorptions behaviors both fullerene and B-band absorption of phthalocyanines, so slight higher absorption intensity is observed when adding the third component **SiPCs**. Meanwhile, a strong Q-band absorption window was exhibited, from 650 to 800 nm for **SiPC-0** and other three dyes in the range from 650 to 750 nm. Overall, such complementary absorption profiles are promising for enhancing solar harvesting for ternary systems.

b) Surface energy studies

Surface energy plays a decisive role in the segregation tendency of each material when employed in blends according to the previous studies.[138,200] This tendency can cause phase separation, and further impact the location of the sensitizer domains or molecules in the ternary blends. Contact angle measurement by dropping different solvents onto the thin film of material is a useful method to estimate the surface energies of the various materials. According to the SCA20-U software and the Owens-Wendt and Kaelble method,[201] the surface energies of pristine P3HT and PCBM are measured. The values are 23.70 mN m^{-1} and 44.09 mN m^{-1}, respectively, which are consistent with our previous report.[200] In a similar way, the surface energies of **SiPC-0**, **SiPC-1**, **SiPC-2**, and **SiPC-3** are measured and listed in **Table 5-1**. The values are between 27.24 and 28.87 mN m^{-1}, which are positioned close to the value of P3HT but generally in between P3HT and PCBM host materials. According to the method introduced in **Chapter 3**, the wetting coefficient of these four **SiPCs** in blends of materials P3HT and PCBM can be calculated, as listed in **Table 5-1**.

As reported, C will be located in domains of A if the wetting coefficient is larger than unity (ω_C>1), and if ω_C < -1 it will be located in domains of B. Consequently, C will be located at the interface of A and B for -1 <ω_C< 1.[200] Herein, it suggests that the sensitizer molecules **SiPC-0**, **SiPC-1**, **SiPC-2**, and **SiPC-3** are likely to be embedded at the interface of P3HT:PCBM with a clear tendency to arrange around P3HT because the calculated values

between 0.66 and 0.98.

Table 5-1 Surface energy, wetting coefficient and predicted location of sensitizers **SiPCs** within the P3HT:PCBM matrices.[182]

Materials	Surface energy ($mN\ m^{-1}$)	Wetting coefficient (ω_C)	Predicted location of **SiPCs** in the blends
SiPC-0	27.24	0.66	interface
SiPC-1	26.94	0.69	interface
SiPC-2	26.27	0.75	interface
SiPC-3	23.87	0.98	interface

c) Film morphology

Atomic force microscopy (AFM): Figure 5-3 shows the surface morphologies investigated by atomic force microscopy (AFM). The surface of reference P3HT:PCBM film is relatively smooth with a root-mean-square RMS of 1.031 in an area of 5×5 μm, and the surface was slightly smoother and remained homogeneous by the addition of 15 wt.% different sensitizers. The ternary films have the RMS of 0.959, 0.963, 0.899, and 0.898 nm, respectively. The similar RMS values in comparison to the binary film indicate that the addition of **SiPC** does not cause any phase separation and no obvious morphology modifications. This result further suggests that **SiPCs** are highly compatible to P3HT/PCBM host matrix without destroying the single phase domains, should be a potential photosensitivity in P3HT:PCBM based ternary solar cells.

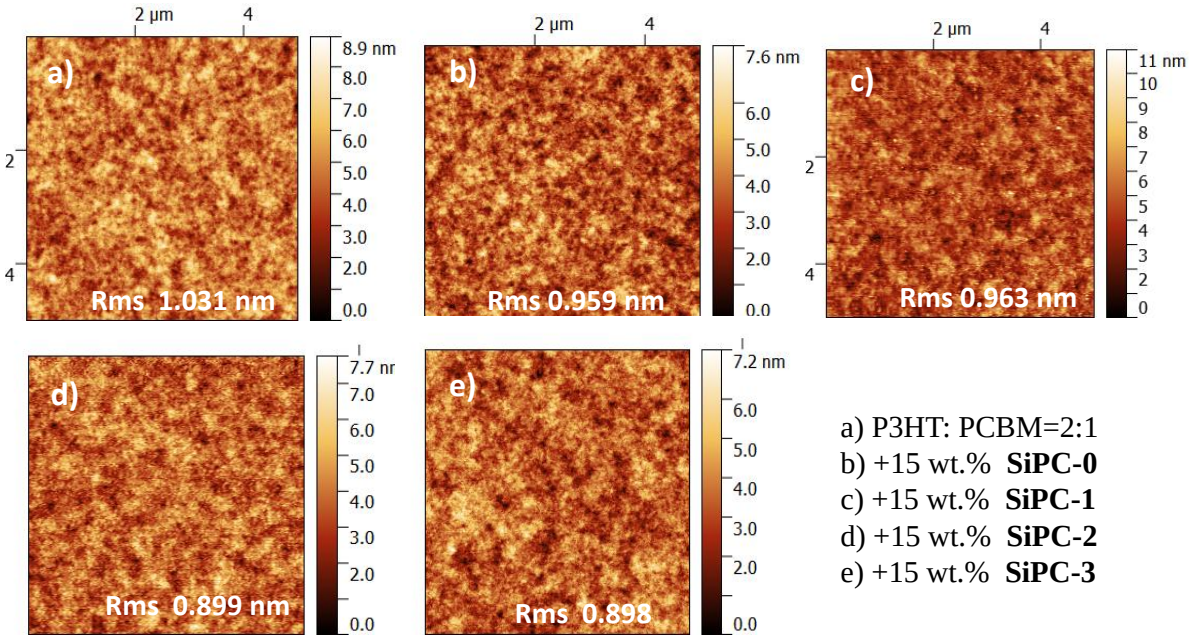

Figure 5-3 Surface topographic AFM images (Size: 5×5 μm^2) of a) binary P3HT:$PC_{61}BM$ film, and ternary blend films with 15 wt.% sensitizer b) **SiPC-0**, c) **SiPC-1**, d) **SiPC-2**, and e) **SiPC-3**.[182]

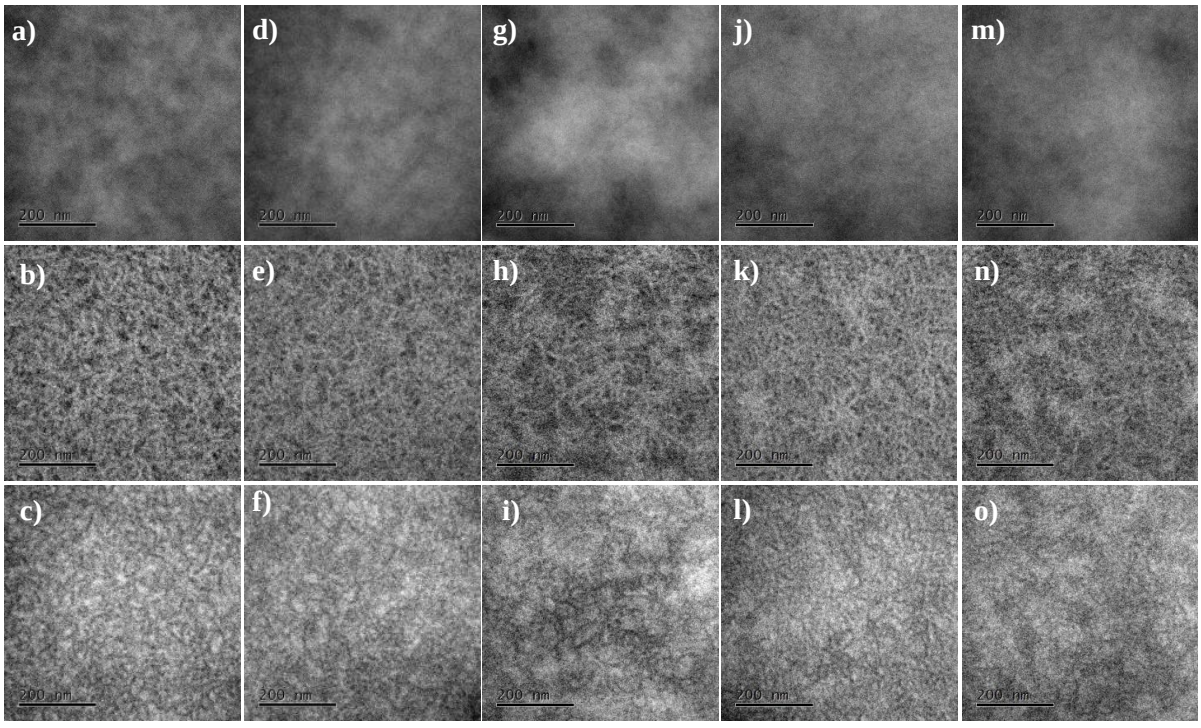

Figure 5-4 TEM bright field images (top row) and elemental maps based on energy filtered TEM (EFTEM) imaging of sulfur (center row) and of carbon (bottom row): binary P3HT:$PC_{61}BM$ film (a–c), and ternary films blended with 15 wt.% sensitizer **SiPC-0** (d–f),

SiPC-1 (g–i), **SiPC-2** (j–l), and **SiPC-3** (m–o).[182]

Transmission electron microscopy (TEM): TEM investigations were performed to get detail information about the morphology.[202] **Figure 5-4** shows TEM bright field images as well as elemental maps based on energy filtered TEM (EFTEM) imaging of sulfur (S) using the S L edge and of carbon (C) using the C K edge for binary and ternary (the dye content is 15 wt.%) films. It is feasible to distinguish P3HT from the other components using the sulfur signal because only P3HT comprises sulfur. The carbon signal can be used to represent PCBM due to the difference of the carbon content of PCBM (81.8 at %) in comparison to P3HT (40.0 at %), **SiPC-0** (50.9 at %), **SiPC-1** (50.3 at %), **SiPC-2** (49.7 at %) and **SiPC-3** (49.2 at %) The Si as well as the N signals of SiPc were too small for EFTEM imaging. By comparing all images, the morphology is preserved even at high sensitizer ratios. The P3HT fibers of the binary films still exist in the ternary cases.

5.3.2 Photovoltaic properties of BHJ devices

Different contents of synthesized **SiPCs** were implemented into P3HT:PCBM system as near IR photosensitizers. The schematic of the inverted devices was depicted in **Figure 5-1**, featuring ZnO as the electron-transporting layer, MoO_X as the hole-transporting layer, and the air stable, high work function metal Ag as the anodic electrode for hole collection. The combined energy band diagram of the fabricated devices are shown in **Figure 5-5**, with HOMO and LUMO values of **SiPCs** calculated from cyclic voltammetry potentials (See **Table 4-1**) and, those of P3HT and PCBM are extracted from previous reports.[81,203] It forms a cascade alignment energy level for the third component used in ternary systems.

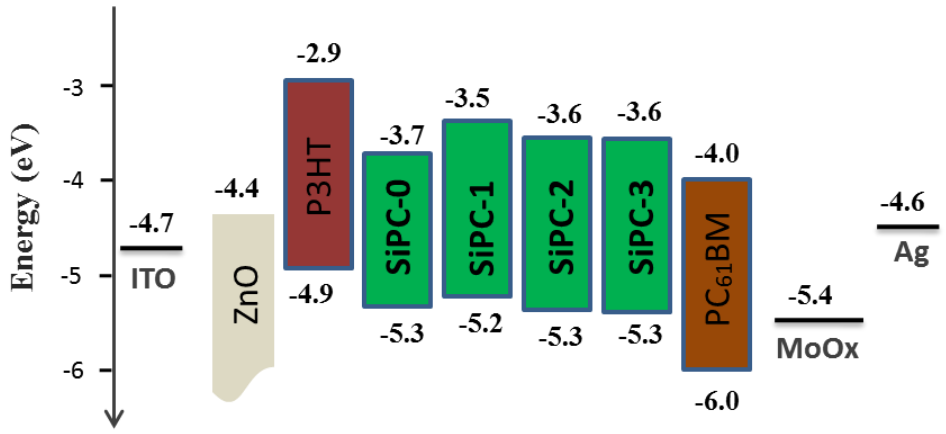

Figure 5-5 The schematic energy band diagram.[182]

In order to certify whether it can form a cascade charge transfer process or not after adding **SiPCs** into P3HT/PCBM matrix, we tested the corresponding binary devices. Because all **SiPCs** molecules have the similar HOMO and LUMO values, it only chooses one of them to give a try. As shown in **Figure 5-6** and **Table 5-2**, **SiPC-1** works well for either using as donor in **SiPC-1**:PCBM binary devices or using as acceptor in P3HT:**SiPC-1** binary device. It means that **SiPCs** molecules can not only transfer hole to P3HT but also can transfer electron to PCBM. Herein, **SiPCs** using as photosensitizer in P3HT:PCBM based ternary devices can form a cascade charge transfer process, and further facilities the charge transfer/transport, which will be decried later in photophysical study part.

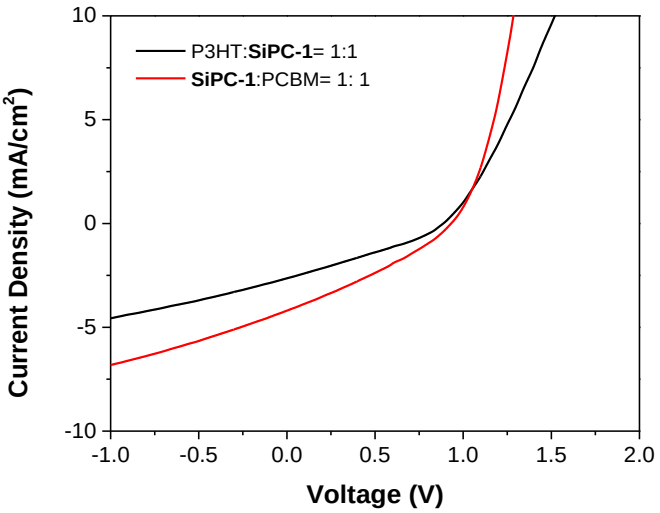

Figure 5-6 *J–V* curves of P3HT:**SiPC-1** and **SiPC-1**:PCBM controlled binary devices.

Table 5-2 Device photovoltaic parameters of P3HT:**SiPC-1** and **SiPC-1**:PCBM controlled binary devices under AM1.5 G, 100 mW cm^{-2}

	V_{OC} [V]	J_{SC} [mA cm^{-2}]	*FF* [%]	*Eff.* [%]
P3HT:**SiPC-1**=1:1	0.89	2.94	28.97	0.76
SiPC-1:PCBM=1:1	0.92	4.23	30.62	1.19

The *J–V* analysis of the binary reference as well as ternary devices varying contents of **SiPCs** are shown in **Figure 5-7** and summarized in **Table 5-3**. By comparing with the state of the art, the efficiency of the P3HT:PCBM reference was rather moderate with a PCE≈2.73% due to the different experiment conditions and material sources. Indeed using the most reported P3HT:PCBM ratio of 1:1, we observed a significant drop in the EQE at the P3HT absorption region by the addition of **SiPCs**. Thus, we used the P3HT:PCBM ratio of 2:1, which was the optimized ratio for the ternary devices. However, we went forward to prove the concept of near IR sensitizing effect of P3HT:PCBM cells.

As expected, the additions of **SiPC-0**, **SiPC-1**, **SiPC-2**, and **SiPC-3** result in increased J_{SC}. This improvement stems from the extended absorption in the near IR region, producing a significantly higher number of photo–generated carriers. Sensitization is most efficient up to 15 wt.% and starts to level out beyond 20 wt.%. For **SiPC-0** as the sensitizer, J_{SC} increases by approximately 25 wt.% from 8.22 to 10.42 mA cm^{-2}, which is slightly better than for the other three dyes (**Table 5-3**). This can be explained by the broader absorption in the near IR region for **SiPC-0** compare to other **SiPCs**, as described in **Figure 4-9.**

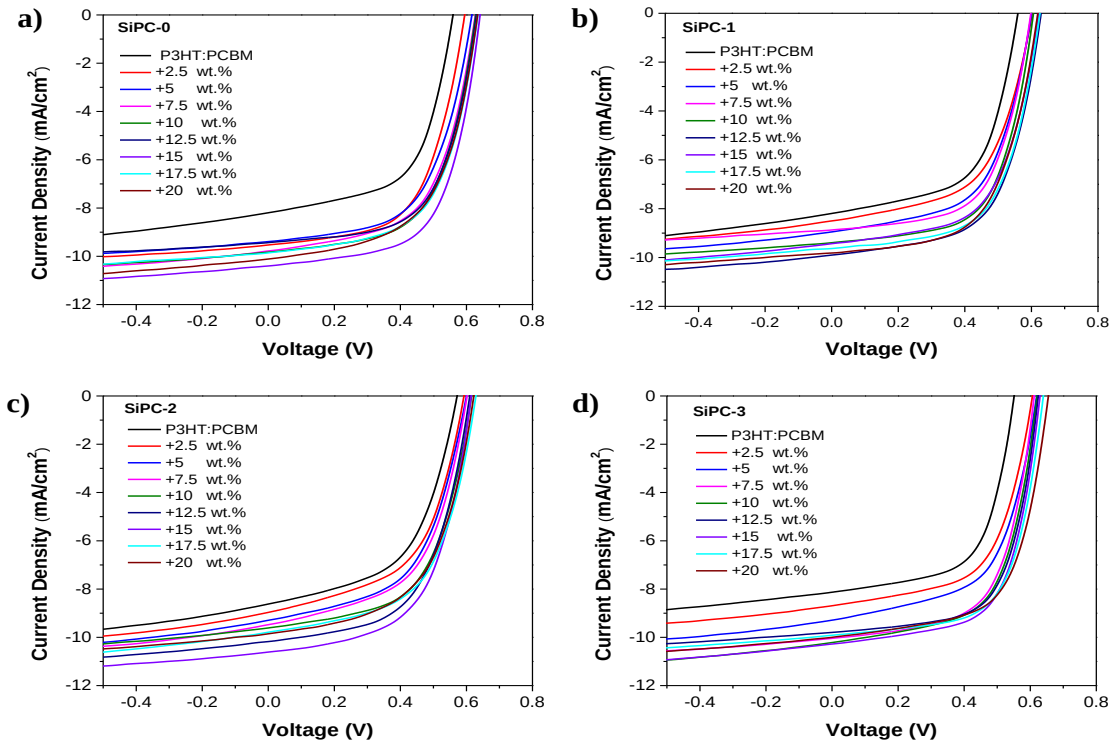

Figure 5-7 Current density *vs* voltage curves for binary and ternary devices by the addition of different contents of **SiPCs** into P3HT:PCBM matrix.[182]

Interestingly, the *FF* increases initially with higher **SiPCs** ratios and levels out at the content around 15 wt.%, showing a similar upward trend with J_{SC}. Over the whole range tested, higher *FF* than for the binary reference device is observed for all **SiPCs**. As for the ternary P3HT:**SiPC-3**:PCBM, *FF* improves around 10% even at the high content of 20 wt.% as compared to the binary system (**Table 5-3**). Slightly better fill factor is observed for **SiPC-3** than other **SiPCs** based ternary systems. A possible explanation could be the weaker intramolecular interactions as well as the higher solubility **SiPC-3**, reducing the trend to form aggregation.

We also found that the V_{OC} increases from 0.56 V for the reference device to 0.65 V by the addition of **SiPCs**. There are many possible factors to influence on V_{OC} in different degrees, such as bulk morphology, CT state, energetic disorder and so on. As shown in **Figure 5-4**, the morphology by the incorporation of **SiPCs** did not show significant differences. Hence, the origin of the gradual increase in V_{OC} probably mainly originates from the changing electronic

structure of the blend as function of composition.[119] It can be also attributed to the decrease of non-radiative recombination pathways between the P3HT and PCBM regions as the sensitizer is intercalated directly at the heterojunction between P3HT and PCBM.[204]

Table 5-3 Device photovoltaic parameters of the P3HT:**SiPCs**:PCBM with different **SiPCs** contents under AM1.5 G, 100 mW cm^{-2}.[182]

Sensitizer	**SiPC** content [wt.%][a]	V_{OC} [V]	J_{SC} [mA cm^{-2}]	*FF* [%]	*Eff.* [%]
	0	0.56	8.22	59.27	2.73 (2.6±0.15)
SiPC-0	2.5	0.59	8.75	59.93	3.17 (3.2±0.18)
	5	0.62	9.40	58.53	3.41 (3.3±0.11)
	7.5	0.62	9.79	59.77	3.63(3.53±0.10)
	10	0.62	9.84	61.32	3.75(3.58±0.16)
	12.5	0.62	9.45	62.72	3.68(3.49±0.19)
	15	0.62	10.42	60.60	3.92(3.90±0.25)
	17.5	0.62	9.88	61.57	3.78(3.55±0.23)
	20	0.62	10.13	59.43	3.74(3.45±0.28)
SiPC-1	2.5	0.56	8.22	59.27	2.73(2.60±0.15)
	5	0.59	8.53	58.57	2.95(2.75±0.20)
	7.5	0.59	8.97	59.63	3.15(3.00±0.15)
	10	0.59	9.15	59.84	3.23(3.15±0.12)
	12.5	0.62	9.63	60.89	3.64(3.40±0.20)
	15	0.62	9.91	61.58	3.79(3.60±0.19)
	17.5	0.62	9.45	60.06	3.52(3.35±0.15)
	20	0.62	9.64	62.33	3.73 (3.65±0.08)
SiPC-2	2.5	0.59	8.99	56.59	3.00 (2.95±0.08)
	5	0.59	9.32	58.21	3.19 (3.13±0.13)
	7.5	0.59	9.49	59.02	3.30 (3.15±0.15)
	10	0.62	9.63	60.10	3.58 (3.44±0.14)
	12.5	0.62	10.19	59.09	3.65 (3.47±0.14)
	15	0.62	9.99	61.46	3.80 (3.61±0.21)
	17.5	0.62	9.81	60.42	3.67 (3.52±0.14)
	20	0.62	9.87	58.75	3.59 (3.46±0.15)
SiPC-4	2.5	0.62	8.71	58.36	3.16 (3.15±0.18)
	5	0.62	9.31	58.71	3.39 (3.29±0.10)

7.5	0.62	10.05	61.91	3.86 (3.72±0.20)
10	0.62	10.23	61.91	3.93 (3.83±0.33)
12.5	0.62	9.81	65.28	3.98 (3.80±0.18)
15	0.62	10.29	64.76	4.13 (3.87±0.26)
17.5	0.65	9.93	63.71	4.12 (4.02±0.10)
20	0.65	10.02	63.54	4.14 (4.10±0.18)

[a]Note: The weight percent is referred to P3HT. The ratio of P3HT:PCBM is 2:1 for all devices. The values are average over 10 devices for each ratio component.

In summary, the best performance is achieved for **SiPC-3** ternaries with a J_{SC} of 10.02 mA cm^{-2}, V_{OC} of 0.65 V, *FF* of 63.54%, and a PCE of 4.14%, resembling an improvement of 51.65% over the reference cell. Maximum PCEs obtained for **SiPC-0**, **SiPC-1**, and **SiPC-2** as photosensitizers are 3.92%, 3.79%, and 3.81%, respectively. As shown in **Table 5-3**, all device parameters experience a relevant improvement even for high sensitizer contents (≈20 wt.% referred to P3HT). This high **SiPCs** addition without destroy the device performance and morphology is different from previous studies, which reported on unfunctionalized **SiPCs** reaching maximum PCE at sensitizer ratio of only 4.8 wt.%. According to Lim et al,[143] four bulky tert-butyl substituents on the periphery of **SiPCs** have a direct impact on the dye molecule incorporation, allowing incorporating larger weight fractions of dye molecules before the morphology of the ternary device is disrupted.

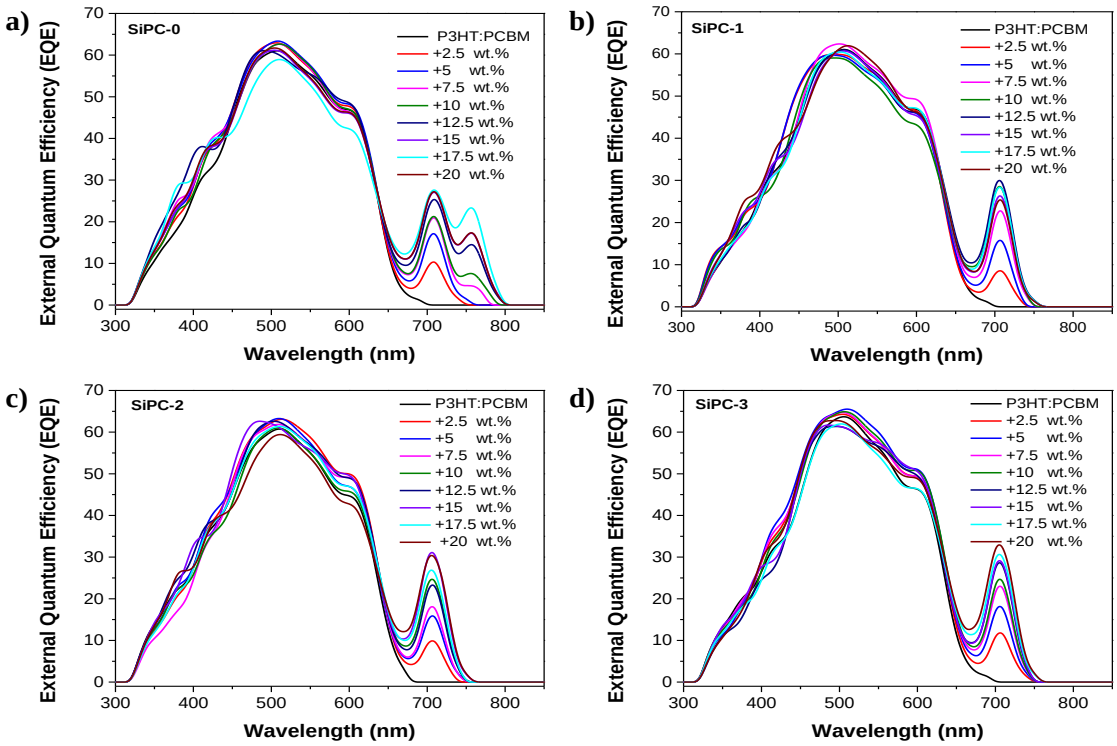

Figure 5-8 EQE spectra of P3HT:PCBM based ternary devices with **SiPCs** at different ratios.[182]

In order to prove the contribution of the sensitizer in solar harvesting and photocurrent generation, external quantum efficiency (EQE) measurements were performed. The EQE spectra for P3HT:PCBM binary and ternary cells with different **SiPCs** and sensitizer ratios are shown in **Figure 5-8.** It was found that the EQE peak increased with increasing **SiPCs** ratio in the near IR region from 650 nm to 800 nm. For example, integrating of this region suggests that the contribution of 15 wt.% of **SiPC-3** results in a J_{SC} enhancement by approximately 25%. Although the relative weight fraction of P3HT is reduced in the photoactive layer for a constant thickness, there is no obvious drop of the EQE in the P3HT absorption part observed even at very high **SiPCs** ratios of 15 wt.%. A possible explanation could be the improvement of the charge transfer and transport by the addition of **SiPCs**, which will be discussed in detail later in the Photo-CELIV part. On the other hand, another reason should be the relatively stable morphology, because the P3HT fibers still exist even in ternary system with high ratio of **SiPCs**, as shown in **Figure 5-4**.

For **SiPC-0** blend ternary devices, an red shift of approximately 50 nm in the near IR region is registered when the dye content exceeds 5 wt.%, allowing further dye addition to significantly improve the photocurrent. This is highly in agreement with the red shift absorption profiles found in both pristine **SiPC-0** and blend ternary thin films as discussed before.

5.3.3 Photophysical studies

a) Photoluminescence (PL) quenching

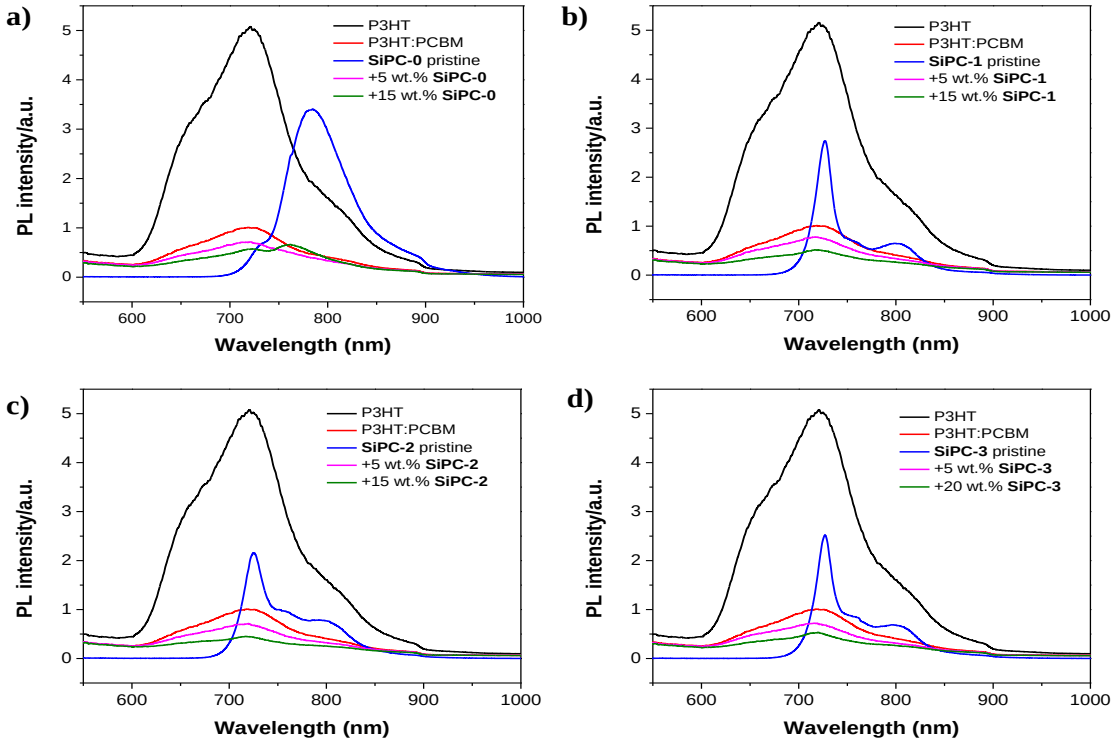

Figure 5-9 PL spectra of pristine P3HT and **SiPCs**, the reference P3HT:PCBM binary, and ternary P3HT: **SiPCs**:PCBM under different **SiPCs** contents.[182]

As shown in **Figure 5-9**, steady state emission spectra of P3HT and **SiPCs** pristine films as well as the reference P3HT:PCBM film and blended ternary thin films were depicted. All samples were excited at 445 nm, except for **SiPCs**, which were excited at 375 nm. In order to eliminate the possible influence of thickness variations on the observed PL intensity, all PL spectra have been normalized to the absorbance of each film at 375 nm or 445 nm, separately,

The **SiPC-0** shows a different PL spectrum compared to the spectra of other **SiPCs**. One main peak around 720 nm and a small shoulder around 800 nm were observed for other **SiPCs**. That is because the PL spectra are somehow the mirror image of the corresponding absorption spectra, exhibiting a main peak often around 700 nm and a small shoulder around 630 nm in the absorption spectra (**Figure 4-9**). While for **SiPC-0**, the case is different since the main absorption peak at 700 nm is broader than the other **SiPCs**.

Taking the PL maximum of P3HT at 720 nm for study, a more efficient quenching for ternary films with a sensitizer ratio of 5 wt.% (≈85%) than for the binary P3HT:PCBM film (≈80%). Interesting, the P3HT PL intensity is quenched further to ≈90% for sensitizer (at a ratio of 15 wt.%) by further increasing the sensitizer content. The peaks associated with **SiPCs** are almost completely quenched, except for **SiPC-0**, which should be due to the stronger intermolecular interaction in the solid state than for the others. Overall, the PL studies indicate the improved charge transfer processes between sensitizers, P3HT, and PCBM.

b) Charge generation

As shown in **Figure 5-10**, the photocurrent density (J_{ph}) as a function of the effective voltage (V_{eff}) was also measured to further study the effect of SiPCs blending on charge generation.[205] The detail evaluation method is as following. Firstly the photocurrent was calculated by the equation $J_{ph}=J_l - J_d$, where J_l and J_d are the current density under illumination at 100 mW cm^{-2} and in the dark, respectively. V_{eff} is given by $V_{eff}=V_0-V$, where V_0 is the compensation voltage defined as $J_{ph}(V_0)=0$, and V is the applied voltage. The *J-V* plots indicated that J_{ph} quickly saturates for V_{eff} >1 V. At full saturation, all generated electron-hole pairs are supposed to be dissociated and collected at the electrodes. In the end, the maximum generation rate of free charge carriers (G_{max}) can be estimated according to $J_{sat}=qG_{max}L$,[206] where q is the electronic charge and L is the active layer thickness. The values of G_{max} for the reference binary and **SiPCs** blended ternary devices are calculated and later listed in the **Table 5-4**. In comparison with the reference binary device, all ternary devices achieve greater G_{max} values. Among them, **SiPC-0** obtain a highest value of 7.80×10^{21} $cm^{-3}s^{-1}$ at a dye

content of 15 wt.%. The trend is consistent with the enhancement of J_{SC} for ternary systems compared to the binary system, indicating more efficient exciton generation and separation in the presence of the sensitizers.

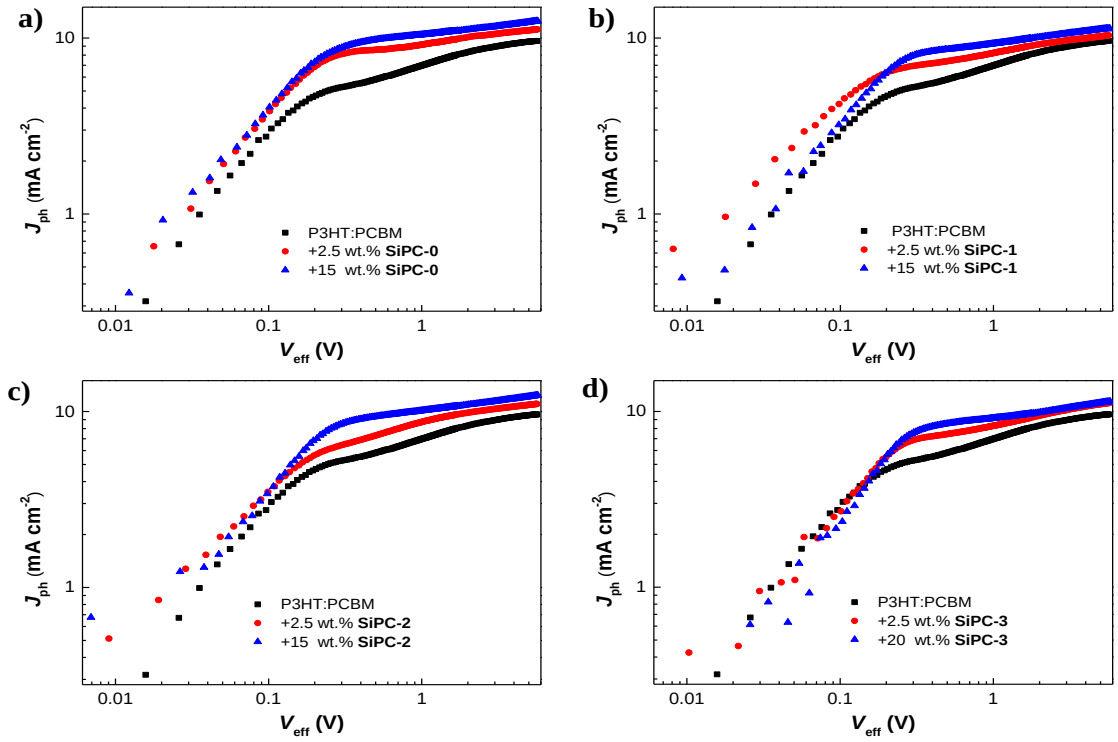

Figure 5-10 Photocurrent density of **SiPCs** based solar cells as a function of the effective voltage under 1 sun illumination.[182]

c) Charge carrier mobility

Furthermore, the charge transport of the aforementioned systems was investigated in detail. By employing the technique of photoinduced charge carrier extraction by linearly increasing voltage (photo-CELIV),[207] the charge carrier mobility (μ) of all devices was investigated. From the measured photocurrent transients, t_{max}, which occurs at the maximum extracted photocurrent, is determined and the charge carrier mobility (μ) is calculated by using the following equation:

$$\mu = \frac{2d^2}{3At_{max}^2\left[1+0.36\frac{\Delta j}{j(0)}\right]} \quad if \quad \Delta j \leq j(0) \qquad (5\text{-}1)$$

Where *d* is the active layer thickness, *A* is the voltage rise speed *A=dU/dt*, *U* is the applied voltage, and *j(0)* is the displacement current.[177,208,209]

The photocurrent transients shown in **Figure 5-11** reveal that t_{max} occurs slightly faster for higher **SiPCs** content than lower **SiPCs** content, and significantly faster than the reference binary device. As exhibited in **Table 5-4**, the calculated average μ increases with increasing **SiPCs** content. The best one is achieved for **SiPC-3** based device at a surprisingly high dye content of 20 wt.%, with an average value of $(4.32\pm0.4)\times10^{-4}$ $cm^2V^{-1}S^{-1}$. This is highly consistent with the tendency of the fill factor discussed before. This higher μ certainly contributes to the improved carrier transport and carrier extraction behaviors and consequently to a higher photovoltaic performance.

Table 5-4 Device photovoltaic device parameters under AM1.5 G, 100 mW cm^{-2}, maximum rate of free charge carrier generation in saturation regime (G_{max}) and charge carrier mobility (μ) by Photo-CELIV.[182]

Dye	Dye content [wt.%]	V_{OC} [V]	J_{SC} [mA cm^{-2}]	*FF* [%]	*Eff.* [%]	G_{max} [$cm^{-3}s^{-1}$]	μ [$cm^2V^{-1}s^{-1}$]
	0	0.56	8.22	59.27	2.73	6.08×10^{21}	$(1.63\pm0.2)\times10^{-4}$
SiPC-0	15	0.62	10.42	60.60	3.92	7.80×10^{21}	$(3.52\pm0.3)\times10^{-4}$
SiPC-1	15	0.62	9.91	61.58	3.79	7.05×10^{21}	$(3.95\pm0.5)\times10^{-4}$
SiPC-2	15	0.62	9.99	61.46	3.81	7.04×10^{21}	$(3.82\pm0.5)\times10^{-4}$
SiPC-3	20	0.65	10.02	63.54	4.14	7.09×10^{21}	$(4.32\pm0.4)\times10^{-4}$

Overall, the calculated G_{max} and μ values for ternary devices are much higher than the reference binary device. Among them, **SiPC-0** has the higher G_{max}, and **SiPC-3** has the best μ. This trend is similar with that of J_{SC} and FF. One the other hand, the increase mobility is definitely in agreement with the measured EQE spectra, which did not show any drop in P3HT part. In short, incorporating dye sensitizer into the P3HT/PCBM matrix not only facilities the exciton generation and separation, but also improves carrier transport and carrier behaviors. The reasonable explanation should be the suitable HOMO/LUMO values and

complementary absorption features of **SiPCs**, as described in **Chapter 4**.

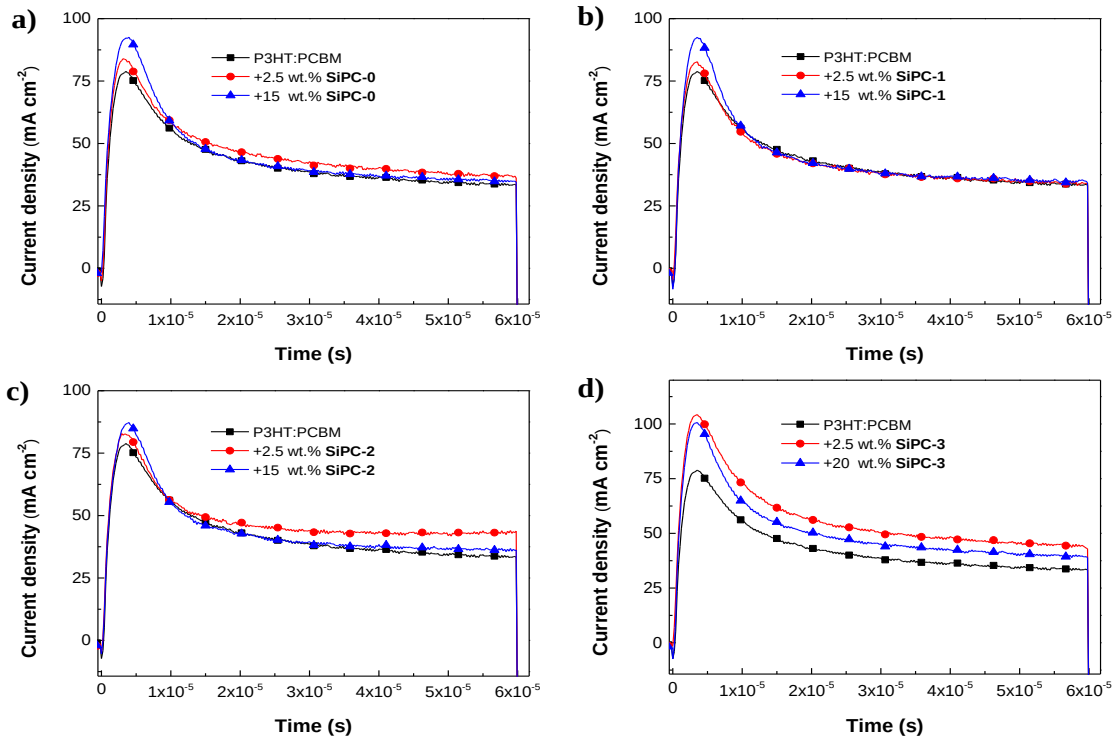

Figure 5-11 Time-dependent photo-CELIV traces of P3HT:PCBM binary and ternary solar cells blended with **SiPCs** after a delay time of 50 μs.[182]

5.4 Conclusion

In this chapter the synthesized **SiPCs** (**SiPC-0**, **SiPC-1**, **SiPC-2**, and **SiPC-3**) were introduced into P3HT/PCBM matrix as near IR photosensitizers in ternary systems. All the compounds exhibited good photosensitivity. **SiPC-0**, which has no alkyl chain as linker group, shows a higher J_{SC} as well as a longer generation rate of free change carriers, compared with the other **SiPCs**. However, **SiPC-3**, which has the longest of alkyl chain as linker group, reveals the overall best *FF* and highest charge carrier mobility. The photo sensitization mechanisms were investigated to yield an increase of up to 21.9% of J_{SC}, 16.1% of V_{OC} and 7.2% of *FF*, leading to an improvement of up to 51.6% of PCE for **SiPC-3** based ternary solar cells compare to the reference P3HT:PCBM binary device.

Notably the EQE spectra showed a strong photosensitivity in the near IR region, up to 800

nm for **SiPC-0** and 750 nm for the other **SiPCs**. Through the photocurrent study and Photo-CELIV measurements, an explanation for the enhanced J_{SC} and *FF* could be higher free charge carrier generation rates and mobility for ternary systems, respectively. A cascade charge transfer between P3HT, **SiPCs** and PCBM is proposed by the photoluminescence study. According to AFM and TEM investigations, the morphology was not disturbed even at high content of **SiPCs**, which was consistent with the increased *FF*. Those findings were highly in agreement with the surface energy studies, predicting that **SiPCs** were mainly located at the interface of P3HT and PCBM domains.

In general, material physical properties and their application of **SiPCs** reveal that the alkyl chain length as a spacer between the core and pyrene ring has an impact on blend film absorption profiles and charge carrier mobility, thereby influencing the photovoltaic properties. The current study can provide an effective insight into concept for tailoring efficient dye sensitizers with enhanced device performance. Such relationships between molecular structure and their corresponding opto-electronic characteristics will be beneficial for the judicious choice of new materials with appropriate ligands and alkyl chain lengths for use in organic photovoltaic.

Chapter 6

Panchromatic ternary/quaternary polymer:fullerene solar cells, based on novel SiNC-1 and SiPCs dye sensitizers

Abstract

More efficient light harvesting throughout the whole solar spectrum by introducing third and fourth components offers a new pathway towards development of high efficiency organic solar cells based on polymer/fullerene blends. Recently, dye molecules have been utilized as promising light harvesting photosensitizers. In **Chapter 4**, novel silicon naphthalocyanine (**SiNC-1**) with a broad near IR absorption window was synthesized. Herein, in this chapter, **SiNC-1** is tested in single dye ternary device as an efficient photosensitizer. On the other hand, multi-colored co-sensitized quaternary devices are fabricated, incorporating both **SiNC-1** and a silicon phthalocyanine (**SiPC-0** or **SiPC-1**) as the third/fourth component. Because these two dyes have complementary absorption spectrum, it allows harvesting a broader fraction of the solar spectrum.

The relative results in detail can be found in the following published article:

L. Ke, N. Gasparini, J. Min, H. Zhang, M. Adam, S. Rechberger, K. Forberich, C. Zhang, E. Spiecker, R. R. Tykwinski, C. J. Brabec and T. Ameri, Panchromatic quaternary polymer/fullerene BHJ solar cells, based on the novel silicon naphthalocyanine and silicon phthalocyanine dye sensitizers, *J. Mater. Chem. A*, **2016**, DOI: 10.1039/C6TA08729A.

6.1 Introduction

In recent years, the most thoroughly studied materials for the active layer are blends of P3HT and PCBM, while the narrow absorption window of P3HT limit its further improvement in device performance. Several strategies are current being pursued to optimize absorption in BHJs. Among them, constructing ternary blend based solar cells, by adding a suitable third component into the P3HT:PCBM matrix and processing the solution in a single-step, has been intensively studied.[77,78,80,82-84] Recently, a variety of dye molecules have been designed and synthesized to act as light-harvesting photosensitizer in the longer wavelength region of the spectrum,[142,196] and the photophysics of systems composed of, for example, polymer/dye/fullerene blends have been studied.[79,81] Little is known, however, about the details of the overall charge transfer/transport mechanism and the role of the dye in ternary blends.

Although some dye molecules have successfully been applied for ternary blend systems, the light absorption is always limited in near IR range of 600–850 nm for various dye molecules.[138,144,145,195] A simple and versatile method using multi-colored dye sensitization by multiple dyes is thus desirable, which could increase the visible light absorption through the use of dyes that have complementary spectral features in the near IR region. This concept has been successfully applied in dye-sensitized solar cells (DSSCs), by selecting a suitable co-absorbing material or constructing a dye-bilayer structure stained with two different dyes.[210-215] To date, however, there is only one report of polymer/fullerene BHJ solar cells based on the concept of multi-colored dye sensitization.[140] The limit success of this concept in BHJ solar cells is often the result of unfavorable interactions between different dye

molecules and formation of dye aggregation, which hinders efficient light harvesting in blends and also limits high dye loading.

In this chapter, the synthesized **SiNC-1** including flexible axial ligands was incorporated into ternary devices, offering favorable intermolecular interactions. The broad sensitization range of the new dye, **SiNC-1**, up to 950 nm, was studied as a means to boost efficient light harvesting in ternary blends. On the basis of the detailed analyses, such as PL and photoinduced absorption (PIA) measurement, a definite charge transfer/transport mechanism has been clarified. On the other hand, multi-colored dye sensitized quaternary solar cells were fabricated by employing **SiNC-1** in combination with **SiPC-0** or **SiPC-1** (see **Scheme 6-1**). The device with **SiNC-1** and **SiPC** as co-sensitizers showed enhanced power conversion efficiency compared to that of the individual blend solar cells with a single dye blending.

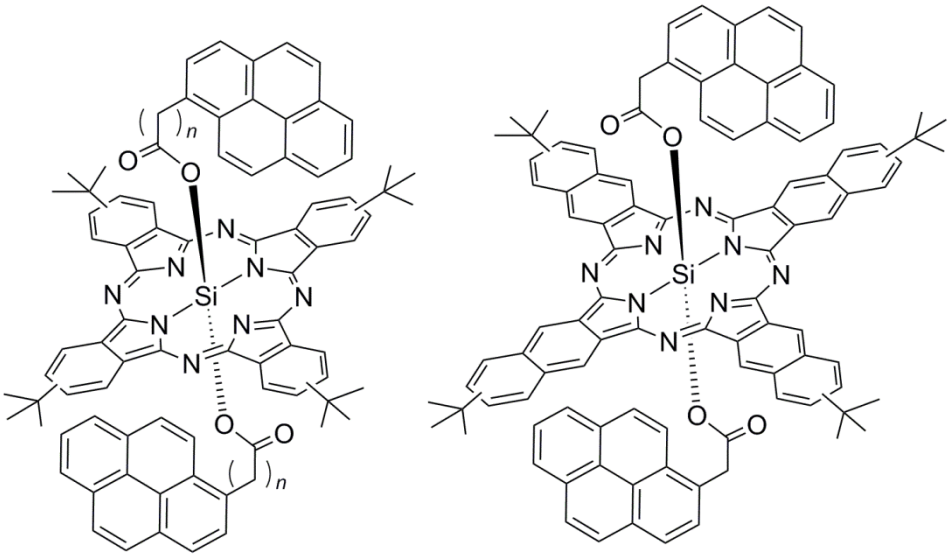

Scheme 6-1 Chemical structures of **SiPC-0**, **SiPC-1**, and **SiNC-1**.[186]

6.2 Experiment methods

6.2.1 Solution preparation

The blend solution was prepared as following: P3HT, PCBM and two sensitizers (**SiPC** and

SiNC-1) were prepared at a concentration of 20 mg/mL in dichlorobenzene, and then left overnight to stir on a hot plate under 85 °C to ensure complete dissolution of all compounds in the solvent. The mixed solutions were allowed to spin on a hot plate for at least 1.5 h at 85 °C to ensure that the solutions were fully mixed before blading.

6.2.2 Device fabrication

All devices were fabricated using doctor–blading under ambient conditions with the inverted structure. Pre–structured indium tin oxide (ITO) substrates were cleaned with acetone and isopropyl alcohol in an ultrasonic bath for 15 minutes each. After drying, the substrates were successively coated with 40 nm of zinc oxide (ZnO), following by annealing in air on a hot plate at 80 °C for 5 min. Finally a 120 nm thick active layer based on P3HT:sensitizers:PCBM (20 mg/mL) was bladed. The whole stack was annealing on a hot plate at 140 °C for 5 min in the glove box. To complete the fabrication of the devices 10 nm of MoOx and 100 nm of Ag were thermally evaporated through a mask (with a 10.4 mm^2 active area opening) under a vacuum of ~$5x10^{-6}$ mbar.

6.2.3 Acknowledgments

Most of measurements shown in this chapter were done by Lili Ke. At the same time, we thank our colleagues for their contributions to some technique measurements as following. Photoinduced charge carrier extraction by linearly increasing voltage (photo-CELIV) was done by N. Gasparini. Transmission electron microscopy (TEM) was done by S. Rechberger. Atomic force microscopy (AFM) was done by H. Zhang. Internal quantum efficiency (EQE) was evaluated by K. Forberich.

6.3 Results and discussion

6.3.1 Ternary BHJ solar cells using SiNC-1 as near IR sensitization

6.3.1.1 Film characterization

a) Absorption properties

Figure 6-1 presented the absorption profiles of ternary films with increasing **SiNC-1** contents. A constant thickness of ca. 120 nm is targeted for all blend films. All films exhibit the distinguished P3HT crystallization vibration bands at around 500–600 nm. Strong absorption window from 650 nm to 950 nm can be exhibited for all ternary film, which is an indicative of **SiNC-1** with near IR absorption profile. The peak related to **SiNC-1** gradually increases when adding more and more **SiNC-1**, while the peak belonged to P3HT part decreases slowly at the beginning and then shows a huge drop when adding 30 wt.% **SiNC-1**. The decreasing from the beginning should due to the dilution of P3HT concentration because the total amount of **SiNC-1** and P3HT keep the same. The main reason for the huge drop is probably due to the destroy morphology of the whole system after 30 wt.% **SiNC-1**, which in further disturb the charge transfer/transport.

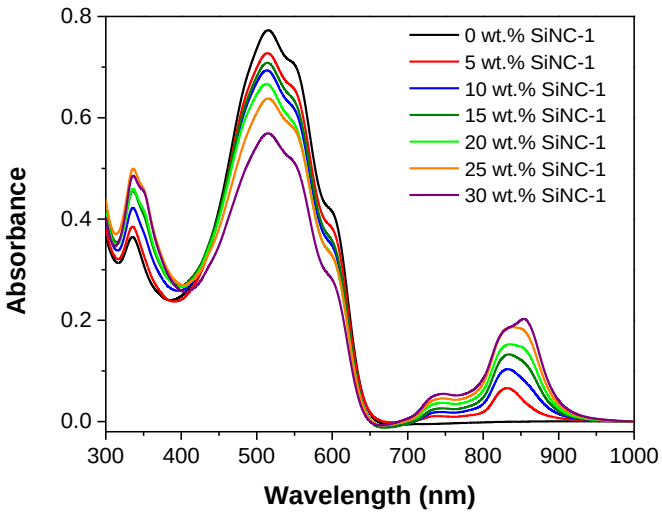

Figure 6-1 Absorption spectra of P3HT:**SiNC-1**:PCBM ternary films with increasing the **SiNC-1** content.[186]

b) Film morphology

In general, the film morphology of bulk heterojunction is needed to be considered as using a third component material in polymer/fullerene blends. Sometimes, the morphology of host system will be destroyed after incorporating a new constituent, in turn, leading to the

decreasing of the device performance.

Atomic force microscopy (AFM): Figure 6-2 showed the surface topographies of active layers investigated by AFM. Both films have similar root-mean-square (RMS) roughness. The RMS value is 1.031 and 0.858 for the binary P3HT:PCBM film and ternary blend film by the addition of 15 wt.% **SiNC-1**. The slight lower RMS for ternary film indicate that **SiNC-1** do not cause any phase separation or any obvious morphology modification, suggesting that **SiNC-1** are highly compatible to the blend of P3HT:PCBM.

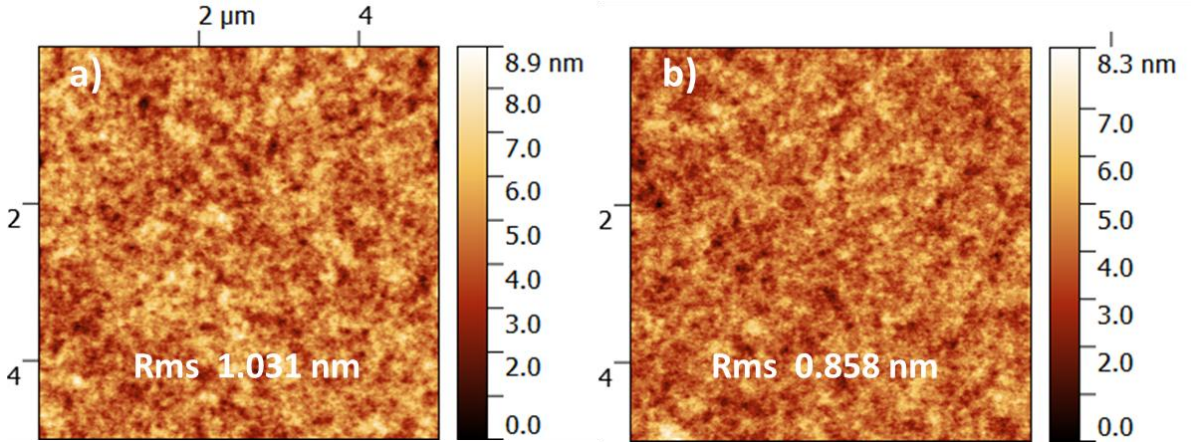

Figure 6-2 Surface topographic AFM images (Size:5×5 µm^2) of a) binary P3HT:PCBM (2:1), b) ternary (15 wt.% **SiNC-1**).[186]

Transmission electron microscopy (TEM): TEM investigations were performed to gain further insights into the morphology. As shown **Figure 6-3**, TEM bright field images as well as elemental maps based on energy filtered TEM (EFTEM) imaging of sulfur (S) using the S L edge and of carbon (C) using the C K edge for P3HT:PCBM binary film and ternary film with 15 wt.% SiNC-1 adding. Similar with test methods shown in **Chapter 5**, the sulfur atoms and the difference of the carbon content can use to distinguish P3HT, PCBM and **SiNC-1**. Comparing the images in **Figure 6-3**, it finds that the morphology is preserved even at high **SiNC-1** loading. The P3HT fibers of the binary films still exist in the ternary case.

Combining the information obtained from AFM and TEM, the morphology of the ternary system and also the P3HT fibers are not destroyed even at high **SiNC-1** loading, which in

further proves that **SiNC-1** is a potential third component.

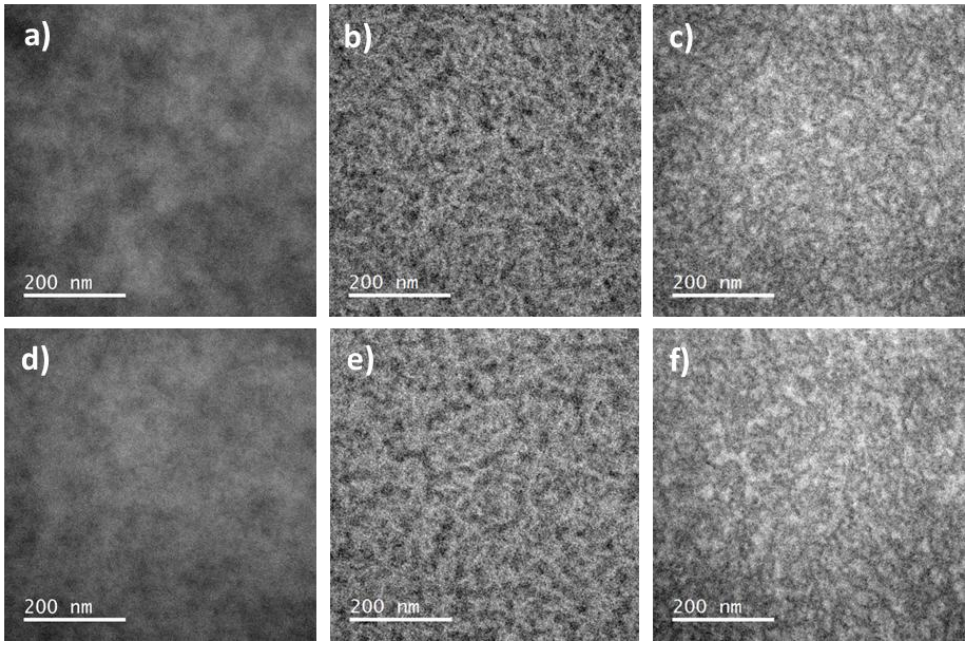

Figure 6-3 TEM bright field images (left row) and elemental maps of sulfur (S L edge, middle row) and of carbon (C K edge, right row): a–c): binary P3HT:PCBM (2:1), d–f): ternary film (15 wt.% **SiNC-1**).[186]

6.3.1.2 Photovoltaic properties

Inverted BHJ ternary solar cells by varying the **SiNC-1** contents were fabricated according to the structure of Glass/ITO/ZnO/P3HT:**SiNC-1**:PCBM/MoOx/Ag. The *J*–*V* characteristics of the ternary cells and the corresponding control P3HT:PCBM binary cell were shown in **Figure 6-4**. The photovoltaic device parameters are further summarized in **Table 6-1**. As expected, the addition of **SiNC-1** results in an increase of J_{SC}. Sensitization turned out to be most efficient at **SiNC-1** concentration of 15 wt.%, leading to almost 10% increase for J_{SC} from 8.83 mA cm^{-2} for the binary control device to 9.66 mA cm^{-2} for ternary based device. For concentrations above 20 wt.%, however, the positive sensitization influence on J_{SC} starts to decline. At low **SiNC-1** content (≤15 wt.%) FF showed also moderate improvement. The latter can be explained based on the fact that no disruptive change in the morphology of ternary blends has been seen, as discussed later in film morphology part. As shown in **Figure 6-3**, P3HT fibers still exist even with 15 wt.% **SiNC-1** loading. Similar to the trend of J_{SC}, FF

started to decrease when **SiNC-1** content is beyond 20 wt.%, suggesting that the sensitizer loading at P3HT/PCBM interface reaches saturation with a content less than 20 wt.%. Previous studies showed that the excess dye sensitizers would not contribute to photocurrent generation if they are located in P3HT or PCBM domains.[138,145]

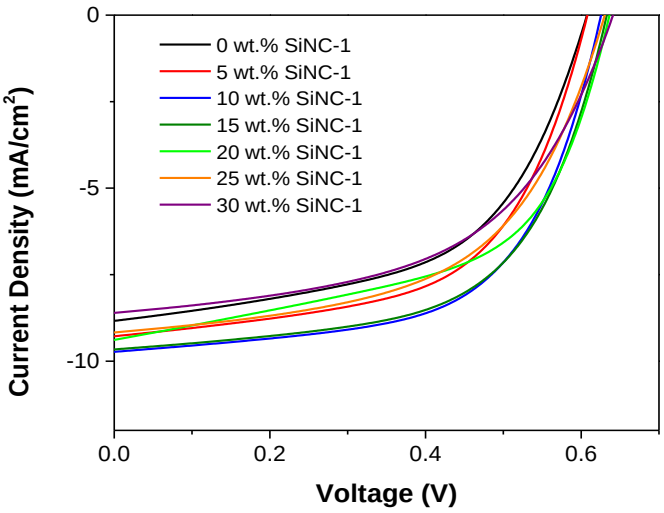

Figure 6-4 *J*–*V* curves of P3HT:PCBM binary device and P3HT:**SiNC-1**:PCBM ternary devices varying **SiNC-1** contents.[186]

As shown, the V_{OC} showed an increase from 0.60 V for the reference device to 0.65 V for the ternary blend with a sensitizer concentration of 10 wt.% and then kept constant. In the end, the ternary solar cells exhibited a substantially improved performance compared to that of the binary control cells. For example, it resulted an increase of 25% in PCE when the SiNC-1 content is 15 wt.%.

Table 6-1 Photovoltaic device parameters of P3HT:**SiNC-1**:PCBM ternary devices by varying the content of **SiNC-1** under AM 1.5G, 100 mW cm^{-2}.[186]

P3HT:**SiNC-1**[wt.%]: PCBM	V_{OC}[V]	J_{SC}[mA cm^{-2}]	J_{SC}/EQE	FF[%]	Eff.[%]
0	0.60	8.83	7.75	56.11	2.97
5	0.60	9.29	8.15	59.01	3.28
10	0.65	9.72	8.53	58.27	3.68

15	0.65	9.66	8.86	57.82	3.63
20	0.65	9.40	8.42	53.73	3.28
25	0.65	9.22	8.42	51.58	3.09
30	0.65	8.61	8.14	52.45	2.93

The external quantum efficiency (EQE) of the corresponding devices were illustrated in **Figure 6-5a**. A broad EQE peak at 650–950 nm was observed for the ternary blend solar cells, corresponding to the absorption of **SiNC-1**. The sensitization effect became stronger when increasing the amount of **SiNC-1**, consistent with the trend seen in the absorption spectra **Figure 6-1**. This increase stems in the near IR region can produce a significantly higher number of photo-generated carriers. The EQE peak associated with P3HT (400–600 nm) features a slight decrease for the **SiNC-1** content less than 15 wt.% and shows a significant drop after the **SiNC-1** content over 20 wt.%. The former can be explained by the stable charge transport of the whole system because the P3HT fibers still exist when adding less than 15 wt.% **SiNC-1** shown in **Figure 6-3** because the crystallization of P3HT is not disturbed. The latter can be explained by the optical loss due to the reduced relative weight fraction of P3HT. On the other hand, it can also be caused by the electrical loss due to the disturb crystallization of P3HT after high **SiNC-1** loading, which in further decrease charge transport of the whole system.

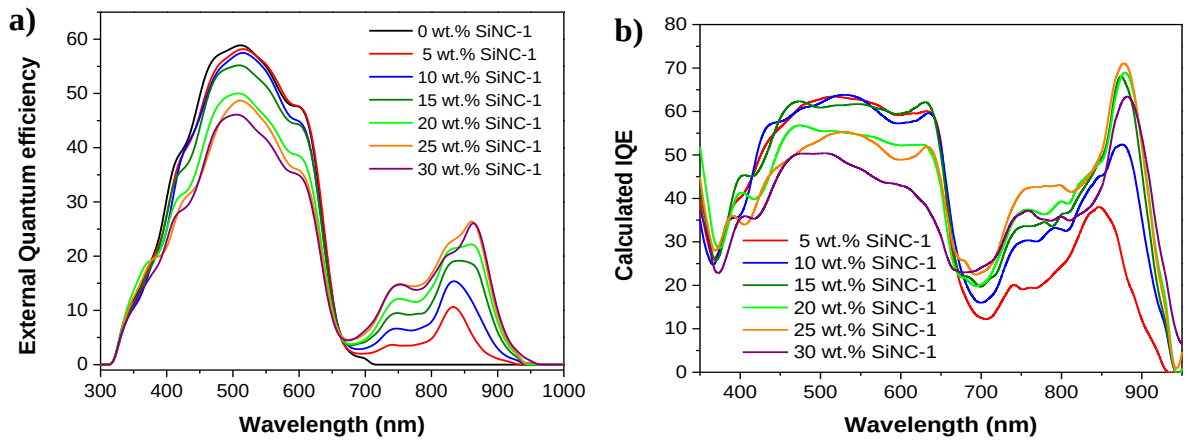

Figure 6-5 a) EQE spectra of the corresponding devices; b) Calculated IQE spectra with

SiNC-1 content from 5 wt.% to 30 wt.%.[186]

In order to evaluate the efficacy of the charge generation and extraction processes, we calculate the internal quantum efficiency (IQE) spectra from the measured EQE spectra according to the following equation.[216]

$$IQE = \frac{EQE}{1-R-T-SPA} \quad (5\text{-}1)$$

Where *R* is the reflection for the total device, and *T* is the corresponding transmission. The *SPA* accounts for the simulated parasitic absorption within the ITO, MoO_X and Ag layers.

The calculated IQE spectra of the **SiNC-1** ternary blend devices by varying **SiNC-1** contents were shown in **Figure 6-5b**. The IQE remains almost constant in the regime where P3HT absorbs when **SiNC-1** contents lower than 15 wt.%. While, a huge photocurrent loss is observed after the concentrations beyond 20 wt.%. This trend is similar to the diminution seen for J_{SC} and FF. As aforementioned, one possible explanation is that the excess **SiNC-1** that desirably need to be located at the interface of P3HT and PCBM, accommodate within the domains of P3HT/PCBM instead, which in turn causes a limitation to the charge transport. Interestingly, it shows a different trend in the near IR region. The IQE features a significant improvement from 5 wt.% to 15 wt.% and levels out beyond 20 wt.%. By forming a mature percolation pathway of **SiNC-1** domains in adjacent to the P3HT crystallites, a parallel-like hole transfer is possibly produced.

In order to verify whether **SiNC-1** is capable to transfer holes by itself, we tested the **SiNC-1**:PCBM binary device. The *J–V* curve and EQE were shown in **Figure 6-6**. The device parameters for **SiNC-1**:PCBM at a ratio of 1: 2 is as following: V_{OC}=0.59 V, J_{SC}= 4.83 mA cm^{-2}, FF=31.89, PCE=0.90 %. The low device efficiency should due to the narrow absorption window of **SiNC-1**. On the basis of these results, it can be concluded that **SiNC-1** is able to transfer holes to the anode by itself to form a parallel-like charge transfer pathway.

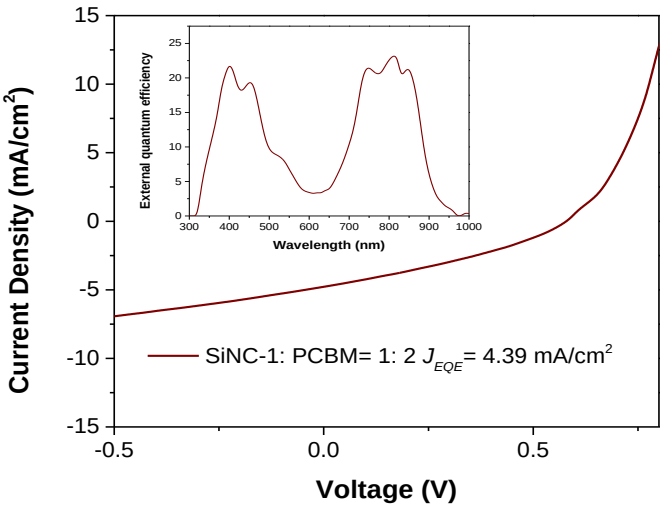

Figure 6-6 The *J–V* curves and EQE spectrum (inside figure) of **SiNC-1**:PCBM binary device.

6.3.1.3 Photophysical studies

a) Photoluminescence (PL) quenching

As shown in **Figure 6-7**, the photoluminescence (PL) of pristine P3HT and **SiNC-1**, the binary blends of P3HT:PCBM and P3HT:**SiNC-1**, and the ternary films with lower and higher **SiNC-1** contents was tested. All samples were excited at 445 nm. After correcting PL spectra according to the absorption and the sensitivity of the sensor, the variation in PL maximum of P3HT at 720 nm indicates that the quenching in ternary films is slightly more efficient with a **SiNC-1** content of 5 wt.% than that of binary P3HT:PCBM film. By increasing **SiNC-1** content, the PL intensity of P3HT is further quenched (over 90% with a **SiNC-1** content of 15 wt.%), meaning that almost all the P3HT excitons are quenched. This trend suggests that a more efficient charge transfer pathway exists in ternary systems compared to binary blends.

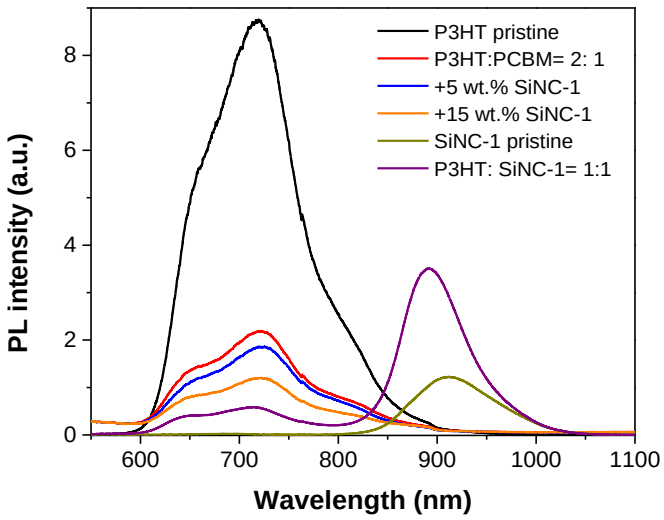

Figure 6-7 PL spectra of pristine P3HT and **SiNC-1** films, P3HT:PCBM and P3HT:**SiNC-1** binary films, and **SiNC-1** and **SiPC-0** based ternary and quaternary films.[186]

b) Energy transfer

Interestingly, as shown in **Figure 6-7**, the PL of P3HT quenches simultaneously by increasing the emission peak of **SiNC-1** in the case of the P3HT:**SiNC-1**=1:1 blend. Hence, PL measurements of other P3HT/**SiNC-1** ratio films were performed to verify this phenomenon. As observed in **Figure 6-8a**, the emission peak of **SiNC-1** becomes larger with increasing P3HT amount even when **SiNC-1** weight ratio decreases, suggesting that there is a non-radiative Förster resonance energy transfer (FRET) between P3HT and **SiNC-1**. As shown in **Figure 6-8b**, there is a strong overlap between donor (P3HT) emission with acceptor (**SiNC-1**) absorption, which fulfills a primary condition for the occurrence of FRET.[217]

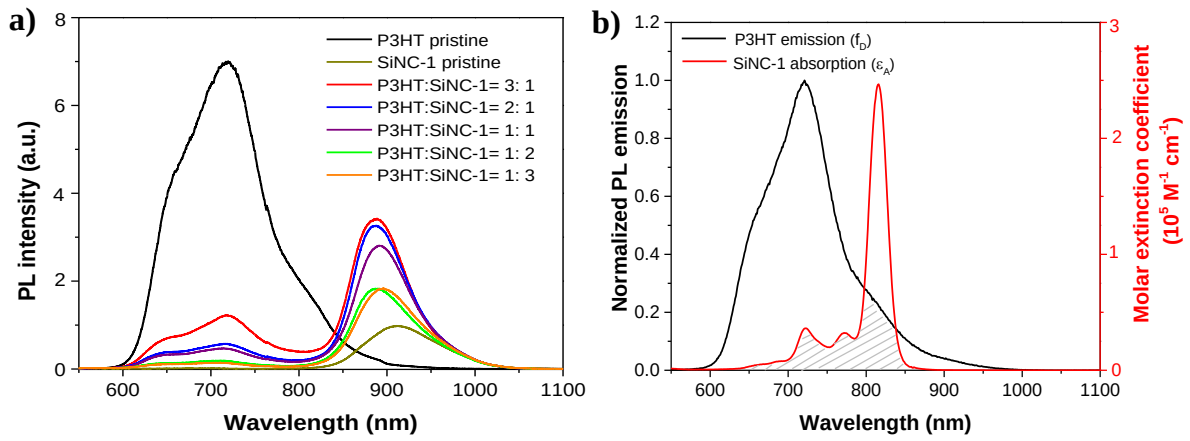

Figure 6-8 a) PL spectra of pristine P3HT and **SiNC-1**, P3HT:**SiNC-1** based binary films varying **SiNC-1** contents.; b) PL emission of P3HT film and extinction coefficient spectrum of **SiNC-1** in dichlorobenzene.[186]

A FRET process between P3HT and polysquaraine dyes in ternary solar cells reported Huang et al. They also provided some experimental evidences to show that FRET enhances the probability of exciton harvesting.[218] Since FRET is a distance-dependent and non-radiative phenomenon, for a favorable system, it is 50% efficient in the donor-acceptor separation distance named as Förster radius (R_0). In order to verify this mechanism in our case, we calculated the Förster radius (R_0) by using the following equations, as previously reported.[217-219]

$$R_0^6 = \frac{9Q_0 \ln(10) k^2 J}{128\pi^5 n^4 N_A} \quad (6\text{-}2)$$

$$J = \int f_D(\lambda)\, \varepsilon_A \lambda^4 d\lambda \quad (6\text{-}3)$$

Where Q_0 is the donor photoluminescence quantum efficiency in the absence of acceptor and can be considered 1% for P3HT. k^2 indicates the dipole orientation factor, which is equal to 2/3 for a random orientation of donor and acceptor molecules. N_A is the Avogadro's number. n is refractive index of the medium, which is approximately 1.4 for organic media. J is the spectral overlap integral and can be calculated by f_D and ε_A, which are the normalized P3HT emission spectrum and **SiNC-1** molar extinction coefficient spectrum.

In the end, R_0 is calculated to be 7 nm, which describes that FRET only acts efficiently between P3HT and **SiNC-1** if the distance between them is 7 nm or less.

c) Photoinduced absorption (PIA)

Normally, steady-state photoinduced absorption (PIA) experiments are utilized to study the charge transfer mechanism. A laser beam is used to excite the molecule and electron-hole pairs are created. Since the HOMO level of **SiNC-1** is similar to that of P3HT, it is hard to be cascaded energy levels from P3HT to **SiNC-1** to PCBM to meet the energetic requirement of an effective ternary system. PIA is recorded for a **SiNC-1** (20 wt.%) based ternary film, further obtaining deeper insights into the charge transfer/transport mechanism in **SiNC-1** ternary blend solar cells

In order to better describe the charge transfer process, the PIA of **SiNC-1**:PCBM binary is also performed. For the PIA experiments, a red pump laser beam (786 nm) is used to selectively excite **SiNC-1** at wavelengths where the P3HT absorption is negligible. PIA of P3HT:PCBM under different laser intensities were measured in order to exclude even the effect of charge transfer (CT) state absorption. As shown in **Figure 6-9**, by using higher laser density, obvious negative peaks at 525 nm, 573 nm, and 623 nm are observed, associating to the bleaching of P3HT ground-state absorption. While, the CT state effect is negligible at laser densities around 14.2 mw cm^{-2}. Herein, all PIA experiments were recorded at this laser light intensity.

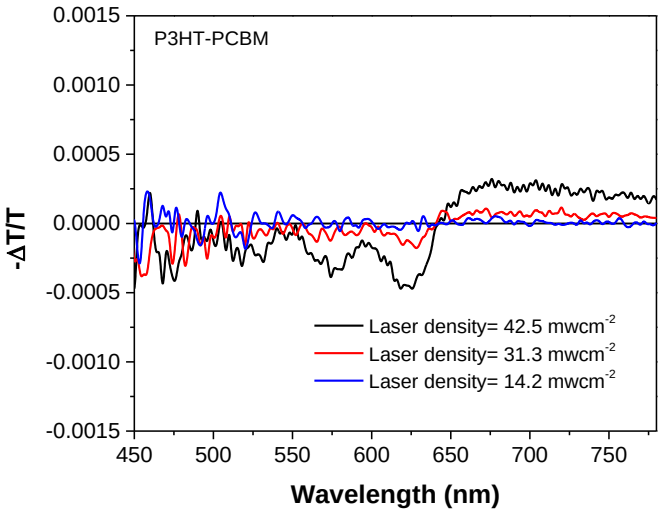

Figure 6-9 PIA spectra recorded at 6.8 mw cm^{-2} light density under different laser intensities.[186]

The polaron formation and polaron features of the pristine P3HT, **SiNC-1** were pre-examined by measuring the photoabsorption of the corresponding iodine doped films. The halogen doping is one of the most widely used doping methods. Particular doping the molecule with iodine induces a strong change in conductivity. By using two different doping methods shown in **Figure 6-10**, the peak position of the positive polarons formed in P3HT, **SiNC-1** and **SiPC-0** films are clearly depicted. The slight difference of two methods can be explained by that the population of polarons and bipolarons increase as the doping levels increase.[220]

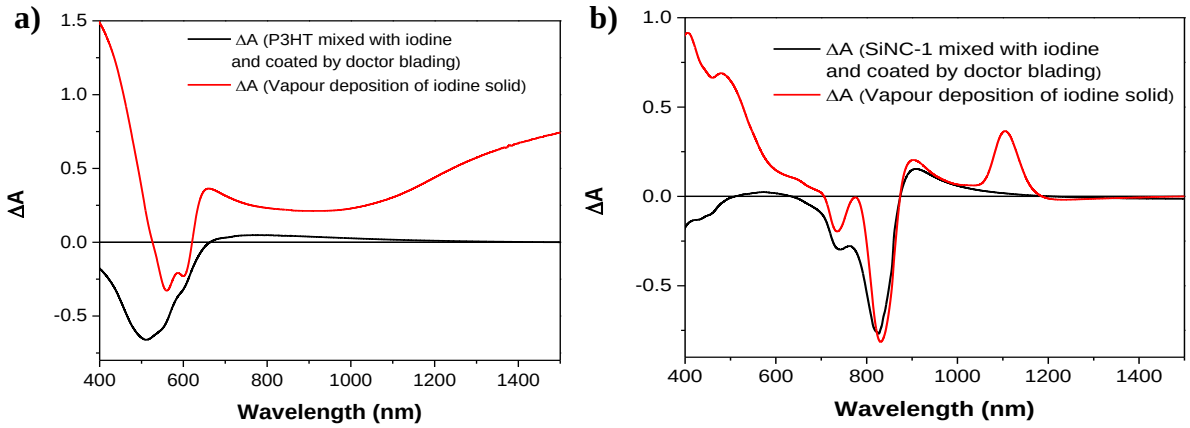

Figure 6-10 The differential absorption spectra of a) P3HT and b) **SiNC-1**, which is obtained as the difference between the doped and undoped spectra under different doping condition.

The PIA experiment spectra were measured by using both Silicon and InGaAs detectors to analyze a broad wavelength region. The negative normalized absorption spectra of the P3HT:PCBM and **SiNC-1** films are also added to explain clearly and more precisely the features related to the ground-state photobleaching of the compounds.

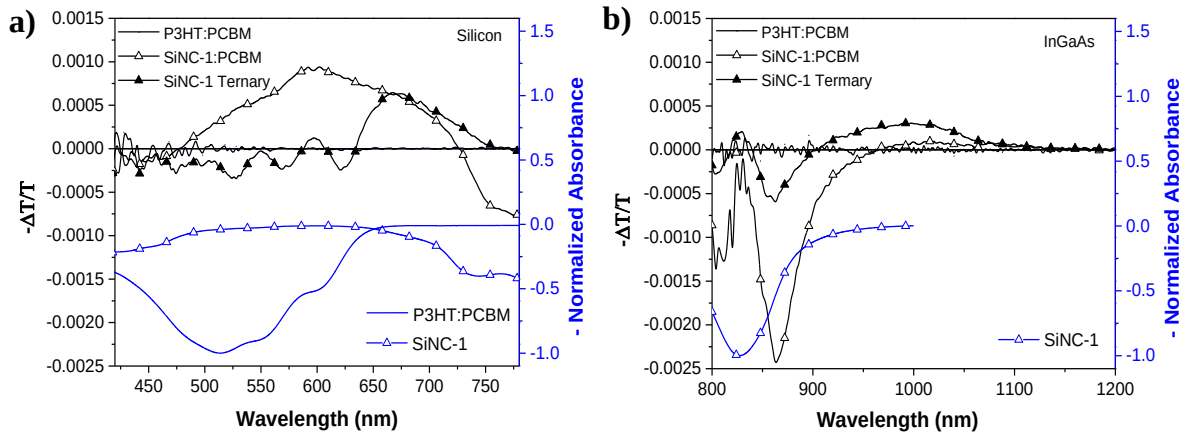

Figure 6-11 PIA spectra recorded at 6.8 mw cm^{-2} light intensity and 14.2 mw cm^{-2} laser intensity of P3HT:PCBM, **SiNC-1**:PCBM , and **SiNC-1** based ternary films measured by a) silicon and b) InGaAs detectors. The normalized absorption spectra of the P3HT:PCBM and **SiNC-1** films are presented on the same graphs for a direct comparison of the peak futures.[186]

Figure 6-11 showed the PIA investigations of the **SiNC-1**:PCBM binary and P3HT: **SiNC-1**:PCBM ternary blends. For **SiNC-1**:PCBM (1:1) film (the line with open triangle symbols), the bleaching peaks at 440 nm, 780 nm and 860 nm are consistent with the absorption feature of **SiNC-1**, and the sharp features from 460 to 730 nm with a peak at 600 nm belong to the **SiNC-1** polaron signals. In contrast, for the corresponding ternary film with 20 wt.% **SiNC-1** content (the line with closed triangle symbols), the measurements shows not only the bleaching peak of **SiNC-1**, but also the bleaching peaks of P3HT at 525 nm, 573 nm and 623 nm. Meanwhile, the enhanced positive polaron regions from 730 to 780 nm and 900 to 1100 nm provide strong evidence for the formation of P3HT polarons. Obviously, P3HT cations are formed upon exciting **SiNC-1**, meaning that a hole transfer from **SiNC-1** to P3HT is happening. As the PIA spectroscopic feature of PCBM extends beyond 1100 nm, the corresponding signal is not observable because of the sensitivity limitation of our detector.[221]

d) Charge transfer/transport mechanism

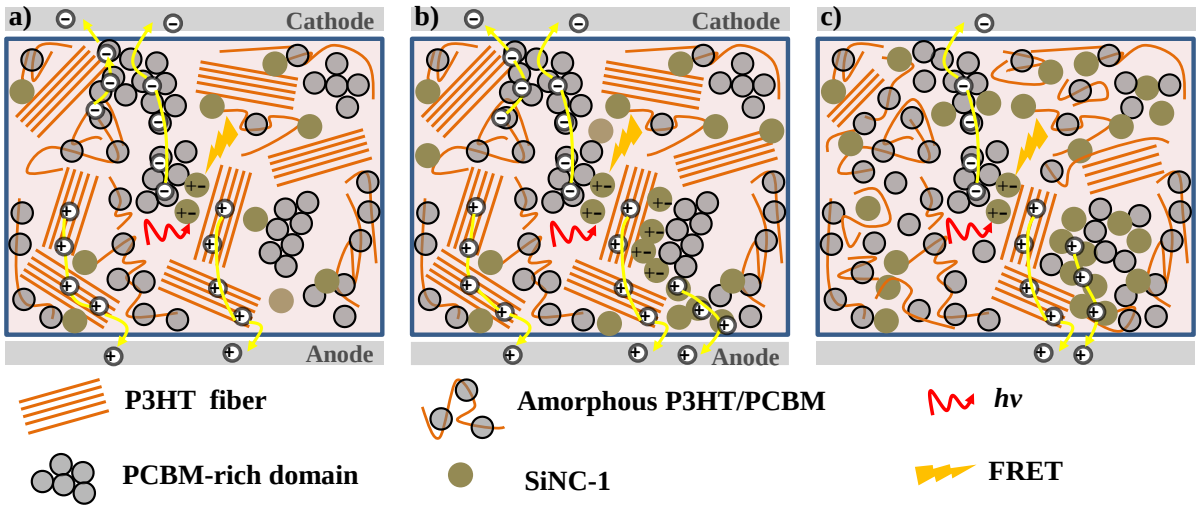

Figure 6-12 Charge transfer and transport mechanism. a) **SiNC-1**≤5 wt.%; b) 5 wt.%≤**SiNC-1**≤15 wt.%; c) **SiNC-1**≥15 wt.%.[186]

In total, a reasonable explanation of the charge transfer/transport mechanism in P3HT:**SiNC-1**:PCBM ternary systems by varying dye contents is schematically illustrated in **Figure 6-12**. When **SiNC-1**≤5 wt.%, the photoinduced excitons in **SiNC-1** molecules are efficiently dissociated at the interface of P3HT:**SiNC-1** and **SiNC-1**:PCBM interfaces because dye molecules located at the amorphous P3HT:PCBM interface. Afterwards, it forms free holes and electrons to transport towards the electrodes through P3HT and PCBM rich domains. In the case of 5 wt.%≤**SiNC-1**≤15 wt.%, a parallel-like hole transport within the **SiNC-1** and P3HT rich domains is very likely because of the aforementioned cascade charge transfer/ transport mechanism. This can explain a huge improvement from 5 wt.% to 15 wt.% at near IR region shown in IQE spectrum. In both cases, efficient energy transfer and/or cascade electron transfer from P3HT to the dye molecules facilitate the P3HT exciton dissociation. When **SiNC-1**≥15 wt.%, dye molecules overload the donor:acceptor amorphous interface volume and start interfering with the crystallites of the P3HT and PCBM host matrices. Consequently, the charge transport and device performance are diminished.

e) Charge generation/ carrier mobility

To elucidate the phenomenon of the increase J_{SC} in P3HT:**SiNC-1**:PCBM ternary system, we discuss the impact of sensitizer addition on charge generation in the following. **Figure 6-13** showed the variation of photocurrent density (J_{ph}) versus effective voltage (V_{eff}).[205] Similarly to **Chapter 5**, the saturation current J_{sat} and the maximum generation rate of free charge carriers G_{max} are estimated according to previous work.[182,206] Herein, J_{sat} and G_{max} values are summarized in **Table 6-2**. The trend of these values is consistent with the difference in J_{SC}. It clearly suggests more efficient exciton generation, leading to higher PCE in the end.

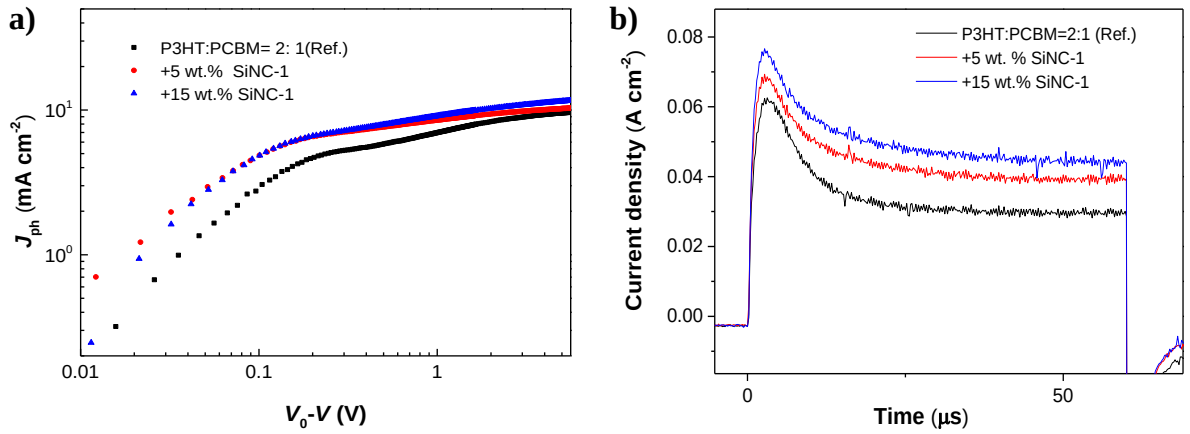

Figure 6-13 a) Photocurrent density of P3HT:PCBM binary and P3HT:**SiNC-1**:PCBM ternary devices versus the effective voltage under 1 sun illumination. b) Time-dependent photo-CELIV traces of the corresponding devices after a delay time of 50 μs.[186]

Table 6-2 Summary of calculated charge generation parameters: saturation current (J_{sat}), G_{max}, and calculated μ by photo-CELIV for P3HT:PCBM binary, and P3HT:**SiNC-1**:PCBM ternary devices under lower and higher **SiNC-1** contents.

Dye content	J_{sat} (mA cm^{-2})	G_{max} (cm^{-3} s^{-1})	μ (cm^{2}V^{-1}s^{-1})
P3HT:PCBM	9.94	6.21x10^{21}	1.38x10^{-4}
+5% **SiNC-1**	10.79	6.74x10^{21}	1.49x10^{-4}
+15% **SiNC-1**	12.11	7.57x10^{21}	1.45x10^{-4}

The charge transport of the aforementioned systems is also investigated in detail to further study the relationship between the addition of SiNC-1 and device performance. Similarly to the method used in **Chapter 5**, photo-CELIV was done, and then the charge carrier mobility

(μ) of devices can be analyzed.[207-209] **Figure 6-13b** showed the photo-CELIV traces after a delay time of 50 μs, which are recorded for the reference binary control device as well as for the P3HT:**SiNC-1**:PCBM ternary devices at low and high dye contents. At the end, a similar μ is achieved for all devices and the values are listed in **Table 6-2**. This is consistent with the similar FFs found for binary and ternary devices shown in **Table 6-1**.

6.3.2 Panchromatic quaternary polymer:fullerene BHJ solar cells

According to our aforementioned studies, both **SiPC** and **SiNC-1** can be incorporated into P3HT:PCBM host system using as potential photosensitizers. As shown in **Chapter 4**, **SiPC** and **SiNC-1** show complementary spectral absorptions at longer wavelengths, making them possible to apply into P3HT:PCBM matrix as co-sensitizers to generate more photocurrent. Herein, in the following, P3HT/**SiNC-1**/**SiPC**/PCBM quaternary blend solar cells were fabricated and studied. The energy level diagram of all components using in quaternary blend solar cells are shown in **Figure 6-14**.

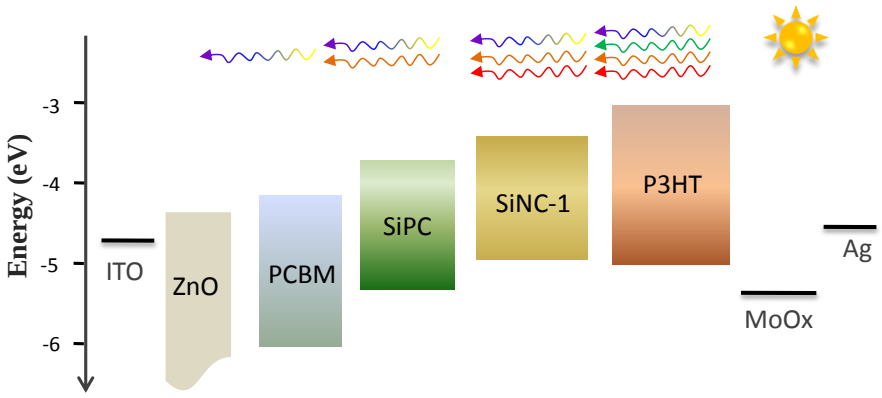

Figure 6-14 Energy level diagram of all components in quaternary blend solar cells.[186]

6.3.2.1 Film characterization

a) Absorption properties

Both **SiPC-0** and **SiPC-1** have been applied into P3HT:**SiPC-0**:**SiNC-1**:PCBM quaternary devices because they exhibit slight different absorption properties. According to the above

discussion, both **SiPCs** exhibit the complementary absorption profiles compared to **SiNC-1**, which do not significantly overlap with those of P3HT:PCBM, promise to allow enhanced solar harvesting. The absorption spectra of two P3HT:**SiPC**:**SiNC-1**:PCBM quaternary systems with increasing the amount of **SiNC-1** are shown in **Figure 6-15**. Both **SiPCs** have similar absorption trend and the same amount of **SiPC** (7.5 wt.%) are choose for comparison. Similarly, two obvious absorption peaks are observed in the near IR range, corresponding respectively to the absorption bands of **SiPCs** (peak at 705 nm) and **SiNC-1** (peak at 830nm). The absorption peak belonged to **SiPCs** keep the same level as we adding the same amount of dye molecules. The absorption peak associated to **SiNC-1** increases with increasing the amount of **SiNC-1**. All films exhibit the distinguished vibration bands at around 500-600 nm, which are indicative of the crystallization of P3HT. It shows slight decreasing in this range with lower content of **SiNC-1**, and then a huge drop after higher amount of **SiNC-1**.

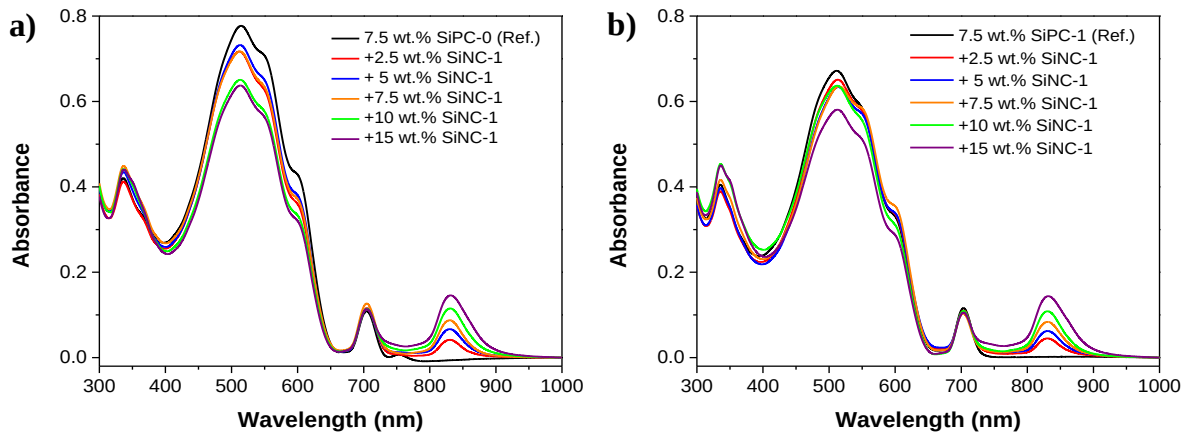

Figure 6-15 a) Absorption spectra of the P3HT:**SiPC-0**:**SiNC-1**:PCBM quaternary films with increasing the **SiNC-1** content; b) Absorption spectra of the P3HT:**SiPC-1**:**SiNC-1**:PCBM quaternary films varying the **SiNC-1** content.[186]

b) Film morphology

The film morphology of bulk heterojunction is a useful method to clarify whether one molecule is suitable as the third or fourth component incorporating into host system or not. The surface topographies of binary P3HT:PCBM film and quaternary P3HT:**SiPC-0** (7.5 wt.%):**SiNC-1** (7.5 wt.%):PCBM film investigated by AFM shown in **Figure 6-16**.

Comparing to P3HT:PCBM binary system, quaternary film even shows a slight small root-meat-square (RMS) roughness. It indicates that there is no any phase separation or any obvious morphology modification even adding two different sensitizers.

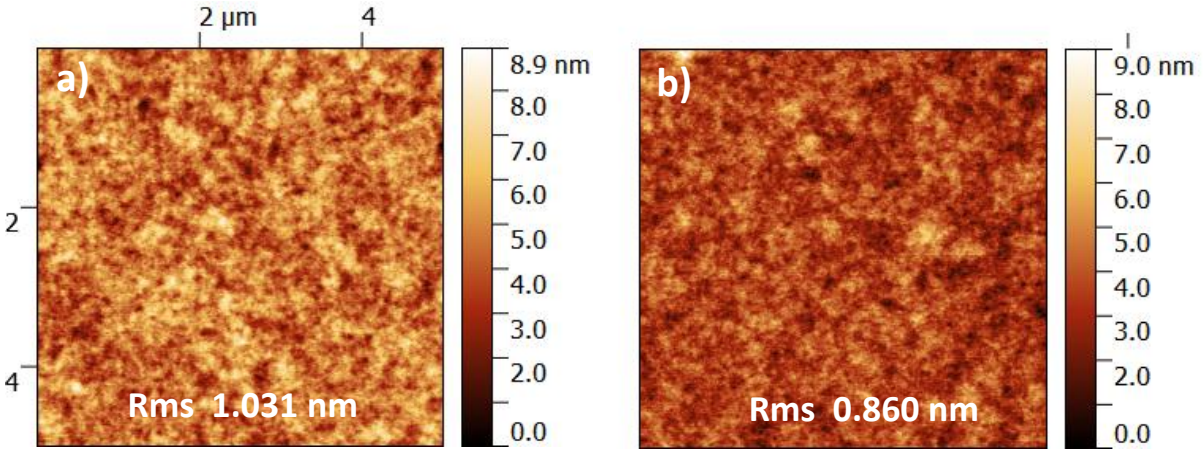

Figure 6-16 Surface topographic AFM images (Size:5×5 µm^2) of a) binary P3HT:PCBM (2:1), b) quaternary (7.5 wt.% **SiNC-1**+7.5 wt.% **SiPC-0**) films.[186]

To gain further understand of the quaternary morphology, TEM investigations are also performed, as shown in **Figure 6-17**. It includes TEM bright field images as well as elemental maps based on energy filtered TEM (EFTEM) imaging of sulfur (S) using the S L edge and of carbon (C) using the C K edge for binary P3HT:PCBM and P3HT:**SiPC-0** (7.5 wt.%):**SiNC-1** (7.5 wt.%):PCBM quaternary films. As observed, the morphology of quaternary film is similar with referenced binary film, and the P3HT fibers exist in both cases. This can explain why in absorption spectra the distinguished vibration bands of P3HT are obvious even in quaternary system.

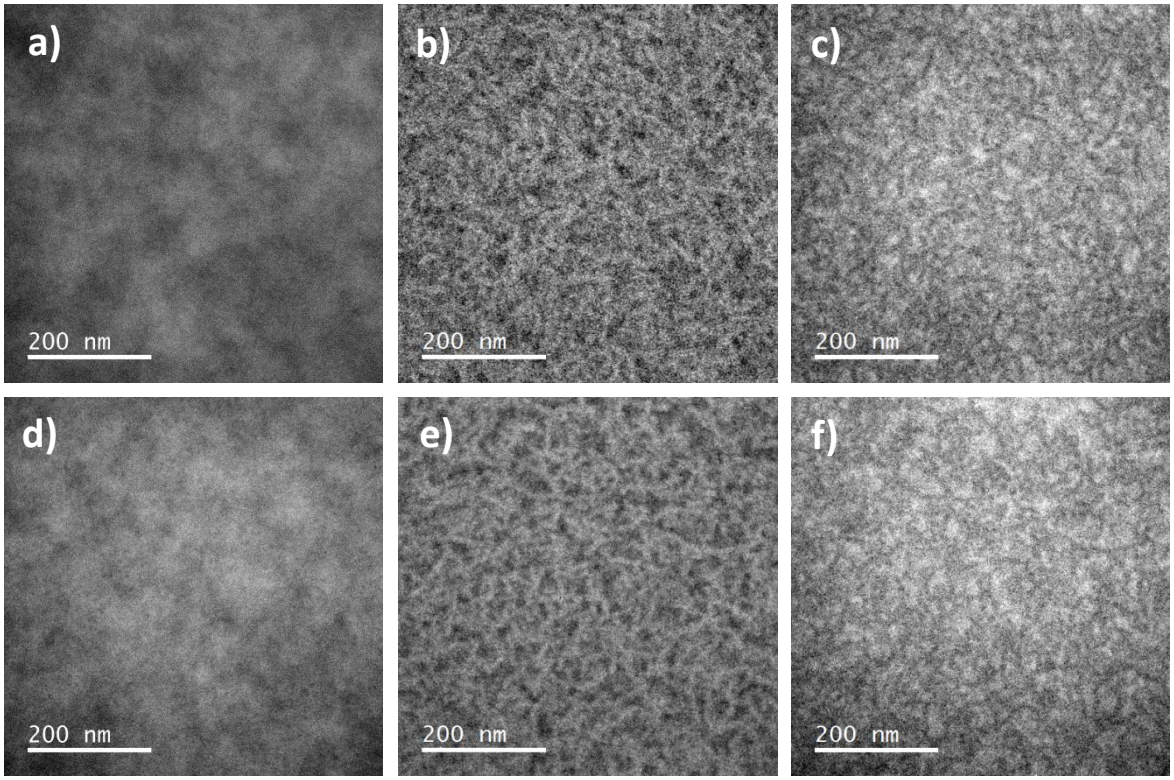

Figure 6-17 TEM bright field images (left row) and elemental maps of sulfur (S L edge, middle row) and of carbon (C K edge, right row): a–c): binary P3HT:PCBM (2: 1), d–f): quaternary (7.5 wt.% **SiNC-1**+7.5 wt.% **SiPC-0**) films.[186]

6.3.2.2 Photovoltaic properties

Quaternary blend solar cells with an active layer configuration of P3HT/**SiNC-1**/**SiPC**/PCBM were fabricated and studied by the incorporation of **SiPCs** or **SiNC-1**, since they show complementary spectral absorption at longer wavelengths. **Figure 6-18** show the *J*–*V* curves of P3HT:**SiPC-0**:**SiNC-1**:PCBM and P3HT:**SiPC-1**:**SiNC-1**:PCBM blended quaternary devices and all the device photovoltaic parameters are summarized in **Table 6-3**. For comparison, the content of **SiPC** is kept constant to be 7.5 wt.% and that of **SiNC-1** slowly increases. As illustrated, the quaternary blend solar cells exhibit an improved performance compared to the reference **SiPC-0** blend ternary solar cells. This increase in PCE is mainly caused by the improvement of J_{SC} due to more photocurrent because of broader absorption window. The sensitization has a positive impact up to 10 wt.% **SiNC-1** and starts to decline for higher content fourth component. A similar trend is seen for the **SiPC-1** quaternary

system. As summarized in **Table 6-3**, the PCE of the quaternary blend solar cells are higher than that of the individual ternary blend solar cells, which means both dyes can effectively contribute to the photocurrent generation without unfavorable interactions between the two sensitizers.

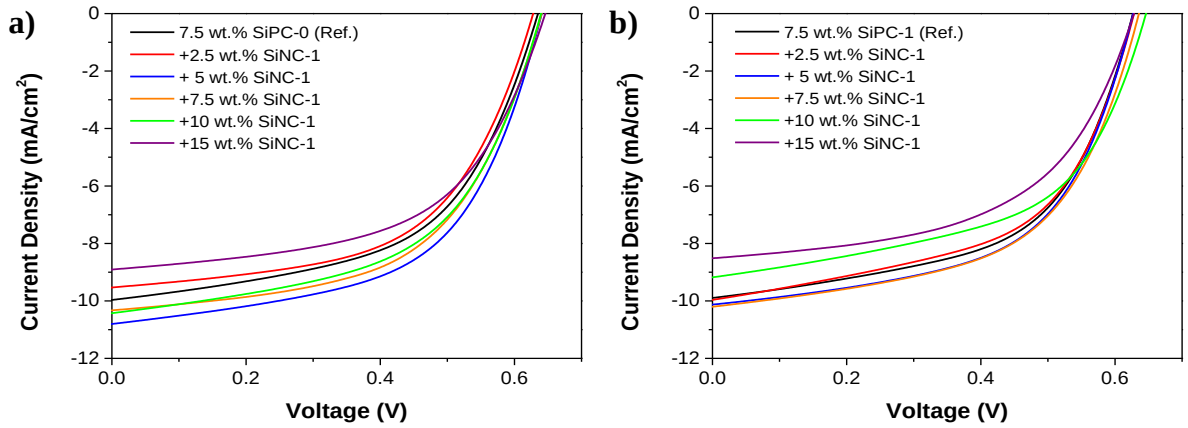

Figure 6-18 a) *J*–*V* curves of P3HT:**SiPC-0**:**SiNC-1**:PCBM quaternary devices varying **SiNC-1** content; b) *J*–*V* curves of P3HT:**SiPC-1**:**SiNC-1**:PCBM quaternary devices varying **SiNC-1** content. The addition of **SiPCs** is kept constant to be 7.5 wt.%.[186]

Table 6-3 Photovoltaic device parameters of P3HT:**SiPCs (SiPC-0** or **SiPC-1)**:**SiNC-1**:PCBM quaternary devices with different **SiNC-1** contents under AM 1.5G, 100 mW cm^{-2}.

	Dye content **SiPCs**[wt.%]+**SiNC-1**[wt.%]	V_{OC}[V]	J_{SC}[$mAcm^{-2}$]	J_{SC}/EQE	FF[%]	Eff.[%]
SiPC-0	7.5%+0%	0.65	9.96	8.39	53.85	3.49
	7.5%+2.5%	0.65	9.95	8.33	54.66	3.39
	7.5%+5%	0.65	10.80	8.45	55.45	3.89
	7.5%+7.5%	0.65	10.33	8.51	55.42	3.72
	7.5%+10%	0.65	10.43	8.50	53.73	3.64
	7.5%+15%	0.65	8.91	8.27	55.35	3.21
	7.5%+0 %	0.65	9.89	8.29	54.15	3.48

	7.5%+ 2.5%	0.65	9.97	8.36	52.65	3.41
SiPC-1	7.5%+5%	0.65	10.13	8.51	54.63	3.59
	7.5%+7.5%	0.65	10.20	8.71	54.35	3.60
	7.5%+10%	0.65	9.18	8.32	54.08	3.23
	7.5% +15%	0.65	8.51	7.75	52.47	2.90

The corresponding EQE spectra of these two quaternary solar cell systems, with broad signals from 350 nm up to 900 nm, are displayed in **Figure 6-19**. It shows two broad peaks at 710 nm and 840 nm, indicating that both **SiPC** and **SiNC-1** act as sensitizers in the P3HT/PCBM matrix. By increasing the amount of **SiNC-1**, the EQE associated with the **SiNC-1** part continuously improves, accompanied by an increasing in J_{SC}. Interestingly, the EQE signal related to **SiPC** remained almost unchanged. The possible explanation is that **SiPC** is always located at the interface of the P3HT/PCBM matrix and that there is no unfavorable interaction between **SiPC** and **SiNC-1**. In the near IR region, the EQE value of **SiPC** is almost the same for the quaternary blend after the addition of **SiNC-1** and the individual ternary solar cells blending only with **SiPC**. However, the peak associated to P3HT (400–600 nm) emerges a slight drop at less than 10 wt.% **SiNC-1** and then a huge decrease at 15 wt.% **SiNC-1**. This trend is similar to the change of J_{SC}. According to the above studies, the interface loading of **SiPC** or **SiNC-1** in P3HT/PCBM blend ternary system is around 15-20 wt.%. A possible deduction is that, no matter whether one or two sensitizers are added, the total amount of sensitizers loading at the interface of P3HT/PCBM is always in the range of 15 to 20 wt.%.

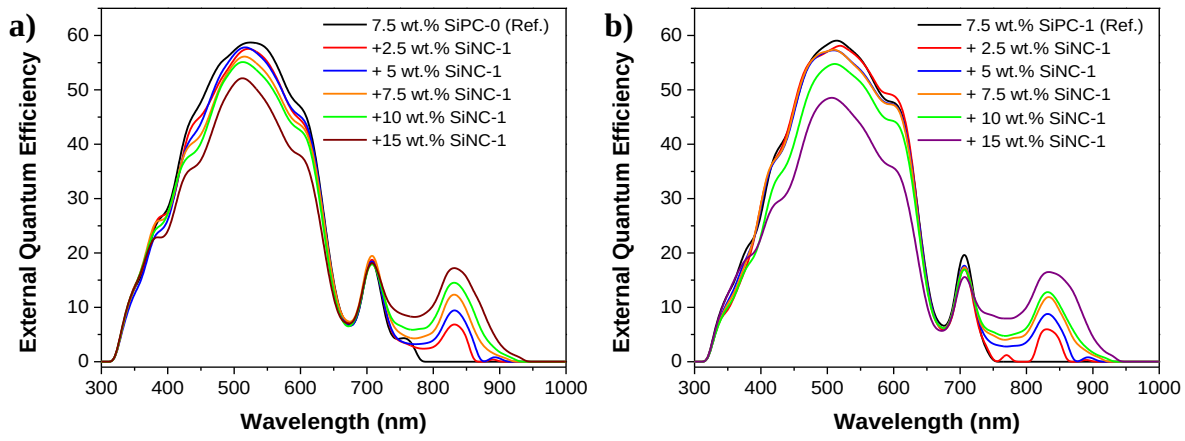

Figure 6-19 EQE spectra of the quaternary devices with increasing the **SiNC-1** content: a) P3HT:**SiPC-0**:**SiNC-1**:PCBM; b) P3HT:**SiPC-1**:**SiNC-1**:PCBM.[186]

6.3.2.3 Photophysical studies

a) Photoluminescence (PL) quenching

As illustrated in **Figure 6-20**, the PL of P3HT in quaternary films is more effectively quenched compared to that of the individual ternary blend solar cells with a single dye. This finding suggests a more efficient charge transfer processes in the quaternary system comparing to the corresponding ternary system.

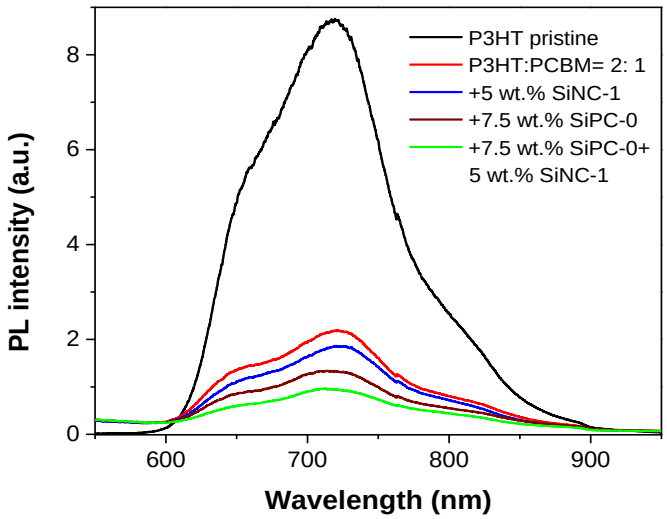

Figure 6-20 PL of pristine P3HT, P3HT:PCBM binary, **SiNC-1** and **SiPC-0** based ternary, and P3HT:**SiPC-0**:**SiNC-1**:PCBM quaternary films.[186]

b) Charge generation/ carrier mobility

In order to elucidate the phenomenon of improved J_{SC} in P3HT:**SiNC-1**:**SiPC**:PCBM quaternary systems, the differences of charge generation before and after adding **SiNC-1** were studied. The variation of J_{ph} as a function of V_{eff} is shown in **Figure 6-21**. According to the same method discuss before, the saturation current J_{sat} and the maximum generation rate of free charge carriers G_{max} are estimated. Herein, J_{sat} and G_{max} values are summarized in **Table 6-4**. These results are consistent with the difference in J_{SC} and clearly suggest more

efficient exciton generation in quaternary system compared to the ternary system, leading to higher PCE in the end.

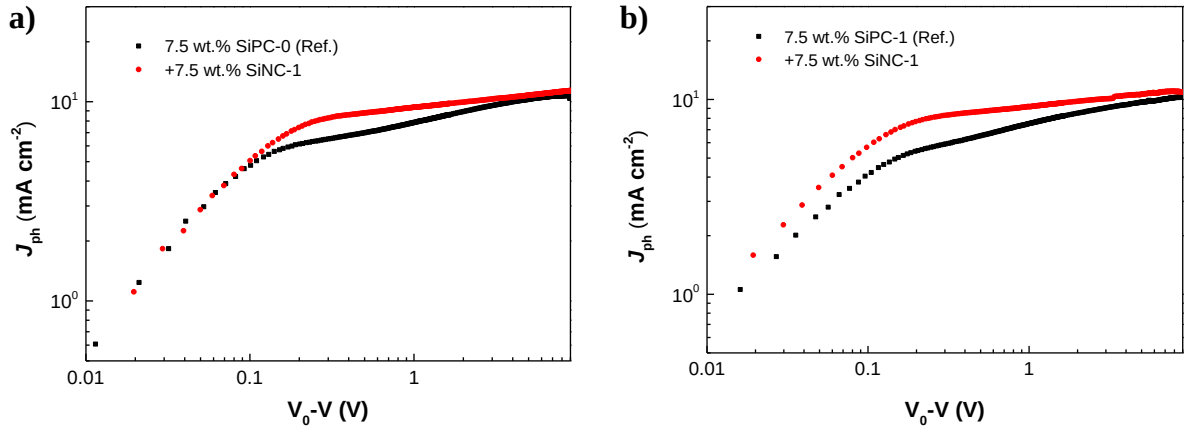

Figure 6-21 Photocurrent density of a) P3HT:**SiPC-0**:PCBM ternary and P3HT:**SiPC-0**:**SiNC-1**:PCBM quaternary devices; and b) P3HT:**SiPC-1**:PCBM ternary and P3HT:**SiPC-1**:**SiNC-1**:PCBM quaternary devices as a function of the effective voltage under 1 sun illumination.[186]

Table 6-4 Summary of calculated charge generation parameters: J_{sat}, G_{max} and μ.

Dye content	J_{sat} (mA cm^{-2})	G_{max} (cm^{-3} s^{-1})	μ (cm^{2}V^{-1}s^{-1})
7.5% **SiPC-0**	10.71	6.69x10^{21}	1.25x10^{-4}
+7.5% **SiPC-0**+7.5% **SiNC-1**	11.48	7.17x10^{21}	1.27x10^{-4}
7.5% **SiPC-1**	10.45	6.53x10^{21}	1.34x10^{-4}
+7.5% **SiPC-1**+7.5% **SiNC-1**	11.13	6.96x10^{21}	1.30x10^{-4}

As discuss before, not only the morphology is not adversely affected by the addition of two sensitizers but also the quaternary devices show comparable values compared to the ternary device. It is necessary to investigate charge transport in detail to further study the relationship between the additions of sensitizers with device performance. Similarly to the above discussion, the charge carrier mobility (μ) can be analyzed by employing the photo-CELIV technique. **Figure 6-22** shows the photo-CELIV traces after a delay time of 50 μs, which are recorded for the reference ternary control device with 7.5 wt.% **SiPC** as well as for the P3HT:**SiNC-1** (7.5 wt.%):**SiPC** (7.5 wt.%):PCBM quaternary devices. At the end, a similar μ

is achieved for all the devices. The μ values are listed in **Table 6-4**, which is consistent with the similar FFs found for the reference ternary and quaternary devices.

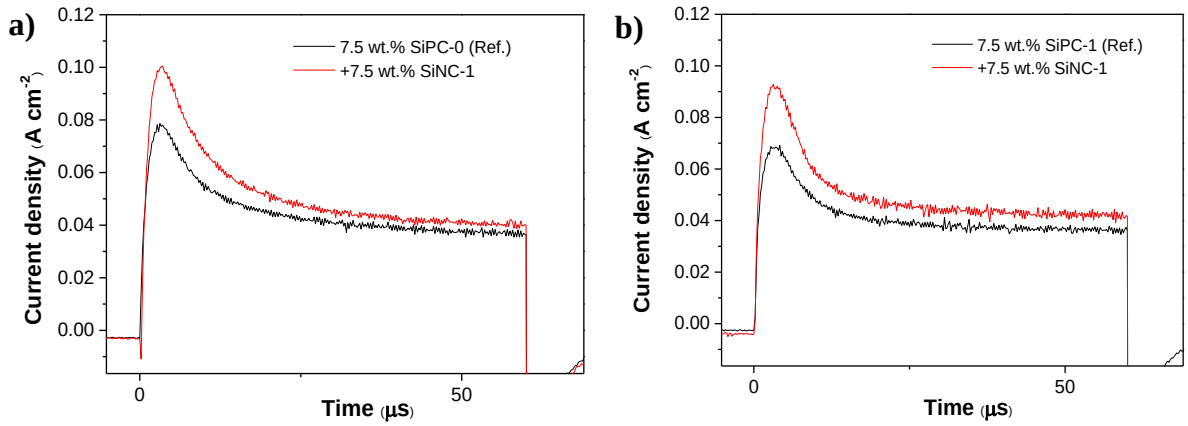

Figure 6-22 Time-dependent photo-CELIV traces of a) P3HT:**SiPC-0**:PCBM ternary and P3HT:**SiPC-0**:**SiNC-1**:PCBM quaternary devices; b) P3HT:**SiPC-1**:PCBM ternary and P3HT:**SiPC-1**:**SiNC-1**:PCBM quaternary devices after a delay time of 50 μs.[186]

6.4 Conclusion

In this chapter, ternary OPV devices have been fabricated using **SiNC-1** as a light-harvesting photosensitizer in the longer wavelength region. Embedded into the P3HT/PCBM matrix, **SiNC-1** provides an additional charge generation pathway. **SiNC-1** shows strong photosensitivity in the near IR region (650–950 nm), as verified by both UV-vis and EQE measurements, yielding an improvement of up to 10% for J_{SC} and 24% for PCE in the blend with P3HT/PCBM. Our in-depth study based on the complementary IQE, PL, and PIA measurements reveals complex charge transfer and transport kinetics, including cascade charge transfer, energy transfer and parallel-like charge transfer mechanisms.

Furthermore, quaternary devices have been fabricated based on multi-colored dye sensitizers (**SiNC-1**+**SiPC-0** or **SiNC-1**+**SiPC-1**) blending into P3HT/PCBM matrix. Complementary spectral absorption is observed in the near IR region shown in EQE spectra for multi-colored dye sensitized device. It covers the UV-vis as well as near IR region from 350 nm up to 900 nm outlining apparent signal characteristics of each single dye, corroborating the effective

contribution of both **SiPC** and **SiNC** dyes in enhancing the J_{SC}. It means that both dyes contribute to the generation of excitons with an efficient charge separation. Quaternary solar cells with 7.5 wt.% **SiPC** and 5–7.5 wt.% **SiNC-1** show an improved PCE compared to the individual ternary blend solar cells. If continue to increase the amount of **SiNC-1**, a huge decreasing happens in the J_{SC} and PCE, which is similar with the trend shown in EQE. A possible deduction is that, no matter one or two sensitizers are added, the total amount of sensitizers loading at the interface of P3HT/PCBM always reach saturation in the range of 15 to 20 wt.%, sensitization turned out to be most efficient at this concentration. AFM and TEM investigations show that the morphology is not disturbed even with 15–20 wt.% dye loading for both ternary and quaternary systems.

Hence, our results further illustrate the potential of the multi-colored dye sensitization concept as a powerful approach to mitigate the non-ideal optical absorption normally encountered in organic-based optoelectronic devices. Incorporation of dye molecules as a third and/or fourth dye component is an efficient approach to pursuit high efficiency in organic solar cells. This simple and versatile method could be applied to efficiently enhance light harvesting and, thus, to increase the PCE and enables an easy access to optimal morphology of solar cells even for highly efficient low-bandgap polymer/fullerene system.

Chapter 7

High efficiency ternary solar cell based on mid bandgap polymer and SiPC sensitizer

Abstract

The **SiPCs** and **SiNC-1** incorporated ternary solar cells were relatively low efficiency, despite a PCE around 4%, owing to the low efficient host matrix of P3HT:PCBM. It could limit the wide application and commercial production of these ternary photovoltaics. In this chapter, SiPC is introduced into two different mid band gap polymers (OPV-46 and PCDTBT) based systems as the near IR sensitizers. The high efficiency of 7.34% and 6.31% are achieved for OPV-46:**SiPC**:PCBM and PCDTBT:**SiPC**:PCBM, respectively. Interesting, different V_{OC} trends are observed for aforementioned ternary systems.

The relative results in detail will be submitted soon. The manuscript is in preparation as following,

L. Ke, X. Tang, H. Chen, S. Chen, C. Zhang, Q. Fan, C. J. Brabec and T. Ameri, Origin of the V_{OC} enhancement in high efficiency ternary solar cells based mid bandgap polymers and SiPC sensitizer. In preparation.

7.1 Introduction

As aforementioned, ternary blend solar cells have attracted much of the interest in the OPV community and have been subject of several review articles.[83,222,223] Ternary blends have shown performance multiple-beneficiaries compared to binary blends. According to the above chapters, our research efforts have been focused on blended material systems based on P3HT and PCBM, as the electron donor and acceptor, respectively. However, one of the drawbacks of P3HT is its limited light harvesting capability, as the whole bandgap of > 1.9 eV can only absorbs a quarter of the total photons of the solar eradiation at best.[224] This leaves plenty of room for improvement of photocurrent by enhancing the spectral sensitivity in the visible as well as in the near IR region of the spectrum.

To overcome absorption limitations in OSCs, several strategies are currently pursuing to achieve enhanced PCE. For example, extensive works have been performed to employ conjugated polymers with smaller band gap, which extend absorption into the near-IR and improve light harvesting.[225-229] In this chapter, the common use of silicon phthalocyanine as near IR photosensitivity is addressed by studying two different polymer:fullerene systems. Hence, **SiPC-3** was incorporated into OPV-46:$PC_{70}BM$ and PCDTBT:$PC_{70}BM$ based host matrix. The improvement of current density (J_{SC}) and broader near IR sensitization were observed in both ternary systems.

7.2 Experiment methods

7.2.1 Solution preparation

The blend solution was prepared as following: for OPV-46:**SiPC-3**:$PC_{70}BM$ ternary blends, the mixture of OPV-46 and $PC_{70}BM$ was prepared at a concentration of 25 mg/mL in chlorobenzene (CB) with OPV-46:$PC_{70}BM$ weight ratio of 1:1.5. Meanwhile, **SiPC-3** was also prepared at a concentration of 25 mg/mL in chlorobenzene (CB) in a separate solution bottle. Then two bottles of solution was left overnight to stir on a hot plate under 75 °C to ensure complete dissolution of the compounds in the solvent. Finally, **SiPC-3** was added into the OPV-46:$PC_{70}BM$ mixture solution according to different contents. The mixed solutions were allowed to spin on a hot plate for at least 1.5 h at 75 °C to ensure that the solutions were fully mixed before blading.

For PCDTBT:**SiPC-3**:$PC_{70}BM$ ternary blends, the mixture of PCDTBT and $PC_{70}BM$ was prepared at a concentration of 20 mg/mL in *o*-dichlorobenzene (ODCB) with PCDTBT:$PC_{70}BM$ weight ratio of 1:4.. Meanwhile, **SiPC-3** was also prepared at a concentration of 20 mg/mL in *o*-dichlorobenzene (ODCB) in a separate solution bottle. Then the mixture PCDTBT:$PC_{70}BM$ solution and **SiPC-3** solution were left overnight to stir on a hot plate under 110 °C and 85 °C separately to ensure complete dissolution of the compounds in the solvent. Finally, **SiPC-3** was added into the PCDTBT:$PC_{70}BM$ mixture solution according to different contents. The mixed solutions were allowed to spin on a hot plate for at least 1.5 h at 85 °C to ensure that the solutions were fully mixed before blading.

7.2.2 Device fabrication

All devices were fabricated in the inverted structure. Pre–structured indium tin oxide (ITO) substrates were cleaned with acetone and isopropyl alcohol in an ultrasonic bath for 15 minutes each. After drying, the substrates were successively coated with 40 nm of zinc oxide (ZnO) using doctor–blading under ambient conditions, following by annealing in air on a hot plate at 80 °C for 5 min. For OPV-46:**SiPC-3**:$PC_{70}BM$ ternary film, a 300 nm thick active layer was coated using spin coating technology in the glove box. For PCDTBT:**SiPC-3**:$PC_{70}BM$ ternary film, a 70 nm thick active layer was also coated using spin coating method under ambient conditions. To complete the fabrication of the devices 10 nm

of MoOx and 100 nm of Ag were thermally evaporated through a mask (with a 10.4 mm² active area opening) under a vacuum of ~5x10^{-6} mbar.

7.3 Results and discussion

7.3.1 OPV-46:SiPC-3:$PC_{70}BM$ system

Glass/ITO/ZnO/OPV-46:**SiNC-3**:$PC_{70}BM$/MoOx/Ag BHJ inverted ternary solar cells with various dye contents were fabricated and characterized. The energy levels of the materials in this ternary device are shown in **Figure 7-1**. As shown, it forms a cascade energy level alignment. The *J–V* characteristics of the ternary blend solar cells and the corresponding control OPV-46:$PC_{70}BM$ binary blend solar cell are shown in **Figure 7-2a**. The photovoltaic device parameters are further summarized in **Table 7-1**.

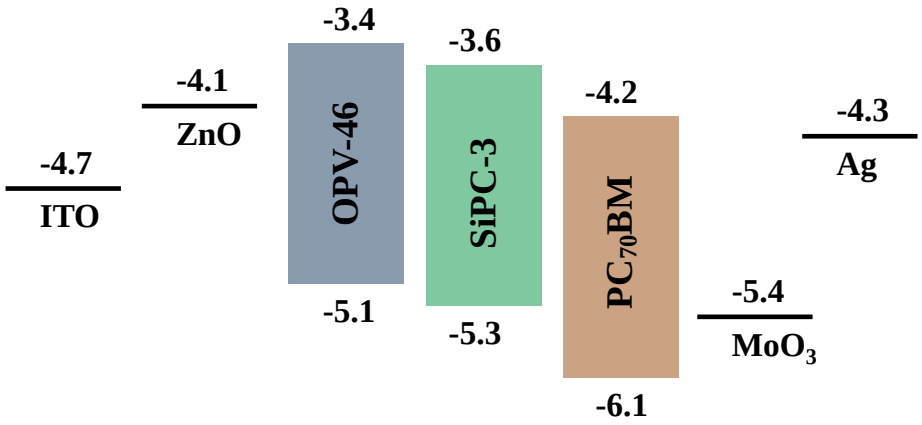

Figure 7-1 The schematic of the energy levels in OPV-46:**SiPC-3**:$PC_{70}BM$ ternary system.

As expected, the addition of **SiPC-3** results in an increase of the short circuit current density (J_{SC}) because of its complementary absorption profiles compared to the host matrix. Sensitization turned out to be most efficient at a dye concentration of 37.5 wt.%, leading to a J_{SC} increase of almost 9% from 15.71 mA cm^{-2} for the binary control device to 17.11 mA cm^{-2} for ternary based device. For concentrations above 50 wt.%, however, the positive influence of sensitization on J_{SC} starts to decline. By comparison, more dye loading is allowed for the amorphous polymer system. For crystalline polymer P3HT system, one can only add 15 wt.%

of dye molecules, as discussed in **Chapter 5**. Regrettably, the fill factor (FF) for the ternary blend cells shows a continuing downward trend when adding the third component **SiPC-3**. It can be attributed to the unfavorable morphology formation in ternary blends.

Interestingly, the V_{OC} shows a continuing increasing trend from 0.72 V for the reference device to 0.83 V for the ternary blend with a sensitizer concentration of 100 wt.% (The weight percent is referred to host polymer OPV-46). Fourier Transform Photocurrent Spectroscopy (FTPS) measurements and electroluminescence (EL) spectra for the ternary devices including different **SiPC-3** contents need to be done to shin light on the origin of V_{OC} increasing trend.

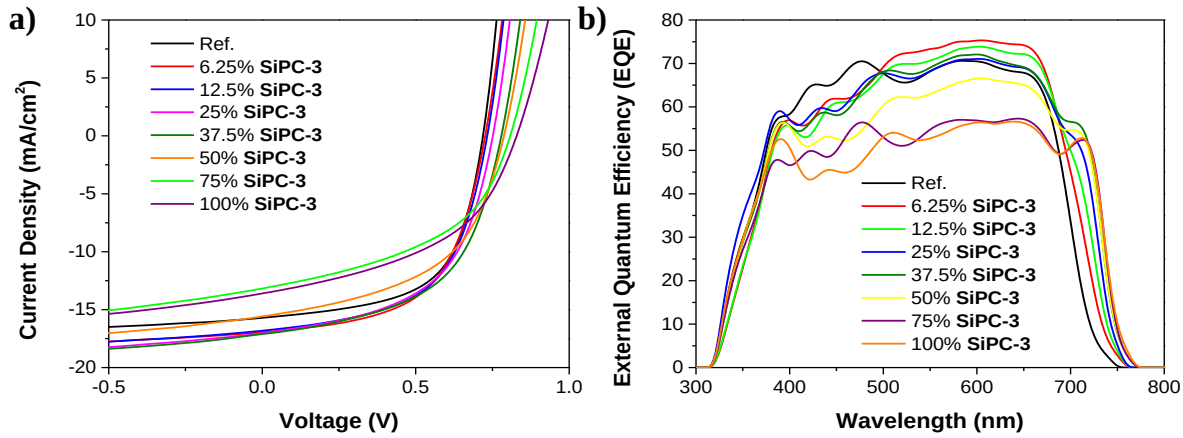

Figure 7-2 (a) J-V curves and (b) EQE spectra for OPV-46:**SiNC-3**:$PC_{70}BM$ devices with various **SiNC-3** contents.

Table 7-1 Photovoltaic device parameters of OPV-46:**SiNC-3**:$PC_{70}BM$ ternary devices for different **SiNC-3** content under AM 1.5G, 100 mW cm^{-2}

Sample	SiPC content	V_{OC}(V)	J_{SC}(mA/cm^2)	J_{SC}(EQE)	FF(%)	PCE(%)
1	0%	0.72	15.71	13.52	0.60	6.79
2	6.25%	0.73	16.94	14.33	0.58	7.17
3	12.5%	0.74	16.82	14.25	0.57	7.09
4	25%	0.76	17.02	14.31	0.55	7.11
5	37.5%	0.78	17.11	14.53	0.55	7.34
6	50%	0.79	15.59	13.48	0.52	6.40

7	75%	0.81	13.49	12.18	0.48	5.24
8	100%	0.83	13.61	11.91	0.47	5.31

Figure 7-2b illustrates the external quantum efficiency (EQE) of the corresponding devices. Because there is some absorption overlap between the host polymer OPV-46 and **SiPC-3**, the EQE contribution of **SiPC-3** is not that obvious, while some difference can still be observed. It shows only a slight red shift to near IR region. When the content of **SiPC-3** is lower than 37.5%, the EQE peak from 500 to 770 nm, which is the combine absorption region for both OPV-46 and **SiPC-3**, increases with increasing the **SiPC-3**'s concentration. It can be explained by the higher number of photo-generated carriers due to the extended absorption in the near IR region and higher absorption coefficient of silicon phthalocyanine molecules. However, the whole region of EQE decreases when the **SiPC-3** loading is more than 50%, showing similar trend with the device performance. One the other side, the EQE associated with OPV-46 (400–500 nm) decrease from the beginning. This can be explained by the optical loss due to the reduced relative weight fraction of OPV-46.

7.3.2 PCDTBT:SiPC-3:$PC_{70}BM$ system

Glass/ITO/ZnO/PCDTBT:**SiNC-3**:$PC_{70}BM$/MoOx/Ag BHJ inverted ternary solar cells with various dye contents were fabricated and characterized. The energy levels of the materials used in this ternary device are shown in **Figure 7-3**. As shown, they also form a cascade energy level alignment. The *J–V* characteristics of the ternary blend solar cells and the corresponding control PCDTBT:$PC_{70}BM$ binary blend solar cell are shown in **Figure 7-4a**. The photovoltaic device parameters are further summarized in **Table 7-2**.

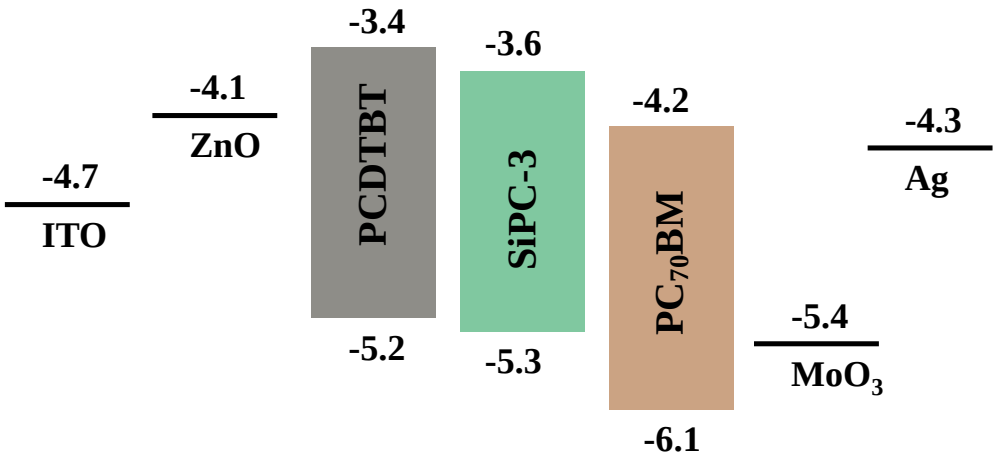

Figure 7-3 The schematic of the energy levels in the PCDTBT:**SiPC-3**:$PC_{70}BM$ ternary system.

As expected, the addition of **SiPC-3** results in an increase of the short circuit current density (J_{SC}) because of its complementary absorption profiles compared to the host polymer PCDTBT. Sensitization turned out to be most efficient at a dye concentration of 37.5 wt.%, leading to a J_{SC} increase of almost 10% from 10.75 mA cm^{-2} for the binary control device to 11.79 mA cm^{-2} for ternary based device. For concentrations above 50 wt.%, however, the positive influence of sensitization on J_{SC} starts to decline. Unfortunately, the fill factor (FF) only keeps constant when **SiPC-3** content is lower than 25 wt.% and at high **SiPC-3** concentrations shows a continuing downward trend. It can be explained by the destroying of the morphology in ternary blends. Interestingly, the V_{OC} increases from 0.85 eV to 0.90 V by adding 6.25 wt.% **SiNC-3** to the reference matrix and keeps almost constant for higher sensitizer concentration up to 100 wt.%.

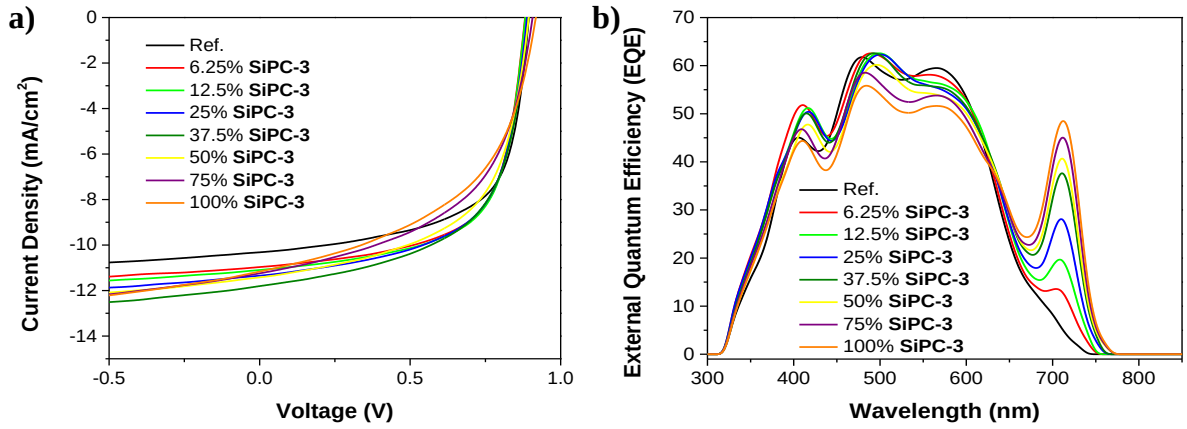

Figure 7-4 (a) J-V curves and (b) EQE spectra for PCDTBT:**SiNC-3**:$PC_{70}BM$ devices with various **SiNC-3** contents.

Table 7-2 Photovoltaic device parameters of PCDTBT:**SiNC-3**:$PC_{70}BM$ ternary devices with different **SiNC-3** contents under AM 1.5G, 100 mW cm^{-2}

Sample	SiPC content	V_{OC}(V)	J_{SC}(mA/cm^2)	J_{SC}(EQE)	FF(%)	PCE(%)
1	0%	0.90	10.32	8.98	63.50	5.90
2	6.25%	0.90	10.95	9.38	63.48	6.26
3	12.5%	0.90	11.13	9.53	63.18	6.31
4	25%	0.90	11.34	9.72	61.12	6.25
5	37.5%	0.90	11.79	10.11	58.98	6.26
6	50%	0.90	11.41	9.95	57.59	5.92
7	75%	0.90	11.23	9.98	53.40	5.34
8	100%	0.90	11.16	9.85	51.24	5.15

Figure 7-4b illustrates the external quantum efficiency (EQE) of the corresponding PCDTBT:**SiPC-3**:PCBM devices. Different from OPV-46:**SiPC-3**:PCBM ternary system, the EQE contribution of **SiPC-3** is very obvious. For the region from 650 nm to 770 nm which **SiPC-3** shows strong absorption profile, the EQE peak shows a significant improvement by increasing the SiPC-3 content from 0 wt.% to 100 wt.%. On the other hand, for only PCDTBT absorption region (350–650 nm), the EQE peak shows the constant trend even the

relative weight fraction of PCDTBT is reduced. It can be contributed to the interferences effect.

7.4 Conclusion

In this chapter, two mid band gap polymer ternary systems of OPV-46:**SiPC-3**:$PC_{70}BM$ and PCDTBT:**SiPC-3**:$PC_{70}BM$ were studied. **SiPC-3** was incorporated into these two systems with various contents. Compared to P3HT:**SiPC-3**:$PC_{70}BM$ system, it allows higher **SiPC-3** loading up to 50 wt.% in these two systems without destroying the device performance. It seems that **SiPC-3** can be dispersed in an amorphous polymer system, while for crystalline polymer system it can only locate at the interface of polymer:PCBM to contribute in current generation.

By adding **SiPC-3** dye molecules, a notable increase trend for J_{SC} was observed in both ternary systems. It is owing to the complementary absorption window and stronger absorption coefficient of **SiPC-3**, which further increase the current generation. The fill factor decrease by adding **SiPC-3** dye molecules particularly at high contents. Interesting, by increase **SiPC-3** content, V_{OC} presents different trend for two ternary systems, although both of them show a cascade alignment of the energy levels of the three components.

Chapter 8

Summary and outlook

Abstract

This chapter summarizes the main achievements presented in this thesis. Limitations and future challenges for organic ternary solar cells are supplied as an outlook.

8.1 Summary

In this thesis, we focused on the synthesis of novel dyes and their application in organic ternary and quaternary solar cells as near IR sensitizer. We carried out a full study on device physics, charge transfer/transport and morphology of various ternary systems, including our novel dye pigments.

In the first part of this thesis, we focused on the synthesis of silicon phthalocyanine and naphthalocyanine dye molecules and studied the relationship between the molecule structures with the electronic properties by cyclic voltammetry and optical properties by UV-vis absorption. **Chapter 4** showed the detail synthesis procedure of a novel series of silicon phthalocyanines (**SiPC-0**, **SiPC-1**, **SiPC-2**, and **SiPC-3**) with varying the length of alkyl chain between the pyrene ring with PC ring, and silicon naphthalocyanine (**SiNC-1**). By cyclic voltammetry measurements, it reveals that the alkyl chain length will not change the electronic properties for all **SiPCs**. Just **SiNC-1** showed smaller HOMO-LUMO gap because its extended π-system, yielding better electronic communication. By testing UV-*vis* in both solution and solid state, the distinguish absorption characteristics for both silicon phthalocyanines/naphthalocyanine and pyrene ring were observed. Meanwhile, **SiNC-1** shows a strong red shift compared to other **SiPCs**, providing a broader absorption in the near IR region. The outcome of research works in this chapter can be summarized as: i) The length of alkyl chain between the pyrene ring and PC ring did not change electronic and optical properties in solution condition. ii) Extending the π-system structure of dye molecule from SiPCs to SiNC showed a significant effect on electronic and optical properties. iii) Owing to their strong near IR absorption and suitable energy levels alignment **SiPC-0**, **SiPC-1**, **SiPC-2**, **SiPC-3**, and **SiNC-1** all had a great potential to be successfully applied in different ternary or quaternary organic solar cells as dye sensitizers.

In the second part of this thesis, we focused on study of the relationship between material structure with their physical properties and their device application. In **Chapter 5**, all silicon phthalocyanines **SiPC-0**, **SiPC-1**, **SiPC-2**, and **SiPC-3** were introduced into P3HT:PCBM

matrix as near IR sensitizer in ternary solar cells. All **SiPCs** showed a strong photosensitivity in the near IR region and nice improvement for all device parameters in ternary systems. By investigating solid state ternary films, it revealed that the alkyl chain length controlled the intermolecular and intramolecular interaction. In particular, **SiPC-0**, which had no alkyl chain as linker group, showed a relatively broaden absorption in the solid state (up to 800 nm photosensitivity in EQE spectra), and a higher J_{SC}. Meanwhile, **SiPC-3**, which had the longest alkyl chain as linker group, revealed the overall best fill factor. It yielded an increase of up to 21.9% of J_{SC}, 16.1% of V_{OC} and 7.2% of FF, leading to an improvement of up to 51.6% of PCE for **SiPC-3** based ternary solar cells compared to the reference P3HT:PCBM binary system. Photocurrent study and Photo-CELIV measurement indicated higher free charge carrier generation rates for **SiPC-0** and higher mobility for **SiPC-3**. AFM and TEM investigations exhibited the morphology was not disturbed by adding **SiPCs**. The outcome of research works in this chapter can be summarized as: i) The length of alkyl chain between the pyrene ring and PC ring had an impact on intermolecular and intermolecular interaction in the solid film, which subsequently affected various properties such as film absorption and charge carrier mobility. ii) This kind of silicon phthalocyanines were suitable sensitizers because then not only improved all device parameters but also did not change the morphology of the host matrix. iii) Tailoring efficient dye sensitizer by changing molecular structure supplied us more rational choice.

In the third part of this thesis, we focused on not only the study of ternary and quaternary concept but also revealing the charge transfer/transport mechanism. In **Chapter 6**, **SiNC-1** was embedded into the P3HT/PCBM matrix as a light harvesting photosensitizer in the longer wavelength region with various contents. It showed the complementary absorption widows compared to the host system, which yielded strong photosensitivity in the near IR region (650-950 nm) verified by both UV-*vis* absorption and EQE measurements. In the near IR region, the photosensitivity effect increased with adding more and more **SiNC-1**. At the end, it yielded an improvement of up to 10% for J_{SC} and 24% for PCE for P3HT:**SiNC-1**:PCBM ternary devices compared to the P3HT:PCBM reference. Our in-depth study based on the complementary IQE, PL and PIA measurements revealed complex charge

transfer and transport kinetic, including cascade charge transfer, energy transfer and parallel-like charge transfer mechanisms. Furthermore, quaternary devices have been fabricated based on two sensitizers (**SiNC-1**+**SiPC-0** or **SiNC-1**+**SiPC-1**) blended with a P3HT/PCBM matrix because of their complementary absorption window. For multi-color dye sensitized device, it showed the apparent signal characteristics of each single dye with two separate absorption peaks in the near IR region, corroborating the effective contribution of both **SiPC** and **SiNC** dyes. Interestingly, the total amount of sensitizers loading at the interface of P3HT:PCBM always get saturated in the range of 15 to 20 wt.%. The outcome of research works in this chapter can be summarized as: i) **SiNC-1** was a wonderful sensitizer used in polymer based ternary system, because of not only its strong photosensitivity in the near IR region up to 950 nm but also its efficient charge transfer/transport mechanism. ii) For crystalline polymer (P3HT) based ternary system, the sensitization turned out to be most efficient with 15–20 wt.% dye loading no matter one or two sensitizers. iii) Multi-colored dye sensitization concept was successfully demonstrated as a powerful approach to broaden the non-ideal narrow absorption window of organic-based optoelectronic devices all over the UV, Vis and near-IR regions.

In the last part of this thesis, we focused on studying mid band gap polymer ternary systems. In **Chapter 7**, the best silicon phthalocyanine **SiPC-3** was individually introduced into OPV-46:$PC_{70}BM$ and PCDTBT:$PC_{70}BM$ host systems with various **SiPC-3** contents. It was found that up to 37.5 wt.% of **SiPC-3** loading is still improving the device performance, in contrast to P3HT-based ternary devices which only around 15-20 wt.% sensitizer loading was allowed. For both systems, **SiPC-3** showed very strong photosensitivity in the near IR region, up to 50% observed in the EQE spectra. Hence, it yielded an increasing of J_{SC} in both ternary systems. Interestingly, different V_{OC} trend were observed for these two ternary systems. The outcome of research works in this chapter can be summarized as: i) compared to the crystalline P3HT systems, amorphous polymer systems allowed more dye sensitizer loading with stronger near IR photosensitivity. ii) Despite the similar cascade alignment of the energy levels and quite similar HOMO/LUMO value, these two ternary systems showed very different V_{OC} change trends.

8.2 Outlook

The results and findings demonstrated in this thesis are a broad investigation of dye sensitized ternary organic solar cells. The goal of this work was to design and synthesize appropriate dye molecules with strong near IR absorption which is fully functional in high efficiency organic ternary solar cells as near IR sensitizer. Incorporating the silicon phthalocyanine/ naphthalocyanine molecules is a simple and versatile method to enhance light harvesting and, thus, to increase the device performance. However, there are still some challenges and limitations.

The visualizing and controlling of the morphology and crystallinity of the ternary blend films are two big challenges for ternary solar cells, which are closely related to the compatibility and miscibility of the sensitizer into the host system. According to the above discussion in this thesis, silicon phthalocyanine/ naphthalocyanine molecules cannot be incorporated into crystalline polymer:fullerene systems with a higher content because its limited loading at the interface of host matrix. As we know, the interface engineering is a particular importance for dye sensitization in ternary blend solar cells. One useful method is to design other types of **SiPC**/ or **SiNC** molecules, with one axial ligand substituent compatible with crystalline polymer with a surface energy of around 25-30 mN/m and another ligand substituent compatible with fullerene with a higher surface energy of around 50 mN/m. At the end, it will allow more dye molecules loading in the interface, which further improve the photocurrent and device performance without disturbing the morphology of host matrix.

Due to the incorporation of the third component, the fundamental working mechanisms of ternary solar cells are much more complicated than the traditional binary devices, which need further investigation for better selection of the active layer materials. Among them, the arguments about the tunable V_{OC} in the ternary solar cells require still further verification and understanding. Actually there are lots of parameters which can influence the V_{OC}, as shown in **Figure 8-1**. Influence of the charge transfer energy and its absorption intensity on the V_{OC} of ternary solar cells can be investigated by *Fourier Transform Photocurrent*

Spectroscopy (*FTPS*) measurements. One the other hand, electroluminescence (EL) can be done to get insight into the non-geminate recombination mechanism in ternary blend devices as compared to the reference binary one.

Figure 8-1 The parameters which influence the V_{OC} directly or indirectly.[230]

Appendix A

Bibliography

1 Delucchi, M. A. & Jacobson, M. Z. Providing all global energy with wind, water, and solar power, Part II: Reliability, system and transmission costs, and policies. *Energy policy* **39**, 1170-1190 (2011).

2 Solangi, K., Islam, M., Saidur, R., Rahim, N. & Fayaz, H. A review on global solar energy policy. *Renewable and sustainable energy reviews* **15**, 2149-2163 (2011).

3 Scharber, M. C. & Sariciftci, N. S. Efficiency of bulk-heterojunction organic solar cells. *Progress in polymer science* **38**, 1929-1940 (2013).

4 Yeh, N. & Yeh, P. Organic solar cells: Their developments and potentials. *Renewable and Sustainable Energy Reviews* **21**, 421-431 (2013).

5 Dou, L. *et al.* 25th anniversary article: a decade of organic/polymeric photovoltaic research. *Advanced Materials* **25**, 6642-6671 (2013).

6 Weinberger, B., Akhtar, M. & Gau, S. Polyacetylene photovoltaic devices. *Synthetic Metals* **4**, 187-197 (1982).

7 Karg, S., Riess, W., Dyakonov, V. & Schwoerer, M. Electrical and optical characterization of poly (phenylene-vinylene) light emitting diodes. *Synth Met* **54**, 427-433 (1993).

8 Tang, C. W. Two‐layer organic photovoltaic cell. *Applied Physics Letters* **48**, 183-185 (1986).

9 Yu, G., Gao, J., Hummelen, J. C., Wudl, F. & Heeger, A. J. Polymer photovoltiac cells: Enhanced efficiencies via a network of internal donor-acceptor heterojunctions. *Science* **270**, 1789 (1995).

10 Chiang, C. K. *et al.* Electrical conductivity in doped polyacetylene. *Physical Review Letters* **39**, 1098 (1977).

11 Brabec, C. J., Dyakonov, V., Parisi, J. & Sariciftci, N. S. *Organic photovoltaics: concepts and realization*. Vol. 60 (Springer Science & Business Media, 2013).

12 Inoue, K. *et al.* Temperature and time dependence of heat treatment of rr-p3ht/pcbm solar cell. *Synthetic metals* **154**, 41-44 (2005).

13 Brabec, C. J. & Durrant, J. R. Solution-processed organic solar cells. *Mrs Bulletin* **33**, 670-675 (2008).

14 Peet, J., Heeger, A. J. & Bazan, G. C. "Plastic" solar cells: self-assembly of bulk heterojunction nanomaterials by spontaneous phase separation. *Accounts of Chemical Research* **42**, 1700-1708 (2009).

15 Price, S. C., Stuart, A. C., Yang, L., Zhou, H. & You, W. Fluorine substituted conjugated polymer of medium band gap yields 7% efficiency in polymer− fullerene solar cells. *Journal of the American Chemical Society* **133**, 4625-4631 (2011).

16 Hawks, S. Device Physics and Recombination in Polymer: Fullerene Bulk-Heterojunction Solar Cells. (2015).

17 Brédas, J.-L., Beljonne, D., Coropceanu, V. & Cornil, J. Charge-transfer and energy-transfer processes in π-conjugated oligomers and polymers: a molecular picture. *Chemical Reviews* **104**, 4971-5004 (2004).

18 Ross, R. B. *et al.* Endohedral fullerenes for organic photovoltaic devices. *Nature materials* **8**, 208-212 (2009).

19 Kooistra, F. B. *et al.* New C84 derivative and its application in a bulk heterojunction solar cell. *Chemistry of materials* **18**, 3068-3073 (2006).

20 Troshin, P. A. *et al.* Material Solubility‐Photovoltaic Performance Relationship in the Design of Novel Fullerene Derivatives for Bulk Heterojunction Solar Cells. *Advanced Functional Materials* **19**, 779-788 (2009).

21 Wright, M. & Uddin, A. Organic—inorganic hybrid solar cells: A comparative review. *Solar energy materials and solar cells* **107**, 87-111 (2012).

22 Benanti, T. L. & Venkataraman, D. Organic solar cells: an overview focusing on active layer morphology. *Photosynthesis research* **87**, 73-81 (2006).

23 Hoppe, H. & Sariciftci, N. S. Morphology of polymer/fullerene bulk heterojunction solar cells. *Journal of Materials Chemistry* **16**, 45-61 (2006).

24 Liu, Y. *et al.* Aggregation and morphology control enables multiple cases of high-efficiency polymer solar cells. *Nature communications* **5** (2014).

25 He, Z. *et al.* Single-junction polymer solar cells with high efficiency and photovoltage. *Nature Photonics* **9**, 174-179 (2015).

26 bin Mohd Yusoff, A. R. *et al.* A high efficiency solution processed polymer inverted triple-junction solar cell exhibiting a power conversion efficiency of 11.83%. *Energy & Environmental Science* **8**, 303-316 (2015).

27 Zhou, H. *et al.* Polymer Homo‐Tandem Solar Cells with Best Efficiency of 11.3%. *Advanced Materials* **27**, 1767-1773 (2015).

28 Cabanetos, C. m. *et al.* Linear side chains in benzo [1, 2-b: 4, 5-b′] dithiophene–thieno [3, 4-c] pyrrole-4, 6-dione polymers direct self-assembly and solar cell performance. *Journal of the American Chemical Society* **135**, 4656-4659 (2013).

29 Li, N. *et al.* Towards 15% energy conversion efficiency: a systematic study of the solution-processed organic tandem solar cells based on commercially available materials. *Energy & Environmental Science* **6**, 3407-3413 (2013).

30 Günes, S., Neugebauer, H. & Sariciftci, N. S. Conjugated polymer-based organic solar cells.

Chemical reviews **107**, 1324-1338 (2007).

31 Kim, J. Y. *et al.* New Architecture for high‐efficiency polymer photovoltaic cells using solution‐based titanium oxide as an optical spacer. *Advanced materials* **18**, 572-576 (2006).

32 Sariciftci, N., Smilowitz, L., Heeger, A. J. & Wudl, F. Photoinduced electron transfer from a conducting polymer to buckminsterfullerene. *Science* **258**, 1474-1476 (1992).

33 Markov, D. E., Amsterdam, E., Blom, P. W., Sieval, A. B. & Hummelen, J. C. Accurate measurement of the exciton diffusion length in a conjugated polymer using a heterostructure with a side-chain cross-linked fullerene layer. *The Journal of Physical Chemistry A* **109**, 5266-5274 (2005).

34 Kim, J. Y. *et al.* Efficient tandem polymer solar cells fabricated by all-solution processing. *Science* **317**, 222-225 (2007).

35 You, J., Dou, L., Hong, Z., Li, G. & Yang, Y. Recent trends in polymer tandem solar cells research. *Progress in polymer science* **38**, 1909-1928 (2013).

36 Sista, S., Hong, Z., Chen, L.-M. & Yang, Y. Tandem polymer photovoltaic cells—current status, challenges and future outlook. *Energy & Environmental Science* **4**, 1606-1620 (2011).

37 Ameri, T., Li, N. & Brabec, C. J. Highly efficient organic tandem solar cells: a follow up review. *Energy & Environmental Science* **6**, 2390-2413 (2013).

38 Ameri, T., Dennler, G., Lungenschmied, C. & Brabec, C. J. Organic tandem solar cells: a review. *Energy & Environmental Science* **2**, 347-363 (2009).

39 Timmreck, R. *et al.* Characterization of tandem organic solar cells. *Nature Photonics* **9**, 478-479 (2015).

40 Wang, D. H., Kyaw, A. K. K. & Park, J. H. Enhanced Fill Factor of Tandem Organic Solar Cells Incorporating a Diketopyrrolopyrrole‐Based Low‐Bandgap Polymer and Optimized Interlayer. *ChemSusChem* **8**, 331-336 (2015).

41 Cheng, Y.-J., Yang, S.-H. & Hsu, C.-S. Synthesis of conjugated polymers for organic solar cell applications. *Chemical reviews* **109**, 5868-5923 (2009).

42 Servaites, J. D., Ratner, M. A. & Marks, T. J. Practical efficiency limits in organic photovoltaic cells: Functional dependence of fill factor and external quantum efficiency. *Applied Physics Letters* **95**, 163302 (2009).

43 Clarke, T. M. & Durrant, J. R. Charge photogeneration in organic solar cells. *Chemical reviews* **110**, 6736-6767 (2010).

44 Sze, S. M. & Ng, K. K. *Physics of semiconductor devices.* (John wiley & sons, 2006).

45 Hains, A. W., Liang, Z., Woodhouse, M. A. & Gregg, B. A. Molecular semiconductors in organic photovoltaic cells. *Chemical reviews* **110**, 6689-6735 (2010).

46 Ohkita, H. *et al.* Charge carrier formation in polythiophene/fullerene blend films studied by transient absorption spectroscopy. *Journal of the American Chemical Society* **130**, 3030-3042 (2008).

47 Ford, T., Avilov, I., Beljonne, D. & Greenham, N. Enhanced triplet exciton generation in polyfluorene blends. *Physical Review B* **71**, 125212 (2005).

48 Guo, J., Ohkita, H., Benten, H. & Ito, S. Charge generation and recombination dynamics in poly (3-hexylthiophene)/fullerene blend films with different regioregularities and morphologies. *Journal of the American Chemical Society* **132**, 6154-6164 (2010).

49 Clarke, T. M. *et al.* Charge photogeneration in low band gap polyselenophene/fullerene blend films. *The Journal of Physical Chemistry C* **114**, 8068-8075 (2010).

50 Veldman, D. *et al.* Compositional and electric field dependence of the dissociation of charge transfer excitons in alternating polyfluorene copolymer/fullerene blends. *Journal of the American Chemical Society* **130**, 7721-7735 (2008).

51 Deibel, C. & Dyakonov, V. Polymer? fullerene bulk heterojunction solar cells. *Reports on Progress in Physics* **73**, 096401 (2010).

52 Brédas, J. L., Cornil, J. & Heeger, A. J. The exciton binding energy in luminescent conjugated polymers. *Advanced Materials* **8**, 447-452 (1996).

53 McBranch, D. *et al.* Signatures of excitons and polaron pairs in the femtosecond excited-state absorption spectra of phenylene-based conjugated polymers and oligomers. *Synthetic metals* **101**, 291-294 (1999).

54 Scully, S. R. & McGehee, M. D. Effects of optical interference and energy transfer on exciton diffusion length measurements in organic semiconductors. *Journal of applied physics* **100**, 034907 (2006).

55 Nunzi, J.-M. Organic photovoltaic materials and devices. *Comptes Rendus Physique* **3**, 523-542 (2002).

56 WEI, F. *et al.* Properties of conducting polymer donor-acceptor composite films and photovoltaic characteristics of junction devices. (2001).

57 Peumans, P. & Forrest, S. R. Separation of geminate charge-pairs at donor–acceptor interfaces in disordered solids. *Chemical Physics Letters* **398**, 27-31 (2004).

58 Ruseckas, A. *et al.* Ultrafast photogeneration of inter-chain charge pairs in polythiophene films. *Chemical Physics Letters* **322**, 136-142 (2000).

59 Ren, G. *et al.* Photoinduced Hole Transfer Becomes Suppressed with Diminished Driving Force in Polymer‐Fullerene Solar Cells While Electron Transfer Remains Active. *Advanced Functional Materials* **23**, 1238-1249 (2013).

60 Bakulin, A. A. *et al.* Charge-transfer state dynamics following hole and electron transfer in organic photovoltaic devices. *The journal of physical chemistry letters* **4**, 209-215 (2012).

61 Bakulin, A. A. *et al.* The role of driving energy and delocalized states for charge separation in organic semiconductors. *Science* **335**, 1340-1344 (2012).

62 Koster, L., Mihailetchi, V., Xie, H. & Blom, P. Origin of the light intensity dependence of the short-circuit current of polymer/fullerene solar cells. *Applied Physics Letters* **87**, 203502 (2005).

63 Winder, C. & Sariciftci, N. S. Low bandgap polymers for photon harvesting in bulk heterojunction solar cells. *Journal of Materials Chemistry* **14**, 1077-1086 (2004).

64 Brabec, C. J. *et al.* Origin of the open circuit voltage of plastic solar cells. *Advanced Functional Materials* **11**, 374-380 (2001).

65 Shuttle, C. G. *et al.* Bimolecular recombination losses in polythiophene: Fullerene solar cells. *Physical Review B* **78**, 113201 (2008).

66 Lu, H., Akgun, B. & Russell, T. P. Morphological Characterization of a Low‐Bandgap Crystalline Polymer: PCBM Bulk Heterojunction Solar Cells. *Advanced Energy Materials* **1**, 870-878 (2011).

67 Wang, M. *et al.* Donor–acceptor conjugated polymer based on naphtho [1, 2-c: 5, 6-c] bis [1, 2, 5] thiadiazole for high-performance polymer solar cells. *Journal of the American Chemical Society* **133**, 9638-9641 (2011).

68 Liang, Y. *et al.* For the bright future—bulk heterojunction polymer solar cells with power conversion efficiency of 7.4%. *Advanced Materials* **22** (2010).

69 Wang, E. *et al.* An Easily Synthesized Blue Polymer for High‐Performance Polymer Solar Cells. *Advanced Materials* **22**, 5240-5244 (2010).

70 Bijleveld, J. C. *et al.* Poly (diketopyrrolopyrrole− terthiophene) for ambipolar logic and photovoltaics. *Journal of the American Chemical Society* **131**, 16616-16617 (2009).

71 Xu, T. & Yu, L. How to design low bandgap polymers for highly efficient organic solar cells. *Materials Today* **17**, 11-15 (2014).

72 Zhou, E., Hashimoto, K. & Tajima, K. Low band gap polymers for photovoltaic device with photocurrent response wavelengths over 1000nm. *Polymer* **54**, 6501-6509 (2013).

73 Bian, L., Zhu, E., Tang, J., Tang, W. & Zhang, F. Recent progress in the design of narrow bandgap conjugated polymers for high-efficiency organic solar cells. *Progress in Polymer Science* **37**, 1292-1331 (2012).

74 Beaujuge, P. M. & Fréchet, J. M. Molecular design and ordering effects in π-functional materials for transistor and solar cell applications. *Journal of the American Chemical Society* **133**, 20009-20029 (2011).

75 Li, N. & Brabec, C. J. Air-processed polymer tandem solar cells with power conversion efficiency exceeding 10%. *Energy & Environmental Science* **8**, 2902-2909 (2015).

76 An, Q. *et al.* Versatile ternary organic solar cells: a critical review. *Energy & Environmental Science* **9**, 281-322 (2016).

77 Kubo, Y. *et al.* Near-infrared absorbing boron-dibenzopyrromethenes that serve as light-harvesting sensitizers for polymeric solar cells. *Organic letters* **13**, 4574-4577 (2011).

78 Rauch, T. *et al.* Near-infrared imaging with quantum-dot-sensitized organic photodiodes. *nature photonics* **3**, 332-336 (2009).

79 Koppe, M. *et al.* Near IR sensitization of organic bulk heterojunction solar cells: towards

optimization of the spectral response of organic solar cells. *Advanced Functional Materials* **20**, 338-346 (2010).

80 Koppe, M. *et al.* Charge carrier dynamics in a ternary bulk heterojunction system consisting of P3HT, fullerene, and a low bandgap polymer. *Advanced Energy Materials* **3**, 949-958 (2013).

81 Löslein, H. *et al.* Transient Absorption Spectroscopy Studies on Polythiophene–Fullerene Bulk Heterojunction Organic Blend Films Sensitized with a Low‐Bandgap Polymer. *Macromolecular rapid communications* **34**, 1090-1097 (2013).

82 Ameri, T. *et al.* Performance Enhancement of the P3HT/PCBM Solar Cells through NIR Sensitization Using a Small‐Bandgap Polymer. *Advanced Energy Materials* **2**, 1198-1202 (2012).

83 Ameri, T., Khoram, P., Min, J. & Brabec, C. J. Organic ternary solar cells: a review. *Advanced Materials* **25**, 4245-4266 (2013).

84 Ameri, T. *et al.* IR sensitization of an indene-C60 bisadduct (ICBA) in ternary organic solar cells. *Energy & Environmental Science* **6**, 1796-1801 (2013).

85 Zhang, J. *et al.* Conjugated polymer–small molecule alloy leads to high efficient ternary organic solar cells. *Journal of the American Chemical Society* **137**, 8176-8183 (2015).

86 Liu, T. *et al.* Ternary Organic Solar Cells Based on Two Highly Efficient Polymer Donors with Enhanced Power Conversion Efficiency. *Advanced Energy Materials* (2015).

87 Zhang, Y. *et al.* Synergistic Effect of Polymer and Small Molecules for High‐Performance Ternary Organic Solar Cells. *Advanced Materials* **27**, 1071-1076 (2015).

88 Lu, L., Chen, W., Xu, T. & Yu, L. High-performance ternary blend polymer solar cells involving both energy transfer and hole relay processes. *Nature communications* **6** (2015).

89 Lu, L., Kelly, M. A., You, W. & Yu, L. Status and prospects for ternary organic photovoltaics. *Nature Photonics* **9**, 491-500 (2015).

90 Chen, C.-H., Hsieh, C.-H., Dubosc, M., Cheng, Y.-J. & Hsu, C.-S. Synthesis and characterization of bridged bithiophene-based conjugated polymers for photovoltaic applications: acceptor strength and ternary blends. *Macromolecules* **43**, 697-708 (2009).

91 Zhen, Y. *et al.* Organic Solid Solution Composed of Two Structurally Similar Porphyrins for Organic Solar Cells. *Journal of the American Chemical Society* **137**, 2247-2252 (2015).

92 Mandoc, M., Kooistra, F., Hummelen, J., De Boer, B. & Blom, P. Effect of traps on the performance of bulk heterojunction organic solar cells. *Applied Physics Letters* **91**, 263505 (2007).

93 Zhang, M. *et al.* High efficient ternary polymer solar cells based on absorption complementary materials as electron donor. *Solar Energy Materials and Solar Cells* **141**, 154-161 (2015).

94 Hu, Z., Tang, S., Ahlvers, A., Khondaker, S. I. & Gesquiere, A. J. Near-infrared photoresponse sensitization of solvent additive processed poly (3-hexylthiophene)/fullerene solar cells by a low band gap polymer. *Applied Physics Letters* **101**, 053308 (2012).

95 Hesse, H. C. *et al.* Perylene sensitization of fullerenes for improved performance in organic photovoltaics. *Advanced Energy Materials* **1**, 861-869 (2011).

96 Sun, Q. *et al.* Doping a DA structural polymer based on benzodithiophene and triazoloquinoxaline for efficiency improvement of ternary solar cells. *Electronic Materials Letters* **11**, 236-240 (2015).

97 An, Q. *et al.* Enhanced performance of polymer solar cells by employing a ternary cascade energy structure. *Physical Chemistry Chemical Physics* **16**, 16103-16109 (2014).

98 Leong, W. L., Cowan, S. R. & Heeger, A. J. Differential Resistance Analysis of Charge Carrier Losses in Organic Bulk Heterojunction Solar Cells: Observing the Transition from Bimolecular to Trap‐Assisted Recombination and Quantifying the Order of Recombination. *Advanced Energy Materials* **1**, 517-522 (2011).

99 Huang, T.-Y. *et al.* Efficient ternary bulk heterojunction solar cells based on small molecules only. *Journal of Materials Chemistry A* **3**, 10512-10518 (2015).

100 Santo, Y., Jeon, I., Yeo, K. S., Nakagawa, T. & Matsuo, Y. Mixture of [60] and [70] PCBM giving morphological stability in organic solar cells. *Applied Physics Letters* **103**, 073306 (2013).

101 Cheng, Y. J., Hsieh, C. H., Li, P. J. & Hsu, C. S. Morphological stabilization by in situ polymerization of fullerene derivatives leading to efficient, thermally stable organic photovoltaics. *Advanced Functional Materials* **21**, 1723-1732 (2011).

102 Bonaccorso, F. *et al.* Functionalized Graphene as an Electron‐Cascade Acceptor for Air‐Processed Organic Ternary Solar Cells. *Advanced Functional Materials* **25**, 3870-3880 (2015).

103 Wei, Q., Nishizawa, T., Tajima, K. & Hashimoto, K. Self‐Organized Buffer Layers in Organic Solar Cells. *Advanced Materials* **20**, 2211-2216 (2008).

104 An, Q. *et al.* Simultaneous improvement in short circuit current, open circuit voltage, and fill factor of polymer solar cells through ternary strategy. *ACS applied materials & interfaces* **7**, 3691-3698 (2015).

105 Lu, L., Xu, T., Chen, W., Landry, E. S. & Yu, L. Ternary blend polymer solar cells with enhanced power conversion efficiency. *Nature Photonics* **8**, 716-722 (2014).

106 Cnops, K. *et al.* 8.4% efficient fullerene-free organic solar cells exploiting long-range exciton energy transfer. *Nature communications* **5** (2014).

107 An, Q. *et al.* Improved efficiency of bulk heterojunction polymer solar cells by doping low-bandgap small molecules. *ACS applied materials & interfaces* **6**, 6537-6544 (2014).

108 Yang, L., Zhou, H., Price, S. C. & You, W. Parallel-like bulk heterojunction polymer solar cells. *Journal of the American Chemical Society* **134**, 5432-5435 (2012).

109 Khlyabich, P. P., Burkhart, B. & Thompson, B. C. Efficient ternary blend bulk heterojunction solar cells with tunable open-circuit voltage. *Journal of the American Chemical Society* **133**, 14534-14537 (2011).

110 Khlyabich, P. P., Rudenko, A. E., Street, R. A. & Thompson, B. C. Influence of polymer compatibility on the open-circuit voltage in ternary blend bulk heterojunction solar cells. *ACS*

applied materials & interfaces **6**, 9913-9919 (2014).

111 Khlyabich, P. P., Rudenko, A. E., Thompson, B. C. & Loo, Y. L. Structural Origins for Tunable Open‐Circuit Voltage in Ternary‐Blend Organic Solar Cells. *Advanced Functional Materials* **25**, 5557-5563 (2015).

112 Street, R. A., Davies, D., Khlyabich, P. P., Burkhart, B. & Thompson, B. C. Origin of the tunable open-circuit voltage in ternary blend bulk heterojunction organic solar cells. *Journal of the American Chemical Society* **135**, 986-989 (2013).

113 Chun, H. J., Kim, E. S. & Cho, B. R. Scope and limitation of label‐free multiphoton microscopy and probe‐labeled two‐photon microscopy for the endomicroscopic diagnosis. *Scanning* **36**, 462-464 (2014).

114 Cho, Y. J., Lee, J. Y., Chin, B. D. & Forrest, S. R. Polymer bulk heterojunction photovoltaics employing a squaraine donor additive. *Organic Electronics* **14**, 1081-1085 (2013).

115 Minnaert, B. & Burgelman, M. Efficiency potential of organic bulk heterojunction solar cells. *Progress in Photovoltaics: Research and Applications* **15**, 741-748 (2007).

116 Li, N. *et al.* Inverted structure organic photovoltaic devices employing a low temperature solution processed WO 3 anode buffer layer. *Organic Electronics* **13**, 2479-2484 (2012).

117 Khlyabich, P. P., Burkhart, B. & Thompson, B. C. Compositional dependence of the open-circuit voltage in ternary blend bulk heterojunction solar cells based on two donor polymers. *Journal of the American Chemical Society* **134**, 9074-9077 (2012).

118 Li, H., Zhang, Z.-G., Li, Y. & Wang, J. Tunable open-circuit voltage in ternary organic solar cells. *Applied Physics Letters* **101**, 163302 (2012).

119 Kouijzer, S., Li, W., Wienk, M. M. & Janssen, R. A. Charge transfer state energy in ternary bulk-heterojunction polymer–fullerene solar cells. *Journal of Photonics for Energy* **5**, 057203-057203 (2015).

120 Cha, H. *et al.* Complementary Absorbing Star‐Shaped Small Molecules for the Preparation of Ternary Cascade Energy Structures in Organic Photovoltaic Cells. *Advanced Functional Materials* **23**, 1556-1565 (2013).

121 Kang, H. *et al.* Effect of fullerene tris-adducts on the photovoltaic performance of P3HT: fullerene ternary blends. *ACS applied materials & interfaces* **5**, 4401-4408 (2013).

122 Hallermann, M. *et al.* Correlation between charge transfer exciton recombination and photocurrent in polymer/fullerene solar cells. *Appl. Phys. Lett* **97**, 1-3 (2010).

123 Zhou, Y. *et al.* Observation of a Charge Transfer State in Low‐Bandgap Polymer/Fullerene Blend Systems by Photoluminescence and Electroluminescence Studies. *Advanced Functional Materials* **19**, 3293-3299 (2009).

124 Vandewal, K., Tvingstedt, K., Gadisa, A., Inganäs, O. & Manca, J. V. Relating the open-circuit voltage to interface molecular properties of donor: acceptor bulk heterojunction solar cells. *Physical Review B* **81**, 125204 (2010).

125 Campoy-Quiles, M., Kanai, Y., El-Basaty, A., Sakai, H. & Murata, H. Ternary mixing: A simple method to tailor the morphology of organic solar cells. *Organic Electronics* **10**, 1120-1132 (2009).

126 Chang, S.-Y. *et al.* Enhancing the efficiency of low bandgap conducting polymer bulk heterojunction solar cells using P3HT as a morphology control agent. *Journal of Materials Chemistry A* **1**, 2447-2452 (2013).

127 Park, S. J. *et al.* Bulk heterojunction polymer solar cells based on binary and ternary blend systems. *Journal of Polymer Science Part A: Polymer Chemistry* **49**, 4416-4424 (2011).

128 Hsin-Yi, C. *et al.* Poly (3-hexylthiophene): indene-C60 bisadduct morphology improvement by the use of polyvinylcarbazole as additive. *Solar Energy Materials and Solar Cells* **113**, 90-95 (2013).

129 Lou, Y., Wang, Z., Naka, S. & Okada, H. Enhanced short-circuit current density in poly (3-hexylthiophene) and 1-(3-methoxycarbonyl)-propyl-1-phenyl-(6, 6) C61 based organic solar cells by doping small molecular perylene. *Applied Physics Letters* **99**, 033305 (2011).

130 Peumans, P., Uchida, S. & Forrest, S. R. Efficient bulk heterojunction photovoltaic cells using small-molecular-weight organic thin films. *Nature* **425**, 158-162 (2003).

131 Peumans, P. & Forrest, S. Very-high-efficiency double-heterostructure copper phthalocyanine/C60 photovoltaic cells. *Applied Physics Letters* **79**, 126-128 (2001).

132 Heutz, S., Sullivan, P., Sanderson, B., Schultes, S. & Jones, T. Influence of molecular architecture and intermixing on the photovoltaic, morphological and spectroscopic properties of CuPc–C 60 heterojunctions. *Solar Energy Materials and Solar Cells* **83**, 229-245 (2004).

133 Chen, L. *et al.* Improvement of the efficiency of CuPc/C 60-based photovoltaic cells using a multistepped structure. *Organic Electronics* **10**, 724-728 (2009).

134 Ltaief, A., Chaâbane, R. B., Bouazizi, A. & Davenas, J. Photovoltaic properties of bulk heterojunction solar cells with improved spectral coverage. *Materials Science and Engineering: C* **26**, 344-347 (2006).

135 Kaulachs, I. *et al.* in *Proceedings of ISES World Congress 2007 (Vol. I–Vol. V).* 1038-1042 (Springer).

136 Johansson, E. M., Yartsev, A., Rensmo, H. & Sundstrom, V. Photocurrent spectra and fast kinetic studies of P3HT/PCBM mixed with a dye for photoconversion in the near-IR region. *The Journal of Physical Chemistry C* **113**, 3014-3020 (2009).

137 Honda, S., Nogami, T., Ohkita, H., Benten, H. & Ito, S. Improvement of the light-harvesting efficiency in polymer/fullerene bulk heterojunction solar cells by interfacial dye modification. *ACS applied materials & interfaces* **1**, 804-810 (2009).

138 Honda, S., Ohkita, H., Benten, H. & Ito, S. Selective dye loading at the heterojunction in polymer/fullerene solar cells. *Advanced Energy Materials* **1**, 588-598 (2011).

139 Honda, S., Yokoya, S., Ohkita, H., Benten, H. & Ito, S. Light-harvesting mechanism in polymer/fullerene/dye ternary blends studied by transient absorption spectroscopy. *The Journal of Physical Chemistry C* **115**, 11306-11317 (2011).

140 Honda, S., Ohkita, H., Benten, H. & Ito, S. Multi-colored dye sensitization of polymer/fullerene bulk heterojunction solar cells. *Chemical communications* **46**, 6596-6598 (2010).

141 Chen, W. *et al.* in *Electron Devices and Solid-State Circuits (EDSSC), 2010 IEEE International Conference of.* 1-4 (IEEE).

142 Xu, Z.-X., Roy, V., Low, K.-H. & Che, C.-M. Bulk heterojunction photovoltaic cells based on tetra-methyl substituted copper (II) phthalocyanine: P3HT: PCBM composite. *Chemical communications* **47**, 9654-9656 (2011).

143 Lim, B., Bloking, J. T., Ponec, A., McGehee, M. D. & Sellinger, A. Ternary bulk heterojunction solar cells: addition of soluble NIR dyes for photocurrent generation beyond 800 nm. *ACS applied materials & interfaces* **6**, 6905-6913 (2014).

144 Lessard, B. H. *et al.* Bis (tri-n-hexylsilyl oxide) silicon phthalocyanine: a unique additive in ternary bulk heterojunction organic photovoltaic devices. *ACS applied materials & interfaces* **6**, 15040-15051 (2014).

145 Xu, H., Ohkita, H., Tamai, Y., Benten, H. & Ito, S. Interface Engineering for Ternary Blend Polymer Solar Cells with a Heterostructured Near‐IR Dye. *Advanced Materials* **27**, 5868-5874 (2015).

146 Calloway, D. Beer-lambert law. *J. Chem. Educ* **74**, 744 (1997).

147 Baran, D. *Smart Concepts for Mapping Optoelectronic Properties of Organic Solar Cells: Strategies for Fast and Contactless Material Optimization*, Friedrich-Alexander-Universität Erlangen-Nürnberg (FAU), (2014).

148 Li, D. & Neumann, A. A reformulation of the equation of state for interfacial tensions. *Journal of Colloid and Interface Science* **137**, 304-307 (1990).

149 Li, D. & Neumann, A. Contact angles on hydrophobic solid surfaces and their interpretation. *Journal of colloid and interface science* **148**, 190-200 (1992).

150 Nalwa, H. S. *Handbook of Advanced Electronic and Photonic Materials and Devices: Conducting polymers. Vol. 8.* (Academic Press, 2001).

151 Wheeler, B. L., Nagasubramanian, G., Bard, A. J., Schechtman, L. A. & Kenney, M. E. A silicon phthalocyanine and a silicon naphthalocyanine: synthesis, electrochemistry, and electrogenerated chemiluminescence. *Journal of the American Chemical Society* **106**, 7404-7410 (1984).

152 de la Torre, G., Claessens, C. G. & Torres, T. Phthalocyanines: old dyes, new materials. Putting color in nanotechnology. *Chemical communications*, 2000-2015 (2007).

153 Mack, J. & Kobayashi, N. Low symmetry phthalocyanines and their analogues. *Chemical reviews* **111**, 281-321 (2010).

154 Claessens, C. G., Hahn, U. & Torres, T. Phthalocyanines: from outstanding electronic properties to emerging applications. *The Chemical Record* **8**, 75-97 (2008).

155 Ince, M. *et al.* Molecular engineering of phthalocyanine sensitizers for dye-sensitized solar cells. *The Journal of Physical Chemistry C* **118**, 17166-17170 (2014).

156 Mori, S. *et al.* Enhancement of incident photon-to-current conversion efficiency for phthalocyanine-sensitized solar cells by 3D molecular structuralization. *Journal of the American Chemical Society* **132**, 4054-4055 (2010).

157 Bottari, G., de la Torre, G., Guldi, D. M. & Torres, T. Covalent and noncovalent phthalocyanine−carbon nanostructure systems: synthesis, photoinduced electron transfer, and application to molecular photovoltaics. *Chemical reviews* **110**, 6768-6816 (2010).

158 García-Iglesias, M. *et al.* Effect of anchoring groups in zinc phthalocyanine on the dye-sensitized solar cell performance and stability. *Chemical Science* **2**, 1145-1150 (2011).

159 Palomares, E., Martínez-Díaz, M. V., Haque, S. A., Torres, T. & Durrant, J. R. State selective electron injection in non-aggregated titanium phthalocyanine sensitised nanocrystalline TiO 2 films. *Chemical communications*, 2112-2113 (2004).

160 Morandeira, A. *et al.* Slow electron injection on Ru-phthalocyanine sensitized TiO2. *Journal of the American Chemical Society* **129**, 9250-9251 (2007).

161 Atilla, D. *et al.* Synthesis and photodynamic potential of tetra-and octa-triethyleneoxysulfonyl substituted zinc phthalocyanines. *Journal of Photochemistry and Photobiology A: Chemistry* **186**, 298-307 (2007).

162 Cheng, G. *et al.* Synthesis, photochemistry, and electrochemistry of a series of phthalocyanines with graded steric hindrance. *The Journal of Physical Chemistry A* **107**, 3503-3514 (2003).

163 Rodríguez-Redondo, J. L. *et al.* Phthalocyanine-modulated isomerization behaviour of an azo-based photoswitch. *Chemical communications*, 1265-1267 (2006).

164 McKeown, N. B. Phthalocyanine-containing polymers. *Journal of Materials Chemistry* **10**, 1979-1995 (2000).

165 Makhseed, S., McKeown, N. B., Msayib, K. & Bumajdad, A. Inducing solid-state isolation of the phthalocyanine macrocycle by its incorporation within rigid, randomly shaped oligomers. *Journal of Materials Chemistry* **15**, 1865-1870 (2005).

166 Koyama, T., Suzuki, T., Hanabusa, K., Shirai, H. & Kobayashi, N. A comparison of the loop-current effect of silicon phthalocyanine and silicon naphthalocyanine rings on their axial ligands. *Inorganica chimica acta* **218**, 41-45 (1994).

167 Kane, A. R., Sullivan, J. F., Kenny, D. H. & Kenney, M. E. Nuclear magnetic resonance spectra and the electronic spectra of some silicon and germanium phthalocyanines. *Inorganic Chemistry* **9**, 1445-1448 (1970).

168 Joyner, R. D. & Kenney, M. E. Phthalocyaninosilicon compounds. *Inorganic Chemistry* **1**, 236-238 (1962).

169 Krueger, P. C. & Kenney, M. E. Dialkoxyphthalocyaninosilicon Derivatives1a. *The Journal of organic chemistry* **28**, 3379-3381 (1963).

170 Martín-Gomis, L., Ohkubo, K., Fernández-Lázaro, F., Fukuzumi, S. & Sastre-Santos, A. Adiabatic photoinduced electron transfer and back electron transfer in a series of axially substituted silicon

phthalocyanine triads. *The Journal of Physical Chemistry C* **112**, 17694-17701 (2008).

171 Martín-Gomis, L., Ohkubo, K., Fernández-Lázaro, F., Fukuzumi, S. & Sastre-Santos, Á. Multistep electron transfer systems based on silicon phthalocyanine,[60] fullerene and trinitrofluorenone. *Chemical communications* **46**, 3944-3946 (2010).

172 Céspedes‐Guirao, F. J. *et al.* Synthesis and Photophysics of Silicon Phthalocyanine–Perylenebisimide Triads Connected through Rigid and Flexible Bridges. *Chemistry–A European Journal* **17**, 9153-9163 (2011).

173 Bartelmess, J. *et al.* Phthalocyanine− pyrene conjugates: a powerful approach toward carbon nanotube solar cells. *Journal of the American Chemical Society* **132**, 16202-16211 (2010).

174 Karabacak, M., Cinar, M., Kurt, M. & Sundaraganesan, N. Experimental and theoretical FTIR and FT-Raman spectroscopic analysis of 1-pyrenecarboxylic acid. *Spectrochimica Acta Part A: Molecular and Biomolecular Spectroscopy* **114**, 509-519 (2013).

175 Sürgün, S., Arslanoğlu, Y. & Hamuryudan, E. Synthesis of non-peripherally and peripherally substituted zinc (II) phthalocyanines bearing pyrene groups via different routes and their photophysical properties. *Dyes and Pigments* **100**, 32-40 (2014).

176 Murata, S., Nakatsuji, R. & Tomioka, H. Mechanistic studies of pyrene-sensitized decomposition of p-butylphenyl azide: generation of nitrene radical anion through a sensitizer-mediated electron transfer from amines to the azide. *Journal of the Chemical Society, Perkin Transactions 2*, 793-799 (1995).

177 McQueen, E. W. & Goldsmith, J. I. Electrochemical analysis of single-walled carbon nanotubes functionalized with pyrene-pendant transition metal complexes. *Journal of the American Chemical Society* **131**, 17554-17556 (2009).

178 Özceşmeci, İ., Gelir, A. & Gül, A. Synthesis and photophysical properties phthalocyanine–pyrene dyads. *Dyes and Pigments* **92**, 954-960 (2012).

179 Ehli, C. *et al.* Interactions in single wall carbon nanotubes/pyrene/porphyrin nanohybrids. *Journal of the American Chemical Society* **128**, 11222-11231 (2006).

180 Ogbodu, R. O., Antunes, E. & Nyokong, T. Physicochemical properties of a zinc phthalocyanine–pyrene conjugate adsorbed onto single walled carbon nanotubes. *Dalton Transactions* **42**, 10769-10777 (2013).

181 Cardona, C. M., Li, W., Kaifer, A. E., Stockdale, D. & Bazan, G. C. Electrochemical considerations for determining absolute frontier orbital energy levels of conjugated polymers for solar cell applications. *Advanced materials* **23**, 2367-2371 (2011).

182 Ke, L. *et al.* A Series of Pyrene‐Substituted Silicon Phthalocyanines as Near‐IR Sensitizers in Organic Ternary Solar Cells. *Advanced Energy Materials* (2016).

183 Mizushima, T. *et al.* Pyrene-sensitized electron transport across vesicle bilayers: dependence of transport efficiency on pyrene substituents. *Organic & biomolecular chemistry* **4**, 4336-4344 (2006).

184 Lo, P.-C. *et al.* Preparation and photophysical properties of halogenated silicon (IV) phthalocyanines substituted axially with poly (ethylene glycol) chains. *Tetrahedron letters* **44**, 1967-1970 (2003).

185 Lim, B. *et al.* Silicon-naphthalo/phthalocyanine-hybrid sensitizer for efficient red response in dye-sensitized solar cells. *Organic letters* **15**, 784-787 (2013).

186 Ke, L. *et al.* Panchromatic quaternary polymer/fullerene BHJ solar cells, based on the novel silicon naphthalocyanine and silicon phthalocyanine dye sensitizers. *Journal of Material Chemistry A*, DOI: 10.1039/C6TA08729A (2016).

187 Martín-Gomisa, L., Barea, E. M., Fernández-Lázaroa, F., Bisquert, J. & Sastre-Santos, Á. Dye sensitized solar cells using non-aggregated silicon phthalocyanines. *Journal of Porphyrins and Phthalocyanines* **15**, 1004-1010 (2011).

188 Barker, C. A. *et al.* Synthesis of new axially-disubstituted silicon-phthalocyanine derivatives: optical and structural characterisation. *Tetrahedron* **62**, 9433-9439 (2006).

189 Jiang, J., Kaafarani, B. R. & Neckers, D. C. Design, synthesis, and properties of new derivatives of pentacene. *The Journal of organic chemistry* **71**, 2155-2158 (2006).

190 Lehnherr, D., Murray, A. H., McDonald, R., Ferguson, M. J. & Tykwinski, R. R. Pentacene‐Based Polycyclic Aromatic Hydrocarbon Dyads with Cofacial Solid‐State π‐Stacking. *Chemistry–A European Journal* **15**, 12580-12584 (2009).

191 Kaur, I. *et al.* Substituent effects in pentacenes: Gaining control over HOMO− LUMO gaps and photooxidative resistances. *Journal of the American Chemical Society* **130**, 16274-16286 (2008).

192 Anthony, J. E., Brooks, J. S., Eaton, D. L. & Parkin, S. R. Functionalized pentacene: improved electronic properties from control of solid-state order. *Journal of the American Chemical Society* **123**, 9482-9483 (2001).

193 Ragoussi, M. E., Ince, M. & Torres, T. Recent Advances in Phthalocyanine‐Based Sensitizers for Dye‐Sensitized Solar Cells. *European Journal of Organic Chemistry* **2013**, 6475-6489 (2013).

194 Honda, S., Ohkita, H., Benten, H. & Ito, S. Adv. Energy Mater. 2011, 1, 588. *S. Hsiao, W.-T. Whang, S.-C. Suen, J.-Y. Shiu, C.-P. Chen, Nanotechno l ogy* **19**, 415603 (2008).

195 Min, J. *et al.* Two Similar Near-Infrared (IR) Absorbing Benzannulated Aza-BODIPY Dyes as Near-IR Sensitizers for Ternary Solar Cells. *ACS applied materials & interfaces* **5**, 5609-5616 (2013).

196 Xiao, X. *et al.* Small‐Molecule Photovoltaics Based on Functionalized Squaraine Donor Blends. *Advanced Materials* **24**, 1956-1960 (2012).

197 Walter, M. G., Rudine, A. B. & Wamser, C. C. Porphyrins and phthalocyanines in solar photovoltaic cells. *Journal of Porphyrins and Phthalocyanines* **14**, 759-792 (2010).

198 Min, J. *et al.* Alkyl Chain Engineering of Solution‐Processable Star‐Shaped Molecules for High‐Performance Organic Solar Cells. *Advanced Energy Materials* **4** (2014).

199 Min, J. *et al.* Effects of Alkyl Terminal Chains on Morphology, Charge Generation, Transport, and

Recombination Mechanisms in Solution‐Processed Small Molecule Bulk Heterojunction Solar Cells. *Advanced Energy Materials* **5** (2015).

200 Ameri, T. *et al.* Morphology analysis of near IR sensitized polymer/fullerene organic solar cells by implementing low bandgap heteroanalogue C-/Si-PCPDTBT. *Journal of Materials Chemistry A* **2**, 19461-19472 (2014).

201 Owens, D. K. & Wendt, R. Estimation of the surface free energy of polymers. *Journal of applied polymer science* **13**, 1741-1747 (1969).

202 Chen, W., Nikiforov, M. P. & Darling, S. B. Morphology characterization in organic and hybrid solar cells. *Energy & Environmental Science* **5**, 8045-8074 (2012).

203 Li, S.-H., Xu, Z., Yang, G., Ma, L. & Yang, Y. Solution-processed poly (3-hexylthiophene) vertical organic transistor. *Applied Physics Letters* **93**, 213301 (2008).

204 Baran, D. *et al.* Role of Polymer Fractionation in Energetic Losses and Charge Carrier Lifetimes of Polymer: Fullerene Solar Cells. *The Journal of Physical Chemistry C* **119**, 19668-19673 (2015).

205 Mihailetchi, V., Wildeman, J. & Blom, P. Space-charge limited photocurrent. *Physical review letters* **94**, 126602 (2005).

206 Mihailetchi, V. D., Xie, H., de Boer, B., Koster, L. A. & Blom, P. W. Charge transport and photocurrent generation in poly (3‐hexylthiophene): methanofullerene bulk‐heterojunction solar cells. *Advanced Functional Materials* **16**, 699-708 (2006).

207 Pivrikas, A., Sariciftci, N. S., Juška, G. & Österbacka, R. A review of charge transport and recombination in polymer/fullerene organic solar cells. *Progress in Photovoltaics: Research and Applications* **15**, 677-696 (2007).

208 Mozer, A. J. *et al.* Time-dependent mobility and recombination of the photoinduced charge carriers in conjugated polymer/fullerene bulk heterojunction solar cells. *Physical Review B* **72**, 035217 (2005).

209 Gasparini, N. *et al.* Photophysics of Molecular‐Weight‐Induced Losses in Indacenodithienothiophene‐Based Solar Cells. *Advanced Functional Materials* **25**, 4898-4907 (2015).

210 Kroon, J. *et al.* Nanocrystalline dye‐sensitized solar cells having maximum performance. *Progress in Photovoltaics: Research and Applications* **15**, 1-18 (2007).

211 Lee, K., Park, S. W., Ko, M. J., Kim, K. & Park, N.-G. Selective positioning of organic dyes in a mesoporous inorganic oxide film. *Nature materials* **8**, 665-671 (2009).

212 Ogura, R. Y. *et al.* High-performance dye-sensitized solar cell with a multiple dye system. *Applied Physics Letters* **94**, 073308 (2009).

213 Inakazu, F., Noma, Y., Ogomi, Y. & Hayase, S. Dye-sensitized solar cells consisting of dye-bilayer structure stained with two dyes for harvesting light of wide range of wavelength. *Applied Physics Letters* **93**, 093304 (2008).

214 Choi, H. *et al.* Stepwise Cosensitization of Nanocrystalline TiO2 Films Utilizing Al2O3 Layers in

Dye‐Sensitized Solar Cells. *Angewandte Chemie International Edition* **47**, 8259-8263 (2008).

215 Olivier, C. *et al.* Fine‐Tuning of Triarylamine‐Based Photosensitizers for Dye‐Sensitized Solar Cells. *ChemSusChem* **4**, 731-736 (2011).

216 Burkhard, G. F., Hoke, E. T. & McGehee, M. D. Accounting for interference, scattering, and electrode absorption to make accurate internal quantum efficiency measurements in organic and other thin solar cells. *Advanced Materials* **22**, 3293-3297 (2010).

217 Sapsford, K. E., Berti, L. & Medintz, I. L. Materials for fluorescence resonance energy transfer analysis: beyond traditional donor–acceptor combinations. *Angewandte Chemie International Edition* **45**, 4562-4589 (2006).

218 Huang, J.-S. *et al.* Polymer bulk heterojunction solar cells employing Forster resonance energy transfer. *Nature Photonics* **7**, 479-485 (2013).

219 Sheng, C.-X., Tong, M., Singh, S. & Vardeny, Z. Experimental determination of the charge/neutral branching ratio η in the photoexcitation of π-conjugated polymers by broadband ultrafast spectroscopy. *Physical Review B* **75**, 085206 (2007).

220 Koizumi, H., Dougauchi, H. & Ichikawa, T. Mechanism of dedoping processes of conducting poly (3-alkylthiophenes). *The Journal of Physical Chemistry B* **109**, 15288-15290 (2005).

221 Sperlich, A. *et al.* Photoinduced C70 radical anions in polymer: fullerene blends. *physica status solidi (RRL)-Rapid Research Letters* **5**, 128-130 (2011).

222 Goubard, F. & Wantz, G. Ternary blends for polymer bulk heterojunction solar cells. *Polymer International* **63**, 1362-1367 (2014).

223 Yang, L., Yan, L. & You, W. Organic solar cells beyond one pair of donor–acceptor: ternary blends and more. *The journal of physical chemistry letters* **4**, 1802-1810 (2013).

224 Smestad, G. P. *et al.* Reporting solar cell efficiencies in solar energy materials and solar cells. *Solar Energy Materials and Solar Cells* **92**, 371-373 (2008).

225 Liao, S. H., Jhuo, H. J., Cheng, Y. S. & Chen, S. A. Fullerene Derivative‐Doped Zinc Oxide Nanofilm as the Cathode of Inverted Polymer Solar Cells with Low‐Bandgap Polymer (PTB7‐Th) for High Performance. *Advanced Materials* **25**, 4766-4771 (2013).

226 Small, C. E. *et al.* High-efficiency inverted dithienogermole-thienopyrrolodione-based polymer solar cells. *Nature Photonics* **6**, 115-120 (2012).

227 Park, S. H. *et al.* Bulk heterojunction solar cells with internal quantum efficiency approaching 100&percnt. *Nature photonics* **3**, 297-302 (2009).

228 Chen, S. *et al.* Photo‐Carrier Recombination in Polymer Solar Cells Based on P3HT and Silole‐Based Copolymer. *Advanced Energy Materials* **1**, 963-969 (2011).

229 Zou, Y. *et al.* A thieno [3, 4-c] pyrrole-4, 6-dione-based copolymer for efficient solar cells. *Journal of the American Chemical Society* **132**, 5330-5331 (2010).

230 Elumalai, N. K. & Uddin, A. Open circuit voltage of organic solar cells: an in-depth review. *Energy & Environmental Science* **9**, 391-410 (2016).

Appendix B

Publications and Presentations

Publications:

(1) **L. Ke**, J. Min, M. Adam, N. Gasparini, Y. Hou, J. D. Perea, W. Chen, H. Zhang, S. Fladischer, A. C. Sale, E. Spiecker, R. R. Tykwinski, C. J. Brabec and T. Ameri, A series of novel pyrene-substituted silicon phthalocyanines as near-IR sensitizers in organic ternary solar cells: Synthesis and device fabrication, *Adv. Energy Mater.* **2016**, *6*, 1502355.

(2) **L. Ke**, N. Gasparini, J. Min, H. Zhang, M. Adam, S. Rechberger, K. Forberich, C. Zhang, E. Spiecker, R. R. Tykwinski, C. J. Brabec and T. Ameri, Panchromatic quaternary polymer/fullerene BHJ solar cells, based on the novel silicon naphthalocyanine and silicon phthalocyanine dye sensitizers, *J. Mater. Chem. A*, **2016**, DOI: 10.1039/C6TA08729A.

(3) **L. Ke**, X. Tang, H. Chen, S. Chen, C. Zhang, Q. Fan, C. J. Brabec and T. Ameri, Origin of the V_{OC} enhancement in high efficiency ternary solar cells based mid bandgap polymers and SiPC sensitizer. In preparation.

(4) H. Zhang, W. Y. Tan, S. Fladischer, **L. Ke**. T. Ameri, N. Li, M. Turbiez, E. Spiecker, X. H. Zhu, Y. Cao and C. J. Brabec, Roll to roll compatible fabrication of inverted organic solar cells with a self-organized charge selective cathode interfacial layer, *J. Mater. Chem. A.* **2016**, *4*, 5032.

(5) C. Zhang, A. Mumyatov, S. Langner, J. Perea, T. Kasser, **L. Ke**, T. Ameri, A. Osvet, T. Unruh, N. Li, P. Troshin and C. J. Brabec, overcoming the thermal instability of efficient polymer solar cells by employing novel fullerene-based acceptors, *Adv. Energy Mater.* **2016**, DOI: 10.1002/aenm. 201601204.

Presentation at Conferences:

(1) A series of novel pyrene-combinated silicon phthalocyanine near IR derivatives with higher efficiency in ternary solar cell and their photophysics, **L. Ke**, J. Min, R. R. Tykwinski, C. J. Brabec. T.Ameri, MatHero Summer School on Organic photovoltaics, Karlsruhe, Germany, 23-27 August 2015. (Post presentation)

(2) A series of pyrene-substituted SiPc and SiNc as near-IR sensitizers in organic ternary and quaternary solar cells: Synthesis and device fabrication, **L. Ke**, J. Min, M. Adam, N. Gasparini, R. R. Tykwinski, C. J. Brabec. T.Ameri, 9th International Symposium on Flexible Organic Electrons (ISFOE 16), Thessaloniki, Greece, 4-7 July 2016. (Oral presentation)

(3) Synthesis of novel silicon phthalocyanines and their applications in organic ternary solar cells as near IR sensitizers**. L. Ke**, J. Min, N. Gasparini, M. Adam, S. Fladischer, E. Spiecker, R. R. Tykwinski, T. Ameri, C. J. Brabec. 3rd International Congress Next Generation Solar Energy -From Fundamental to Applications, Erlangen, Germany, 23-25 November 2016. (Poster Presentation)